Hochschule Anhalt

Fachbereich Angewandte Biowissenschaften und Prozesstechnik

Studiengang Biotechnologie

Development of a new method for the characterisation of bioreactors concerning heat and mass transfer

Abschlussarbeit zur Erlangung des akademischen Grades

Master of Science (M.Sc.)

vorgelegt von

Ulf Dehio

Mat. Nr. 4059423

Gutachter: Prof. Dr.-Ing. habil. Wolfram Meusel

Zweitgutachter: Prof. Dr. Klaus Lorenz

Datum der Abgabe:

Danksagung

Zuallererst möchte ich mich bei Herrn Prof. Dr.-Ing. habil. W. Meusel für die Übernahme des Referates und bei Herrn Prof. Dr. K. Lorenz für das Korreferat der Masterarbeit herzlich bedanken.

Genauso möchte ich auch Herrn M. Müller, Herrn T. Dreher, Frau U. Husemann sowie Herrn C. Zahnow sowohl für die Themenstellung, als auch für die kompetente Betreuung der Arbeit und die zahlreichen Ratschläge meinen Dank aussprechen. Ebenso danke ich Herrn A. Helling für die freundliche Unterstützung am Rasterelektronenmikroskop.

Weiterhin gilt mein Dank auch allen anderen Mitarbeitern der R&D-Abteilung „Upstream Technology“ der Sartorius Stedim Biotech GmbH für die Unterstützung und die vielen hilfreichen Tipps.

Ein herzliches Dankeschön gilt auch meinen Eltern und meiner Verlobten für ihren stetigen Rückhalt während meines Studiums.

Content

Zusammenfassung

Da der spezifischen Wärmedurchgangskoeffizienten UA und der volumetrische Stofftransportkoeffizienten k_La eine wichtige Rolle bei der Auslegung biotechnologischer Prozesse spielen, wurden in der Vergangenheit verschiedene Methoden zur Bestimmung dieser Parameter entwickelt. Allerdings nutzen diese häufig ungenaue dynamische Verfahren zur Beschreibung von stationären Prozessen und sind hinsichtlich der Größe und Geometrie des Bioreaktors nur beschränkt einsetzbar. Deshalb war es das Ziel dieser Arbeit eine neue Methode zu entwickeln, die diese Limitationen überwindet. Der hier vorgestellte neue Ansatz basiert auf der gleichmäßigen Freisetzung von Wärme und Sauerstoff durch die Zersetzung von Wasserstoffperoxid in einer kontinuierlichen Betriebsweise. Da der Abbau von H_2O_2 unter Normalbedingungen nur unter Einwirkung eines Katalysators abläuft, wurden verschiedene Kandidaten auf ihre Eignung (u.a. bezüglich Sicherheitsaspekten und ihrer Kinetik) untersucht. Mangan-(IV)-oxid wurde als geeignet befunden. Um die Inaktivierung des MnO_2 zu kompensieren wurde ein kontinuierlicher Prozess mit wiederholter Zugabe von frischem MnO_2 etabliert. Weiterhin wurde ein Scale-up, ausgehend von 100 mL bis zu einem 5 Liter Glasbioreaktor (UniVessel®), erfolgreich durchgeführt.

Um die Eignung der neuen Methode zur Charakterisierung von Bioreaktoren zu zeigen, wurde sie mit herkömmlichen Ansätzen verglichen. Sowohl mit dem neu entwickelten als auch mit einem bereits etablierten Verfahren, dass auf einer elektrisch betriebenen Wärmequelle basiert, wurden bei Leistungseinträgen von ca. 50 – 70 $\frac{W}{L}$ spezifische Wärmedurchgangskoeffizienten zwischen 17,1 und 24,8 $\frac{W}{K}$ gemessen. Erste Testergebnisse bzgl. des Stofftransportes ergaben bei unterschiedlichen Verdünnungsraten bis 0,04 h^{-1} allerdings keine konstanten k_La-Werte.

In nachfolgenden Studien sollten nun bezüglich des k_La höhere Zuflussraten aufgrund von gleichmäßigeren Volumenströmen überprüft werden. Darüber hinaus sind weitere Untersuchungen empfehlenswert, um den Wärmeübergang auch in größeren herkömmlichen und ebenfalls in single-use-Bioreaktoren zu analysieren.

Abstract

Since the specific heat transfer coefficient (UA) and the volumetric mass transfer coefficient (k_La) play an important role for the design of biotechnological processes, different techniques were developed in the past for the determination of these parameters. However, these approaches often use imprecise dynamic methods for the description of stationary processes and are limited towards scale and geometry of the bioreactor. Therefore, the aim of this thesis was to develop a new method, which overcomes these restrictions. This new approach is based on a permanent production of heat and oxygen by the constant decomposition of hydrogen peroxide in continuous mode. Since the degradation of H_2O_2 at standard conditions only takes place by the support of a catalyst, different candidates were investigated for their potential (regarding safety issues and reaction kinetic). Manganese-(IV)-oxide was found to be suitable. To compensate the inactivation of MnO_2, a continuous process with repeated feeds of fresh MnO_2 was established. Subsequently, a scale-up was successfully carried out from 100 mL to a 5 litre glass bioreactor (UniVessel®)

To show the applicability of this new method for the characterisation of bioreactors, it was compared with common approaches. With the newly established technique as well as with a conventional procedure, which is based on an electrical heat source, specific heat transfer coefficients were measured in the range of 17.1 – 24.8 $\frac{W}{K}$ for power inputs of about 50 – 70 $\frac{W}{L}$. However, a first proof of concept regarding the mass transfer showed no constant k_La for different dilution rates up to 0.04 h^{-1}.

Based on this, consecutive studies concerning the mass transfer should be made with higher volume flows, due to more even inflow rates. In addition, further experiments are advisable, to analyse the heat transfer in single-use bioreactors and in larger common systems.

List of figures

List of tables

Abbreviations

DCU	Digital control unit
EDTA	Ethylenediaminetetraacetic acid
kDa	kilo Dalton
PBS	Phosphate buffered saline
PESU	Polyethersulfone
RO	Reverse osmosis
Vvm	Volume gas per volume medium per minute

Symbols

Name	Formula symbol	Unit
Acid constant	pK_a	$-$
Activation energy	E_A	$\frac{J}{mole}$
Amount of rotations of the stirrer per time	N	$\frac{1}{s}$
Amount of substance flow	$\dot{n}$	$\frac{mole}{s}$
Area, surface	A	m^2
Average reaction rate for two adjacent measurement points	$k_{i,i+1}$	$\frac{1}{h}$
Average temperature for two adjacent measurement points	$\overline{T}_{i,i+1}$	K
Biomass concentration	c_x	$\frac{g}{L}$
Boltzmann constant	σ	$\frac{W}{m^2 \cdot K^4}$
Carbon dioxide mole fraction (inlet gas flow)	$x_{CO_2,in}$	$-$
Carbon dioxide mole fraction (outlet gas flow)	$x_{CO_2,out}$	$-$
Catalyst concentration	$c(CAT)$	$\frac{g}{L}$
Concentration of active catalase	$c(Catalase_{active})$	$\frac{mg}{L}$
Corrected reaction rate	$k_{corrected}$	$\frac{1}{h}$
Density	ρ	$\frac{kg}{L}$
Density of H_2O_2	$\rho_{H_2O_2}$	$\frac{kg}{L}$

Name	Formula symbol	Unit
Diameter of the stirrer	d	m
Diffusion coefficient	D_c	$\frac{m^2}{s}$
Diffusion coefficient of the gas boundary film	$D_{c,g}$	$\frac{m^2}{s}$
Diffusion coefficient of the liquid boundary film	$D_{c,l}$	$\frac{m^2}{s}$
Dilution rate	D	$\frac{1}{h}$
Energy difference	ΔE	J
Energy flow density	$\dot{e}_s$	$\frac{W}{m^2}$
Labour, heat, energy, which is tied to a mass transport	W, Q, E_m	J
Gas flow rate	$\dot{V}_{gas}$	$\frac{L}{min}$
Gas volume flow at the reactor inlet	$\dot{V}_{g,i}$	$\frac{L}{s}$
Gas volume flow at the reactor outlet	$\dot{V}_{g,o}$	$\frac{L}{s}$
Gas-side mass transfer coefficients	$k_{O_2,g}$	$\frac{m}{s}$
Grade of emission	ε	$-$
H_2O_2 concentration	$c(H_2O_2)$	$\frac{mole}{L}$
H_2O_2 concentration at the measurement point i	$c(H_2O_2)_i$	$\frac{mole}{L}$
H_2O_2 concentration at the measurement point i+1	$c(H_2O_2)_{i+1}$	$\frac{mole}{L}$

Name	Formula symbol	Unit
Hatta number	Ha	$-$
Heat conductivity of the liquid	λ_l	$\frac{W}{m \cdot K}$
Heat flow	$\dot{Q}$	W
Heat flow by the evaporating oxygen	$\dot{Q}_{Evaporation}$	W
Heat flow by the inflowing cooling water	$\dot{Q}_{Jacket,in}$	W
Heat flow by the inflowing H_2O_2	$\dot{Q}_{H_2O_2,in}$	W
Heat flow from the jacket chamber to the environment	$\dot{Q}_{loss\,2}$	W
Heat flow by the outflowing cooling water	$\dot{Q}_{Jacket,out}$	W
Heat flow by the outflowing medium	$\dot{Q}_{Medium,out}$	W
Heat flux density	$\dot{q}$	$\frac{W}{m^2}$
Heat flux density through a plane wall	$\dot{q}_W$	$\frac{W}{m^2}$
Heat flow from the reactor through the lid to the environment	$\dot{Q}_{loss\,1}$	W
Heat flow from the reactor to the double jacket	$\dot{Q}_{Jacket}$	W
Heat transfer coefficient	α	$\frac{W}{m^2 \cdot K}$
Heat transfer coefficient after the layer	α_2	$\frac{W}{m^2 \cdot K}$
Heat transfer coefficient in front of the layer	α_1	$\frac{W}{m^2 \cdot K}$

Name	Formula symbol	Unit
Henry constant (dimensionless)	H^{cc}	$-$
Henry constant (with regard to the partial pressure)	H^{pc}	$\frac{L \cdot Pa}{mole}$
Henry constant for PBS/MnO_2 medium (dimensionless)	${H_{PBS,MnO_2}}^{cc}$	$-$
Henry constant for pure water (dimensionless)	${H_{Water}}^{cc}$	$-$
Inactivation rate	k''	$\frac{1}{h}$
Inflowing H_2O_2 concentration	$c(H_2O_2)_i$	$\frac{mole}{L}$
Inflowing volume flow rate	$\dot{V}_E$	$\frac{L}{s}$
Layer thickness	δ	m
Liquid-side mass transfer coefficients	$k_{O_2,l}$	$\frac{m}{s}$
Mass flow of the cooling water	$\dot{m}_{H_2O}$	$\frac{kg}{s}$
Mass flow of the evaporating O_2	$\dot{m}_{O_2}$	$\frac{kg}{s}$
Mass flow of the inflowing H_2O_2	$\dot{m}_{H_2O_2}$	$\frac{kg}{s}$
Mass flow of the outflowing medium	$\dot{m}_{Medium}$	$\frac{kg}{s}$
Measured H_2O_2 concentration	$c_{measured}(H_2O_2)$	$\frac{mole}{L}$
Molarity of O_2	M_{O_2}	$\frac{g}{mole}$
Newton number	Ne	$-$

Name	Formula symbol	Unit
Nusselt number	Nu	$-$
Outflowing H_2O_2 concentration	$c(H_2O_2)_o$	$\frac{mole}{L}$
Overall heat flow from the H_2O_2 inflow and the medium outflow	$\dot{Q}_{in-and\ outflow}$	W
Overall heat transfer resistance	U	$\frac{W}{K \cdot m^2}$
Overall mass transfer coefficient	K_l	$\frac{m}{s}$
Overall specific power input	$P_{spec.}$	$\frac{W}{L}$
Overflowed length of a stationary layer	L	m
Oxygen concentration in the gas phase at the reactor inlet	$c_{g,i}$	$\frac{mole}{L}$
Oxygen concentration in the gas phase at the reactor outlet	$c_{g,o}$	$\frac{mole}{L}$
Oxygen concentration in the medium at t = 0	c_0	$\frac{mole}{L}$
Oxygen concentrations in the bulk liquid	c_l	$\frac{mole}{L}$
Oxygen concentrations in the gas-liquid boundary phase	c_l^*	$\frac{mole}{L}$
Oxygen mole fraction (inlet gas flow)	$x_{O_2,in}$	$-$
Oxygen mole fraction (outlet gas flow)	$x_{O_2,out}$	$-$
Oxygen partial pressure in the gas bubble	$p_{O_2,g}$	Pa
Oxygen partial pressure in the gas-liquid boundary phase	$p_{O_2,g}^*$	Pa

Name	Formula symbol	Unit
Oxygen saturation concentration in PBS medium	c_s	$\frac{mole}{L}$
Oxygen saturation concentration of PBS/MnO_2 medium	$c_{l,\ PBS,MnO_2}{}^*$	$\frac{mole}{L}$
Oxygen saturation concentration of pure water	$c_{l,\ Water}{}^*$	$\frac{mole}{L}$
Oxygen transfer rate	OTR	$\frac{mole}{s \cdot L}$
Oxygen uptake rate	OUR	$\frac{mole}{s \cdot L}$
Percentage dissolved oxygen saturation concentration in PBS medium	p_{O_2}	%
Power input by the reaction to the reactor	$P_{Reaction}$	W
Power input by the stirrer to the reactor	$P_{Stirrer}$	W
Pre-exponential factor	B	$\frac{1}{h}$
Pressure	p	Pa
Pseudo reaction rate	k'	$\frac{L}{h \cdot g}$
Reaction enthalpy	ΔH_R	$\frac{J}{mole}$
Reaction rate	k	$\frac{1}{h}$
Reaction rate at 30 °C	$k(30\ °C)$	$\frac{1}{h}$
Reaction rate at the temperature $\overline{T}_{i,i+1}$	$k(\bar{T}_{i,i+1})$	$\frac{1}{h}$
Sample volume	V_{Sample}	L

Name	Formula symbol	Unit
Simplified overall mass coefficient	k_L	$\frac{m}{s}$
Sodium thiosulfate concentration	$c(Na_2S_2O_3)$	$\frac{mole}{L}$
Sodium thiosulfate volume	$V_{Na_2S_2O_3}$	L
Specific gas flow rate	$\dot{V}_{spec.gas}$	$\frac{L}{L \cdot s}$
Specific heat capacity of H_2O_2	c_{p,H_2O_2}	$\frac{J}{K \cdot kg}$
Specific heat capacity of the medium	$c_{p,Medium}$	$\frac{J}{K \cdot kg}$
Specific heat capacity of water	c_{p,H_2O}	$\frac{J}{K \cdot kg}$
Specific heat transfer coefficient	UA	$\frac{W}{K}$
Specific heat transfer coefficient for the outer wall of the jacket chamber	UA_3	$\frac{W}{K}$
Specific heat transfer coefficient for the reactor lid	UA_2	$\frac{W}{K}$
Specific length	r, y	m
Specific phase boundary interface	a	$\frac{1}{m}$
Specific oxygen uptake rate	q_{O_2}	$\frac{mole}{s \cdot g}$
Standardisation factor	$\bar{\kappa}_{i,i+1}$	$-$
Standardised reaction rate	$k_{i,i+1}(30\ °C)$	$\frac{1}{h}$
Superficial gas velocity	u_G	$\frac{m}{s}$

Name	Formula symbol	Unit
Temperature at the measurement point i	T_i	K
Temperature at the measurement point i + 1	T_{i+1}	K
Temperature field	ϑ	K
Temperature gradient	$\frac{dT}{dx}, \frac{dT}{dy}$	$\frac{K}{m}$
Temperature in experiment number 1	T_1	K
Temperature in experiment number 2	T_2	K
Temperature in the fluid	T_F	K
Temperature in the wall	T_W	K
Temperature of the inflowing cooling water	$T_{Jacket,in}$	K
Temperature of the environment	$T_{Environment}$	K
Temperature of the outflowing cooling water	$T_{Jacket,out}$	K
Temperature of the reactor	$T_{Reactor}$	K
Theoretical H_2O_2 concentration	$c_{theoretical}(H_2O_2)$	$\frac{mole}{L}$
Thermoconductivity	λ	$\frac{W}{m \cdot K}$
Thickness of the gas boundary film	δ_g	m
Thickness of the liquid boundary film	δ_l	m
Time at the beginning of the measurement	t_0	h

Name	Formula symbol	Unit
Time at the end of the measurement	t_{end}	h
Time at the measurement point i	t_i	h
Time at the measurement point i + 1	t_{i+1}	h
Time dependent oxygen concentration in the medium	$c_l(t)$	$\frac{mole}{L}$
Torque	M_t	$N \cdot m$
Turnover	X	%
Universal gas constant	R	$\frac{J}{mole \cdot K}$
Velocity	w	$\frac{m}{s}$
Volume	V	L
Volume flow rate of the H_2O_2 inflow	$\dot{V}_i$	$\frac{L}{s}$
Volume flow rate of the H_2O_2 inflow and the medium outflow	$\dot{V}_{i,o}$	$\frac{L}{s}$
Volume-specific power input	$\frac{P}{V}$	$\frac{W}{L}$
Volumetric mass transfer coefficient	$k_L a$	$\frac{1}{s}$

Chapter 1

Introduction

Many biotechnological processes include strong exothermic reactions. The formed reaction heat sums up to 500 kJ per mole consumed oxygen (Storhas, 1994). This generated heat has to be removed from the bioreactor in order to guarantee controlled temperature conditions. While this is not problematic in small scale fermentations, cooling of bioreactors is a challenging task in greater scales, due to the decreased surface to volume ratio. For the dimensioning of bioreactors, the knowledge about the heat transfer through the walls of the reactor is very important. Overheating leads to safety issues, product loss or a decreased product quality. Therefore, procedures for a precise estimation of the heat transfer are required. By today, only one static approach with a calibration heater as a heat source is published (Regestein, 2012; Zühlke, 2015). However, it is restricted towards the bioreactor scale and its geometry. Furthermore it is not usable in single use bioreactors, which are nowadays often used in the pharmaceutical industry (Storhas, 1994; Türker, 2004).

Another key challenge for microbial fermentations and mammalian cultivations is the supply of oxygen to the cells, and therefore, to the medium. Due to the low solubility of oxygen in water and the relative high oxygen uptake rates by the cells, a steady aeration is necessary to prevent anaerobe conditions. The absorption velocity is hereby directly proportional to the phase boundary and to the concentration gradient. On that score, dispersing by stirrer or nozzles and aeration with air or pure oxygen is often applied to increase the transferred oxygen (Zlokarnik, 1999). Up to now, different measurement procedures are published. Some operate with dynamic attempts (the gassing-out method) other work with steady state measurements (the sulphite method and the exhaust gas analysis), but every method has its pros and cons and lead to different results. Therefore, new approaches, which are easy to handle, feasible for high mass transfers and result in precise outcomes, are desired (Martin, 1996; Stanbury *et al.*, 1995).

Chapter 2

Aim and Scope

Different approaches exist for the characterisation of the heat and mass transfer in bioreactors. In case of the heat transfer, only one method is published, which is limited by the bioreactor geometry and scale. In view of the mass transfer, often applied techniques use dynamic approaches, which fall short due to the long response time of the dissolved oxygen probes. Furthermore, these dynamic measurements differ from the static mode, which occurs in fermentations. Steady state attempts like the sulphite method deliver more accurate results, but are related with the expensive catalyst disposal. Therefore, the research question of this thesis was to develop a new method for the characterisation of bioreactors regarding heat and mass transfer, which overcomes the limitations mentioned above. This new attempt is based on a chemical heat and oxygen production by the permanent breakdown of H_2O_2, which is realised in a steady state of a continuous procedure.

The main contributions described in this thesis are multifold: First a method for the measurement of the H_2O_2 turnover by the catalysed degradation reaction is presented. This is necessary to compute the heat and the oxygen, which is set free in the reactor. Secondly, an appropriate catalyst is found and its kinetic is clarified. Thirdly, a process is developed, which allows an even heat and oxygen production by the decomposition of H_2O_2. Finally, the whole procedure is scaled up from 100 mL up to a 5 litre glass bioreactor (UniVessel®).

After the successful establishment of this process, its usability is analysed in the UniVessel® (5 L) by a comparison of different conventional techniques with the newly developed procedure.

Chapter 3

Theoretical Background

3.1 Heat transfer

3.1.1 Types of energy transfer

The first law of thermodynamics predicates that a change of energy in an existing system is only possible if a transport of energy in or out of the system consists. Possible transports of energy are labour, heat and energy, which is conveyed by a mass flow (equation (1)) (Stephan, 2013).

$$\Delta E = W + Q + E_M \tag{1}$$

Energy difference	ΔE	$[J]$
Labour, Heat	W, Q	$[J]$
Energy, which is tied to a mass transport	E_m	$[J]$

Heat transport as a change of energy is driven by differences in temperatures. The heat flow represents the transferred heat per time unit:

$$\dot{Q} = \frac{dQ}{dt} \tag{2}$$

Heat flow	$\dot{Q}$	$[W]$

Based on that, the heat flow density is defined as:

$$\dot{q} = \frac{d\dot{Q}}{dA} \tag{3}$$

Heat flux density	$\dot{q}$	$\left[\frac{W}{m^2}\right]$
Area, surface	A	$[m^2]$

Conduction

There are three types of heat transport. One of them is the conduction, whereby the energy transfer is caused by interactions of the molecules in a temperature-shifted material. Besides that, free electrons transport heat in metals as well. For a temperature

gradient in the direction of the coordinate x the heat flux density depends only on a material coefficient, the so called thermoconductivity:

$$\dot{q} = -\lambda \cdot \frac{dT}{dx} \; (Fourier's\ law) \tag{4}$$

Thermoconductivity	λ	$\left[\frac{W}{m \cdot K}\right]$
Temperature gradient	$\frac{dT}{dx}$	$\left[\frac{K}{m}\right]$

For isentropic materials, which have an identic thermoconductivity in all directions in space, $\dot{q}$ is defined proportional to the temperature gradient:

$$\vec{\dot{q}} = -\lambda \cdot grad\ T \tag{5}$$

According to the heat flow, which is always directed to a sink, the equation is negative. Typical values of thermoconductivity are listed up in Table 1. λ depends on the temperature, the pressure and in materials, which are made out of different compounds, on the composition as well.

Table 1: Typical values of thermoconductivities for gases, liquids and solid materials (VDI-Gesellschaft Verfahrenstechnik und Chemieingenieurwesen, 2013).

Physical state	$\lambda \left[\frac{W}{m \cdot K}\right]$
Gaseous	0.015 – 0.15
Liquid	0.1 – 0.65
Solid	1 – 450

The entirety of all temperatures in the material results in a temperature field (ϑ). All points of an object, which has the same temperature at the same time, are defined as isothermal areas. The heat transfer through a plane wall is illustrated by Figure 1. Since r_1 and r_2 are isotherms, their temperature does not differ. $\vartheta(r_1)$ is given as ϑ_{W1} and $\vartheta(r_2)$ as ϑ_{W2}. For $\vartheta_{W1} > \vartheta_{W2}$ the heat flows from r_1 to r_2.

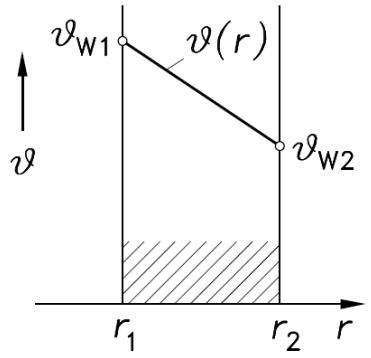

Figure 1: Schematical depiction of the heat flow through a plane wall (Baehr and Stephan, 2013).

The heat flow $(\dot{Q})$ is equal on every isotherm and unaffected by the position in the wall, because no energy can be stored in the wall under steady state conditions. Besides that, for a wall, which has a temperature independent thermoconductivity, Fourier's law is compressed from

$$d\dot{Q} = \dot{q}(r) \cdot A(r) = -\lambda(\vartheta) \cdot \frac{dT}{dr} \cdot A(r) \tag{6}$$

Specific length	r	$[m]$

to

$$d\dot{Q} = -\lambda \cdot \frac{dT}{dr} \cdot A \tag{7}$$

Convective heat transfer through the plane wall

In flowing liquids, the energy transfer does not depend only on the conductivity but on the macroscopic movements, too. It is influenced by properties of the fluid and different process parameters (e.g. flow velocity and grade of turbulence). Special regard is given to the case of the heat transfer from a liquid to a solid phase. Ludwig Prandtl developed hereto the boundary layer theory.

At the boundary the velocity changes from zero to the maximal speed within a narrow boundary layer. Directly at the wall only conduction takes place:

$$\dot{q}_W = -\lambda \left(\frac{dT}{dy}\right)_W \tag{8}$$

Heat flux density through a plane wall	$\dot{q}_W$	$\left[\frac{W}{m^2}\right]$
Specific length	y	$[m]$
Temperature gradient	$\frac{dT}{dy}$	$\left[\frac{K}{m}\right]$

The heat transfer is driven by the temperature difference between the wall and the fluid.

$$\dot{q}_W = \alpha \cdot (T_W - T_F) \tag{9}$$

Heat transfer coefficient	α	$\left[\frac{W}{m^2 \cdot K}\right]$
Temperature in the wall	T_W	$[K]$
Temperature in the fluid	T_F	$[K]$

The heat transfer coefficient condenses the complex pattern of the velocity and temperature profile. It depends on the geometry and surface roughness. Aside from that, the process parameters (e.g. velocity, grade of turbulence or direction of the stream relatively to the wall) and the properties of the fluid play an important role.
Equation (8) and (9) result in

$$\alpha = -\lambda \frac{\left(\frac{dT}{dy}\right)_W}{(T_W - T_F)} \tag{10}$$

so that α depends on the temperature difference between the wall and the fluid and on the slope of the temperature profile in the wall. If the temperature progression is plotted against the wall distance, Figure 2 is formed. The heat flux density through the wall emerges from the slope of the temperature profile. The ratio of $\frac{\lambda}{\alpha}$ signifies the magnitude of the boundary layer, therefore a thick layer implies a small α (and thus in a minor heat transfer) and vice versa (Baehr and Stephan, 2013; Stephan, 2013).

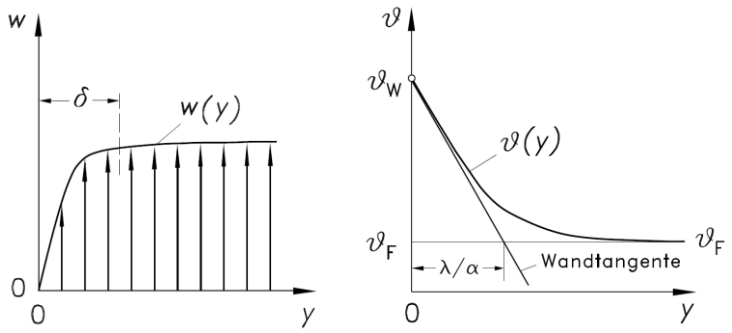

Figure 2: Profile of the flow velocity (left) and the temperature (right) of a streaming fluid next to a wall. (Baehr and Stephan, 2013).

For the determination of α, the temperature profile is needed. That is why for several technical relevant configurations α-values have been calculated out of known values for $\dot{q}$ and the temperature difference $(T_W - T_F)$.

Due to the complex flow profiles next to the wall, it is often assumed that only conduction takes place in the laminar boundary layer. Therefore, the heat transfer in a bioreactor from the liquid phase in the vessel to the cooling jacket outside of it is described with a linearization approach (Türker, 2004).

$$\dot{Q}_{Jacket} = U \cdot A \cdot \Delta T \tag{11}$$

Heat flow from the reactor to the double jacket	$\dot{Q}_{Jacket}$	$[W]$
Overall heat transfer resistance	U	$\left[\frac{W}{K \cdot m^2}\right]$

In case of a heat transfer through a plane wall the overall heat transport coefficient can be expressed as the sum of different individual resistances (Figure 3).

$$\frac{1}{U} = \frac{1}{\alpha_1} + \frac{\delta}{\lambda} + \frac{1}{\alpha_2} \tag{12}$$

Heat transfer coefficient in front of the layer	α_1	$\left[\frac{W}{m^2 \cdot K}\right]$
Layer thickness	δ	$[m]$
Heat transfer coefficient after the layer	α_2	$\left[\frac{W}{m^2 \cdot K}\right]$

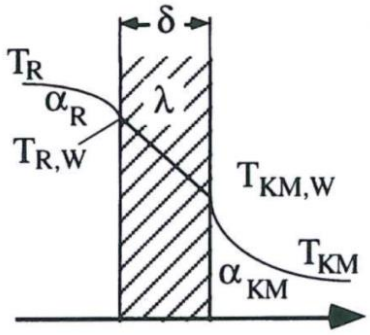

Figure 3: Illustration of the occurring resistances during the heat transfer through a plane wall (Storhas, 1994).

The flow velocity, fluid properties and the vessel geometry influence the overall heat transfer resistance, which describes the conductivity of the system. Since the surface of the reactor is often difficult to measure, U and A are combined and expressed together as the specific heat transfer coefficient (UA) (Stanbury *et al.*, 1995).

In the special case of a liquid medium at the one side of the wall, it is possible to express the relation between the entire heat transfer and the heat transfer by conduction. Therefore, α has to be multiplied with the overflowed length of the stationary layer and divided by the heat conductivity of the liquid. The resulting dimensionless number is called the Nusselt number (Chmiel, 2011; Stanbury *et al.*, 1995).

$$Nu = \frac{\alpha \cdot L}{\lambda_l} = \frac{entire\ heat\ transfer}{heat\ transfer\ by\ conduction} \tag{13}$$

Overflowed length of a stationary layer	L	$[m]$
Heat conductivity of the liquid	λ_l	$\left[\frac{W}{m \cdot K}\right]$
Nusselt number	Nu	$[-]$

Radiation

Every body with a temperature higher than 0 K emits radiation, so that the following formula is valid:

$$\dot{q} = \dot{e}_s = \sigma \cdot T^4 \ (Boltzmann´s\ law) \tag{14}$$

Energy flow density	$\dot{e}_s$	$\left[\frac{W}{m^2}\right]$
Boltzmann constant	σ	$\left[\frac{W}{m^2 \cdot K^4}\right]$

For real bodies, which do not emit 100 % of the possible radiation, it is applied

$$\dot{e} = \varepsilon \cdot \dot{e}_s = \varepsilon \cdot \sigma \cdot T^4 \tag{15}$$

Grade of emission	ε	$[-]$

The grade of emissions depends on the material characteristics, the surface conditions, the temperature and the direction of radiation, as well (Stephan, 2013). In this thesis, radiation is predominantly neglected.

3.1.2 Measurement methods of UA

A static method for the determination of the heat transfer, published by Regestein, is based on a constant electrical power input (Regestein, 2012). This is performed by a calibration heater, which is dipped into the medium. By means of a high performance alternating voltage regulator a defined power input is set and the reactor is tempered by the double jacket or additional cooling fingers. Then, the specific heat transfer coefficient (UA) is calculable by the different heat flows occurring in the double jacket. Advantages of this technique are the easy handling, the low costs and the resulting reproducible outcomes. However, this approach is limited by the bioreactor scale. Further, investigations regarding heat transfer in single-use reactors are not possible with this technique. Other methods are still rare and only focus on the determination of the heat transfer coefficient (α_1) at the inner wall of the bioreactor, which is why new approaches are desired (Zühlke, 2015; Regestein, 2012; Zlokarnik, 1999).

3.2 Mass transfer

In microbial fermentations, the oxygen supply for cells is another important factor during the process. Due to the low solubility of oxygen in water (2.18 $\frac{mmol}{L}$ (0 °C), 1.03 $\frac{mmol}{L}$ (40 °C), respectively (Chmiel, 2011)) an additional aeration with air is usually needed. For a higher supply, air enriched with oxygen or pure oxygen is sometimes added. Another way of increasing the mass transfer is dispersing the gas bubbles by stirring, with the result of an increased total surface. Any more, stirring counteracts concentration gradients and thus, supports an evenly high mass transfer. In addition to that, the average gas bubble diameter is decreased. A malfunction of the aeration system may be a severe threat to the microorganisms. This problem gets special relevance for high cell density cultures. Due to the fact that an insufficient supply with oxygen may lead to a change of the metabolism, product losses or impurities are possible consequences (Chmiel, 2011; Knoll *et al.*, 2005).

3.2.1 Derivation of k_La

A common theory to describe the mass transfer between two different boundary layers is the two-film theory: Each boundary layer has a narrow, laminar film, in which no storage and only diffusion takes place. At the boundary border, the oxygen concentration is in equilibrium with the respective phase. The cores of the phases are assumed as ideal mixed and thus have constant concentrations (Figure 4) (Reiss, 2015; Chmiel, 2011).

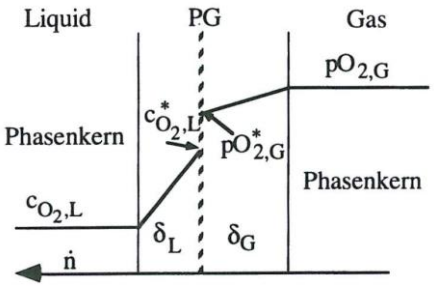

Figure 4: Schematic illustration of oxygen transfer from a gas bubble to the medium (Storhas, 1994).

The gas-side and, respectively, liquid-side mass transfer coefficients $k_{O_2,g}$ and $k_{O_2,l}$ are defined by the corresponding film thickness and the diffusion coefficient:

$$k_{O_2,g} \sim \frac{D_{c,g}}{\delta_g} \qquad k_{O_2,l} \sim \frac{D_{c,l}}{\delta_l} \tag{16}$$

Gas-side mass transfer coefficients	$k_{O_2,g}$	$\left[\frac{m}{s}\right]$
Diffusion coefficient of the gas boundary film	$D_{c,g}$	$\left[\frac{m^2}{s}\right]$
Film thickness of the gas boundary film	δ_g	$[m]$
Liquid-side mass transfer coefficients	$k_{O_2,l}$	$\left[\frac{m}{s}\right]$
Diffusion coefficient of the liquid boundary film	$D_{c,l}$	$\left[\frac{m^2}{s}\right]$
Film thickness of the liquid boundary film	δ_l	$[m]$

The oxygen flow in the liquid film ($\dot{n}$) can be expected as follows.

$$\dot{n} = k_{O_2,l} \cdot a \cdot (c_l{}^* - c_l) \tag{17}$$

Amount of substance flow	$\dot{n}$	$\left[\frac{mole}{s}\right]$
Specific phase boundary interface	a	$\left[\frac{1}{m}\right]$
Oxygen concentrations in the gas-liquid boundary phase	$c_l{}^*$	$\left[\frac{mole}{L}\right]$
Oxygen concentrations in the bulk liquid	c_l	$\left[\frac{mole}{L}\right]$

The oxygen flow in the gas film ($\dot{n}$), which correspond to the oxygen transfer rate (OTR), is given by:

$$OTR = \dot{n} = \frac{k_{O_2,g} \cdot a}{R \cdot T} \cdot (p_{O_2,g} - p_{O_2,g}{}^*) \tag{18}$$

Oxygen transfer rate	OTR	$\left[\frac{mole}{s \cdot L}\right]$
Universal gas constant	R	$\left[\frac{J}{mole \cdot K}\right]$
Oxygen partial pressure in the gas bubble	$p_{O_2,g}$	$[Pa]$
Oxygen partial pressure in the gas-liquid boundary phase	$p_{O_2,g}{}^*$	$[Pa]$

These equations can be transformed to

$$OTR = \dot{n} = K_l \cdot a \cdot (\frac{p_g}{R \cdot T} - c_l) \tag{19}$$

Overall mass transfer coefficient	K_l	$\left[\frac{m}{s}\right]$

where the overall mass transfer coefficient is described by

$$K_l = \frac{1}{\left(\frac{1}{k_{O_2,l}} + \frac{1}{k_{O_2,g}}\right)} \tag{20}$$

The main resistance is represented by the liquid boundary layer, because $k_{O_2,g}$ is much greater than $k_{O_2,l}$. This means that equation (20) can be simplified, which leads to equation (21), where K_l can be equated with $k_{O_2,l}$.

$$K_l \approx \frac{1}{\left(\frac{1}{k_{O_2,l}}\right)} \approx k_{O_2,l} = k_L \tag{21}$$

Simplified overall mass transfer coefficient	k_L	$\left[\frac{m}{s}\right]$

Furthermore, it can be assumed, that $p_g \approx p_g{}^*$ is valid. All in all, the mass transfer is described by

$$OTR = k_L \cdot a \cdot (c_l{}^* - c_l) \tag{22}$$

The oxygen concentrations in the gas-liquid boundary phase ($c_l{}^*$), which is in balance with the core of the gas phase, is given by Henry's law:

$$c_l{}^* = \frac{p_g{}^*}{H^{pc}} \approx \frac{p_g}{H^{pc}} \tag{23}$$

Henry constant (with regard to the partial pressure)	H^{pc}	$\left[\frac{L \cdot Pa}{mole}\right]$	

Since k_L and a are difficult to measure, they are often combined to the volumetric oxygen transfer coefficient (k_La) (Storhas, 1994; Chmiel, 2011). Therefore, the oxygen transfer rate can be expressed as

$$OTR = k_La \cdot (c_l{}^* - c_l) \tag{24}$$

Volumetric mass transfer coefficient	k_La	$\left[\frac{1}{s}\right]$	

3.2.2 Process technological and biological meaning of k_La

The k_La, which characterises the velocity of the mass transfer, can be described as well with a correlation of the volume-specific power input and the superficial gas velocity:

$$k_La = C \cdot \left(\frac{P}{V}\right)^{\alpha} \cdot u_G^{\beta} \quad \text{(Van't Riet, 1979)} \tag{25}$$

Volume-specific power input	$\frac{P}{V}$	$\left[\frac{W}{L}\right]$	
Superficial gas velocity	u_G	$\left[\frac{m}{s}\right]$	

The mass balance for a biological system, which describes the relationship between the introduced and the consumed oxygen, is given as follows:

$$\frac{dc_l}{dt} = OTR - OUR \tag{26}$$

Oxygen uptake rate	OUR	$\left[\frac{mole}{s \cdot L}\right]$

The OUR stands for the oxygen uptake rate of the organisms and is described by the multiplication of the specific oxygen uptake rate with the biomass concentration (Garcia-Ochoa and Gomez, 2009):

$$OUR = q_{O_2} \cdot c_x \tag{27}$$

Specific oxygen uptake rate	q_{O_2}	$\left[\frac{mole}{s \cdot g}\right]$
Biomass concentration	c_x	$\left[\frac{g}{L}\right]$

3.2.3 Measurement methods of k_La

There are different measurement methods for the determination of the volumetric mass transfer coefficient (k_La), which can be split in two groups: The dynamic and the static procedures. While the dynamic approach is based on a changing oxygen level during the measurement ($\frac{dc_l}{dt} \neq 0$), the static strategy works with a steady state concentration of the inflowing gas in the liquid ($\frac{dc_l}{dt} = 0$). This can be achieved by an oxygen sink, e.g. a microbial or chemical one.

An example for a dynamic k_La-determination is the gassing-out method where the aimed gas (e.g. oxygen) in the examined solution is previously degasified with nitrogen. Afterwards, the solution is aerated with air and the increasing oxygen concentration is registered. With the aid of the differential algorithm (equation (28) and (29), respectively), the k_La is calculable. Since equation (29) has the shape of a linear equation, k_La represents the slope of this function (Meusel *et al.*, unpublished; Garcia-Ochoa and Gomez, 2009; Koepp-Bank, 2012).

$$\frac{dc_l}{dt} = k_L a \cdot (c^*{}_l - c_l(t)) \tag{28}$$

$$\ln\left(\frac{c^*{}_l - c_0}{c^*{}_l - c_l(t)}\right) = k_L a \cdot t \tag{29}$$

Time dependent oxygen concentration in the medium	$c_l(t)$	$\left[\frac{mole}{L}\right]$
Oxygen concentration in the medium at t = 0	c_0	$\left[\frac{mole}{L}\right]$

The main advantages of this approach are the quick evaluation and the low costs. The determination is possible under non-sterile settings and the utilised chemicals are harmless considering safety issues. Further, a wide span of different process conditions can be studied without limitations due to biological influences and a comparison of different systems is easily applied. However, due to constantly changing oxygen concentration in the medium, this strategy is vulnerable, due to the response time of the dissolved oxygen probe. Furthermore, the difference between the current and the saturation concentration decreases over time. Hence, the driving force for the mass transfer decreases gradually. Therefore, the k_La determined with dynamic methods will be smaller compared to steady state approaches (Meusel *et al.*, unpublished; Garcia-Ochoa and Gomez, 2009).

For this reason, the stationary sulphite method has to be mentioned (Chmiel, 2011). Under the influence of a catalyst like copper or cobalt, sulphite is oxidized by the dissolved oxygen to sulphate (equation (30)). The amount of non-converted sodium sulphite is determined iodometrically.

$$2\,Na_2SO_3 + O_2 \xrightarrow{Catalyst} 2Na_2SO_4 \tag{30}$$

The oxygen concentration is always zero, because the entire supplied oxygen is consumed in the reaction described above. The O_2-mass-flow is determined by the time-dependent change of the normality of the sulphite-solution. By the fast reaction rate, it can be assumed that the consumption of O_2 takes place next to the boundary layer and

consequently, increases the difference between the gas bubble and the boundary layer as well as the mass-transfer-driving-force. Thus, the obtained k_La will be overestimated compared to biological systems (Martin, 1996; Zlokarnik, 1999; Chmiel, 2011; Garcia-Ochoa and Gomez, 2009; Storhas, 1994).
Another disadvantage of this method is the disposal of cobalt. Furthermore, in single-use bioreactors only one measurement per bag is possible, due to residues of the catalyst, whereas the gassing-out method allows multiple measurements with one bag.

Another static method to determine the k_La is based on the exhaust gas analysis during a microbial fermentation (Nagraik, 2015). The oxygen uptake rate is calculable by equation (31).

$$OUR = \frac{\dot{V}_{spec.gas} \cdot p}{V \cdot R \cdot T} \cdot \left(x_{O_2,in} - \frac{1 - x_{O_2,in} - x_{CO_2,in}}{1 - x_{O_2,out} - x_{CO_2,out}} \cdot x_{O_2,out} \right) \tag{31}$$

Specific gas flow rate	$\dot{V}_{spec.gas}$	$\left[\frac{L}{L \cdot s}\right]$
Pressure	p	$[Pa]$
Volume	V	$[L]$
Oxygen mole fraction (inlet gas flow)	$x_{O_2,in}$	$[-]$
Oxygen mole fraction (outlet gas flow)	$x_{O_2,out}$	$[-]$
Carbon dioxide mole fraction (inlet gas flow)	$x_{CO_2,in}$	$[-]$
Carbon dioxide mole fraction (outlet gas flow)	$x_{CO_2,out}$	$[-]$

Assumed that the velocity of the oxygen transfer is quicker than the biological process this method is quasi-stationary. If the oxygen uptake rate (OUR) is equated with the oxygen transfer rate (OUR), the k_La is defined by equation (32) (Chmiel, 2011).

$$k_L a = \frac{OUR}{c^*_l - c_l} \tag{32}$$

The main advantage of this steady state technique is the independency of model-systems and the related realistic conditions. However, the process parameters are comparatively fixed. They cannot be changed during the fermentation to study different experimental settings.

3.3 Decomposition of hydrogen peroxide as a potential source of heat and oxygen for thermodynamic experiments

For the characterisation of bioreactors, the decomposition of H_2O_2 is a potential source of heat by its high reaction enthalpy (-98.2 $\frac{kJ}{mole}$) and oxygen. Hydrogen peroxide is a highly reactive liquid with a density of 1.1 $\frac{kg}{L}$ (at 20 °C and a concentration of 30 wt. %) and a molarity of 34.0 $\frac{g}{mole}$. Furthermore, it is a cheap compound[1] and the formed products are considered as harmless. However, hydrogen peroxide as the educt is corrosive and oxidizing. The chemical reaction is described as

$$2\ H_2O_2 \rightarrow 2\ H_2O + O_2 \tag{33}$$

and should be supported by a catalyst to ensure a steady and safe process. Possible catalysts are the enzyme catalase, $Fe(NO_3)_3$ and MnO_2 among others (Müller, 2015).
Compared to a calibration heater for the heat production in bioreactors (Regestein, 2012), the hydrogen peroxide-method has the advantage to work independently of the bioreactor scale and geometry. Thus, it can be used in very small, very big and wave-mixed bioreactors and allows an evenly heat production throughout the whole system. In addition, the breakdown of H_2O_2 delivers high amounts of oxygen, which can be used for the measurement of the volumetric mass transfer coefficient (k_La) (Müller, 2015). As distinct to common methods, this procedure leads to a supersaturation of the dissolved oxygen concentration by the formation of dissolved gas in the liquid phase. Values of

[1] 25 L for 84.70 € (Data obtained on the 11.09.2015 at www.carlroth.com)

130-300 % have been published in the literature (Martin, 1996). However, it has to be considered that the accomplished k_La measured with this method was higher compared to the results of other procedures, because of bubble nucleation. This effect was observed especially in non-coalescing media with low k_La-values because newly formed bubbles strongly increased the interfacial surface and caused turbulences (Linek *et al.*, 1996; Martin, 1996; Hickman, 1988).

3.3.1 Different catalysts for the digestion of H_2O_2 and their reaction mechanisms

3.3.1.1 Catalase

Catalase (E.C. 1.11.1.6) naturally occurs in the liver, the kidney, conjunctive tissue and red blood cells. It is present in plants as well, in particular in some storage organelles like potato nodules. It regulates the hydrogen peroxide-level and protects SH-proteins like haemoglobin from the oxidizing effect of H_2O_2 (Reißmann, 2015).

Catalase has a quaternary structure with four subunits (similar to haemoglobin). Each subunit has a haem group, more than 500 amino acids and weighs about 60 kDa. In contrast to haemoglobin, the iron atom at the centre of the porphyrin ring has a charge of +III instead of +II. The metal ion can be transformed to +V during the catalysis. In comparison to free iron ions, the enzyme reaction is distinctly faster. Nevertheless, the homogenous catalysis with Fe^{3+} has been investigated as well (Eduard-Job-Stiftung für Thermo- und Stoffdynamik, 2015).

3.3.1.2 Iron nitrate

Two mechanisms have been found for the iron driven decomposition of H_2O_2 (Eduard-Job-Stiftung für Thermo- und Stoffdynamik, 2015): The Kremer-Stein-mechanism describes the reaction with a changing oxidation number of iron from (+III) to (+V) and back:

$$Fe^{3+} + H_2O_2 \leftrightarrow [Fe^{+III}OOH]^{2+} + H^+ \tag{34}$$

$$\leftrightarrow [Fe^{+V}O]^{3+} + H_2O \xrightarrow{+H_2O_2} Fe^{3+} + 2H_2O + O_2$$

The Haber-Weiss-mechanism depicts the process with a radical chain reaction, where iron (+III) is oxidized to iron (+II) and back. Apart from the high reaction enthalpy, this explains the fast reaction kinetics.

Initiation: $$Fe^{3+} + H_2O_2 \leftrightarrow [Fe^{+III}OOH]^{2+} + H^+ \leftrightarrow Fe^{2+} + HOO\cdot + H^+ \quad (35)$$

Continuation: $$Fe^{2+} + H_2O_2 \rightarrow Fe^{3+} + 2\,OH\cdot$$
$$Fe^{3+} + H_2O_2 + OH\cdot \rightarrow Fe^{3+} + HOO\cdot + H_2O$$
$$\rightarrow Fe^{2+} + H^+ + O_2 + H_2O$$

3.3.1.3 Manganese-(IV)-oxide

Furthermore, manganese dioxide (also known as pyrolysite) has been used as a heterogeneous catalyst in the process described above. Thus, the size of the surface can be a limiting factor for the decomposition of H_2O_2 (Martin, 1996; Eduard-Job-Stiftung für Thermo- und Stoffdynamik, 2015; Hickman, 1988; Reißmann, 2015).
The reaction mechanism is proposed as followed (Broughton and Wentworth, 1947):

$$MnO_2 + H_2O_2 + 2\,H^+ \rightarrow Mn^{++} + 2\,H_2O + O_2 \quad (36)$$
$$Mn^{++} + 2\,H_2O_2 \leftrightarrow Mn(OH)_2 + 2H^+$$
$$Mn(OH)_2 + H_2O_2 \rightarrow MnO_2 + 2\,H_2O$$

Overall reaction: $$2\,H_2O_2 \rightarrow 2\,H_2O + O_2$$

Different publications showed, that the decomposition of H_2O_2 is benefitted in alkaline medium compared to neutral or acidic medium (maximum of catalytic activity: pH 11.5 – 12.0 (Kanungo *et al.*, 1981; Omar, 2014)). The literature mentions for the MnO_2 supported digestion activation energies of $58\,\frac{kJ}{mole}$ and, respectively, $82\,\frac{kJ}{mole}$ (Elprince and Mohamed, 1992; Dolhun, 2015).

3.3.2 Reaction kinetics of the decomposition of H_2O_2

The breakdown of hydrogen peroxide follows a first order reaction. Hence, the change of the H_2O_2 concentration per time is given by

$$\frac{dc(H_2O_2)}{dt} = -k \cdot c(H_2O_2) \tag{37}$$

H_2O_2 concentration	$c(H_2O_2)$	$\left[\frac{mole}{L}\right]$
Reaction rate	k	$\left[\frac{1}{h}\right]$

Because the reaction rate depends on the amount of catalyst, it is defined as

$$k = k' \cdot c(CAT) \tag{38}$$

Pseudo reaction rate	k'	$\left[\frac{L}{h \cdot g}\right]$
Catalyst concentration	$c(CAT)$	$\left[\frac{g}{L}\right]$

Therefore, k' is one of the most important parameters for the dimensioning of experiments (Do *et al.*, 2009; Elprince *et al.*, 2008; Akhtar *et al.*, 2012).

As mentioned before, the pH has an influence on the reaction kinetics (3.3.1). For a defined range, the literature brings up the following coherence for MnO_2 (Elprince *et al.*, 2008):

$$k = k' \cdot c(CAT) \cdot 10^{\frac{-pH}{4}} \tag{39}$$

Since this range refers to soil samples and not to pure MnO_2, it is not completely transferable. Nevertheless, the pH has still to be taken into account. However, if the MnO_2 is suspended in PBS buffer, the pH will not change during the experiment and the additional factor can be integrated in the pseudo reaction rate k'.

In a continuous mode the steady state balance equations for the hydrogen peroxide concentration in an ideally mixed vessel is given by

$$0 = D \cdot c(H_2O_2)_i - D \cdot c(H_2O_2)_o - k' \cdot c(CAT) \cdot c(H_2O_2)_o \tag{40}$$

Dilution rate	D	$\left[\frac{1}{h}\right]$
Inflowing H_2O_2 concentration	$c(H_2O_2)_i$	$\left[\frac{mole}{L}\right]$
Outflowing H_2O_2 concentration	$c(H_2O_2)_o$	$\left[\frac{mole}{L}\right]$

The equation can be transformed to

$$0 = D \cdot c(H_2O_2)_i - (D + k' \cdot c(CAT)) \cdot c(H_2O_2)_o \tag{41}$$

Since the turnover is described by

$$X = \left(1 - \frac{c(H_2O_2)_o}{c(H_2O_2)_i}\right) \cdot 100 \tag{42}$$

Turnover	X	[%]

converting and insertion of equation (41) in equation (42) leads to

$$X = \frac{k' \cdot c(CAT) \cdot \frac{1}{D}}{1 + k' \cdot c(CAT) \cdot \frac{1}{D}} \tag{43}$$

If a constant turnover is adjusted, which is feasible in continuous mode, it is possible to calculate precisely the reaction rate.

3.3.3 Determination of the H_2O_2 turnover

For the calculation of the exact H_2O_2 turnover, a measurement of the current concentration is helpful. The literature recommends a two-step colorimetric method (Vogel and Mendham, 2000; Dokuzovic, 2015). First of all, the colourless hydrogen peroxide solution is mixed with an acidified potassium iodide solution. Attributable to the formation of elementary iodine the liquid changes its colour instantly to dark red and, respectively, brown. In this step, the complete H_2O_2 is depleted due to an overflow of the other components in the solution.

$$\underset{\text{(colourless)}}{H_2O_2 + 2\,HCl + 2\,KI} \rightarrow \underset{\text{(dark red / brown)}}{2\,H_2O + I_2 + 2\,KCl} \tag{44}$$

Afterwards, a sodium thiosulfate solution is titrated until the colour almost reaches the colourless shape again.

$$\underset{\text{(dark red / brown)}}{2\,Na_2S_2O_3 + I_2} \rightarrow \underset{\text{(colourless)}}{2\,NaI + Na_2S_4O_6} \tag{45}$$

Subsequently, a starch solution is added to improve the sensitivity of the colorimetric determination. By the incorporation of polyiodide into the helix shaped starch molecules the liquid turns dark purple and black, respectively. Next, more sodium thiosulfate is titrated until the dark dye is completely ceased. Since the H_2O_2 reacts stoichiometrically with the iodide, the initial amount of H_2O_2 is calculable.

Compared with the often used permanganate method (which is based on equation (46)) the procedure described above has the advantage to be less effected by stabilisers, which are sometimes added to the hydrogen peroxide solution. Furthermore, too high concentrations of H_2O_2 result in the formation of MnO_2, which would decompose the compound of interest (Vogel and Mendham, 2000).

$$2\,MnO_4^- + 5\,H_2O_2 + 6\,H^+ \rightarrow 2\,Mn^{2+} + 5\,O_2 + 8\,H_2O \tag{46}$$

Chapter 4

Material and Methods

4.1 Material

Chemicals, enzymes and devices are listed up in Table 10 and, respectively, Table 11 in the appendix.

4.2 Preparation of the solutions

1 wt. % starch solution (100 mL)

For the preparation of the starch solution, 1 ± 0.05 g starch was weighed out in a beaker and 10 ± 0.5 mL RO-water was added to the starch. The mixture was stirred thoroughly with a scoop before it was added to 80 ± 0.5 mL of boiling RO-water. The starch residues were transferred from the beaker with 10 ± 0.5 mL RO-water and the starch solution was agitated with a magnetic stir bar until it got clear. Finally, the starch solution was cooled down to room temperature and stored at 5 °C.

0.1 M sodium thiosulfate solution (100 mL)

The sodium thiosulfate solution was prepared by weighing of 1.58 ± 0.05 g $Na_2S_2O_3$. After the salt was transferred to a graduated flask (100 mL), a magnetic stir bar and 80 ± 0.5 mL RO-water were added. The solution was stirred until the sodium thiosulfate was completely dissolved. Then, the graduated flask was filled up to 100 mL.

0.24 M potassium iodide solution (500 mL)

For the production of the potassium iodide solution, 20 ± 0.05 g potassium iodide was weighed out and the salt was added to a graduated flask (500 mL). Next, a magnetic stir bar and 400 ± 0.5 mL RO-water were added. The liquid was stirred until the potassium iodide was completely dissolved. Subsequently, the flask was filled up to 500 mL. As much 50 mL tubes as samples were expected were filled with 32 mL KI-solution.

10x PBS-buffer (1000 mL)

The 10-fold PBS-buffer was prepared by weighing out 80 ± 0.1 g NaCl, 2.0 ± 0.05 g KCl, 14.2 ± 0.1 g Na_2HPO_4 and 2.4 g ± 0.05 KH_2PO_4. The salts were transferred to a graduated flask (1 L) and dissolved completely by means of a magnetic stir bar and 800 mL RO-water. After that, the graduated flask was filled up to the calibration mark. Before the PBS-buffer was used, a 10-fold dilution was carried out.

4.3 Determination of the H_2O_2 turnover

The prefilled KI-solution was added to 4 mL of hydrochloric acid (32 wt. %) in another 50 mL tube and subsequently, the sample was added. The recommended sample volume was estimated by Table 2. The sealed 50 mL tube was shaken and the solution was filled to a 50 mL beaker. Afterwards, the solution was stirred with a magnetic stir bar. After the fluid was completely mixed, the sodium thiosulfate solution was titrated until the solution turned almost colourless. Next, 0.8 mL of the starch solution was added. After 15 seconds, the $Na_2S_2O_3$ solution was titrated again until the mixture bleached. The colour changes during the procedure are shown in Figure 5.

Table 2: Recommended sample volume for different estimated H_2O_2 concentrations.

Concentration ($\frac{mole}{L}$)	Turnover [%]*	Sample volume [mL]
9.79	0.0	0.02
4.90	50.0	0.04
2.45	75.0	0.08
1.22	87.5	0.16
0.61	93.8	0.32
0.31	96.9	0.64
0.15	98.4	1.28
0.05	99.5	4.00

*Turnover of H_2O_2 in regard to an initial concentration of 9.80 $\frac{mole}{L}$ and 30 wt. %, respectively.

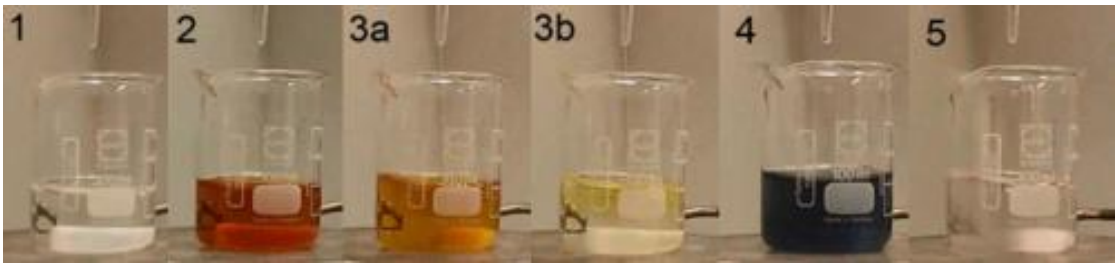

Figure 5: Colour changes during the measurement of the H_2O_2 concentration. From left to right: 1. Acidified KI-solution before the addition of the H_2O_2 sample / 2. Acidified KI-solution after the addition of the H_2O_2 sample / 3a. and 3b. Titration of $Na_2S_2O_3$ / 4. Addition of the starch solution / 5. End point of the titration.

Since every H_2O_2 molecule forms one iodine molecule, which reduces two thiosulfate molecules, the initial concentration of H_2O_2 is calculated by the following equation:

$$c(H_2O_2) = \frac{V_{Na_2S_2O_3} \cdot c(Na_2S_2O_3) \cdot \frac{1}{2}}{V_{Sample}} \tag{47}$$

Sodium thiosulfate volume	$V_{Na_2S_2O_3}$	$[L]$
Sodium thiosulfate concentration	$c(Na_2S_2O_3)$	$\left[\frac{mole}{L}\right]$
Sample volume	V_{Sample}	$[L]$

Subsequently, the turnover is computable by equation (42).

4.4 Establishment of an appropriate catalyst for the decomposition of H_2O_2

Several catalysts were examined for their ability and suitability to decompose H_2O_2. Therefore, batch-experiments in a scale of 0.1 L with different catalyst-concentrations were performed in order to approximately determine the pseudo reaction rate. The experiments were carried out with an initial hydrogen peroxide concentration of 1.5 $\frac{mole}{L}$. This concentration was chosen, because this amount of H_2O_2 can lead to a maximal temperature increase of about 35 °C in the medium and is therefore harmless in view of safety issues. A 250 mL beaker, placed on a stir plate, served as a reaction

vessel. It was insulated to reduce the cooling effect by the environment. The magnetic stirrer was adjusted in a way so that ideal mixing was guaranteed (Figure 6).

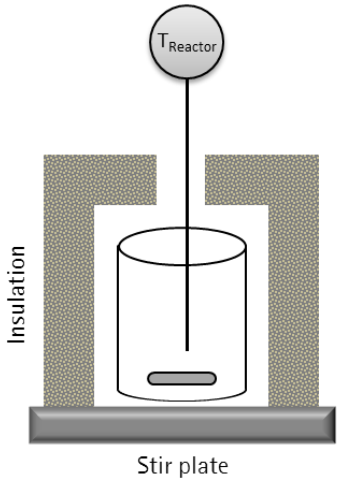

Figure 6: Experimental setup for investigations of different catalysts concerning their ability to decompose H_2O_2.

The H_2O_2 concentration was measured with the previously mentioned procedure (4.3). Since the kinetic of the H_2O_2 decomposition is given by equation (37) and (38), k' is calculable by:

$$k' = \frac{k}{c(CAT)} \tag{48}$$

The time depended temperature profile was registered continuously (measurements every 5 seconds).

The experiments with catalase were executed in potassium phosphate buffer (pH 7), whereas RO-water was utilised for $Fe(NO_3)_3$. PBS-Buffer (pH 7) was used for MnO_2, because manganese oxide does not inhibit coalescence, due to its insolubility in water. In the case of $Fe(NO_3)_3$, the catalyst dissociates by itself in Fe^{3+} and NO^{3-} and therefore, lead to a non-coalescent medium.

4.5 Establishment of a continuous heat production method based on the decomposition of H_2O_2

For the calculation of the specific heat transfer coefficient (UA) and the volumetric mass transfer coefficient (k_La) a continuous process was established with the aim of a constant heat and oxygen release by the steady degradation of hydrogen peroxide. Furthermore, with such a process it is possible to determine different kinetic parameters very precisely. The experimental setup was installed as follows: Hydrogen peroxide was pumped into a 250 mL beaker and later on in a 2 and 5 litre reactor, respectively (UniVessel®, multi-use) by a Watson Marlow peristaltic pump. Depending on the needed flow rate, tubes with different diameters were used. The exact determination of the flow rate was carried out by weighing the H_2O_2 supply bottle and, respectively, the waste bottle. The transfer of the medium was performed by a tube, which was dipped into the medium. The 2 and 5 litre bioreactor were equipped with baffles and a double jacket, which was used for temperature regulation. The cooling water was supplied by the Frigomix 1000. The 2 L reactor was only used for small scale experiments with very low amounts of medium (0.35 L and 1 L) during the establishment of the new method and the scale-up. Therefore, a 3-blade segment impeller (diameter of 54 mm) offered an ideally mixed system. In the 5 L reactor (3.5 L medium) the 6-blade disk-impeller (diameter of 75 mm) was chosen, due to its comparatively better mixing properties in larger scales (Figure 7- Figure 10).

Figure 7: 3-blade segment impeller (left), 6-blade disk impeller (center) and schematic illustration of the UniVessel® (2 L and 5 L) (right).

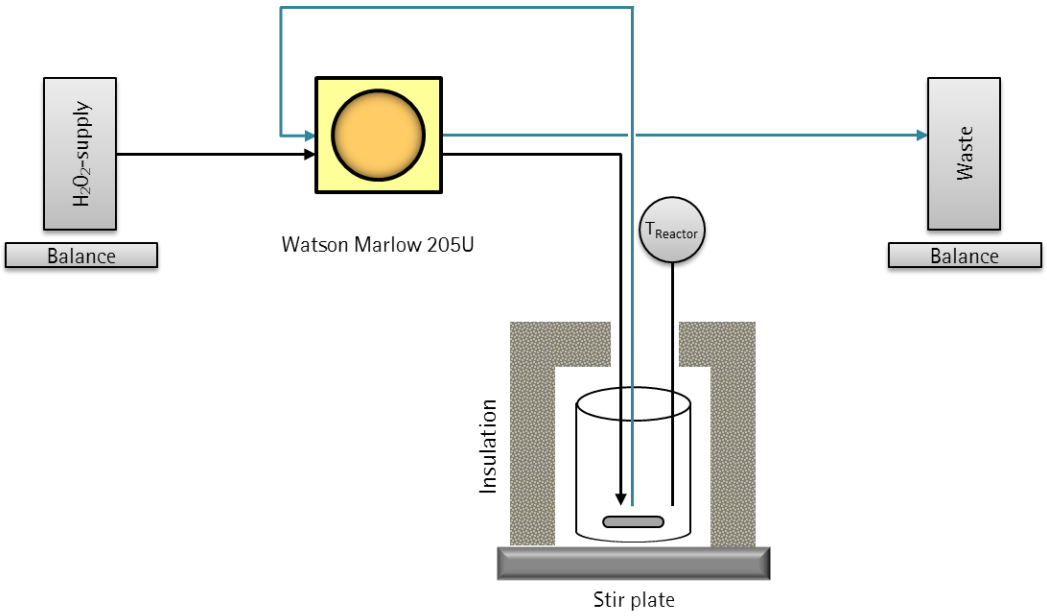

Figure 8: Experimental setup for the establishment of a constant heat and oxygen production method in a 250 mL beaker based on the decomposition of H_2O_2.

Samples for the determination of H_2O_2 were taken out of the 250 mL beaker directly by a pipette and, in case of the UniVessel® (2 L and 5 L, respectively), by two syringes: One for rinsing the tubing (3 mL) and the other one for the taking out of the sample (1.5 mL). The samples were transferred to a micro reaction vessel (Eppendorf), wherefrom a defined volume was taken, added to a KI-solution, which was freshly acidified with HCl, and analysed as described above (4.3).

Subsequently, the medium, taken from the reactor to wash the tubing (and, in case of the UniVessel® (2 L), the leftover in the micro reaction vessel), were pushed back into the system by a third syringe. In case of the Univessel® (5 L), the pass back of the leftover was renounced, due to the insignificance of the small catalyst traces compared to the reactor volume and for reasons of simplifications. Afterwards, 5 mL of ambient air was pushed through the syringes to remove residues from the sampling system and to make both the catalyst and the substrate available to the reaction again.

The sampling system as well as the outflow was placed next to the stirrer in a zone of high mixing and fastened with cable tie at the temperature probe.

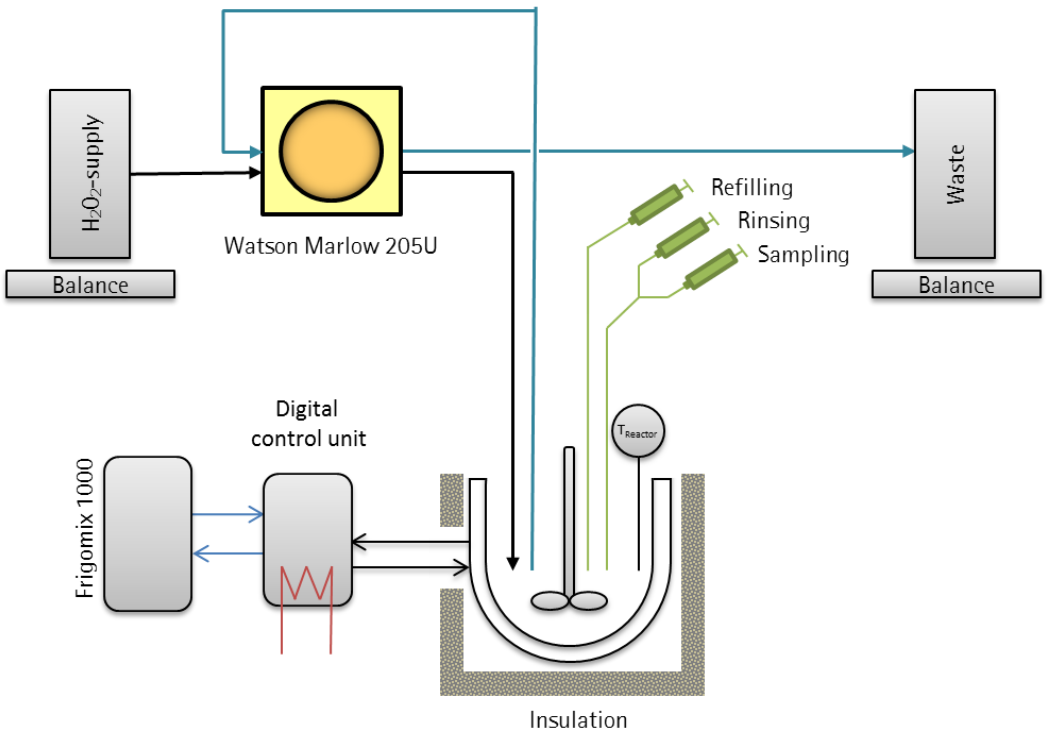

Figure 9: Experimental setup for the establishment of a constant heat and oxygen production method in the UniVessel® (2 L) based on the decomposition of H_2O_2.

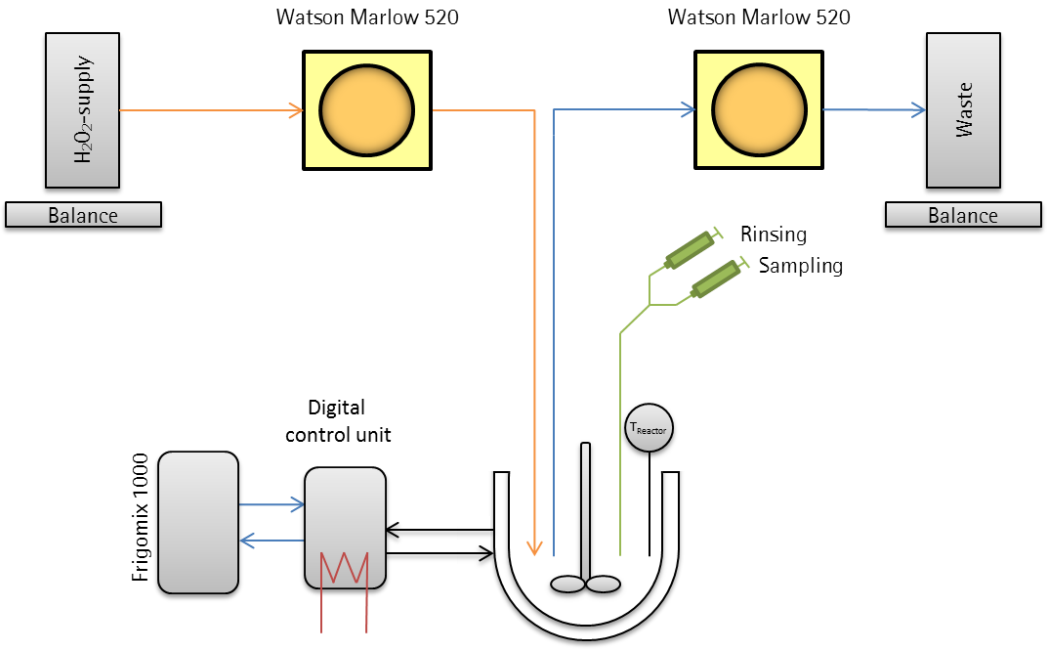

Figure 10: Experimental setup for the establishment of a constant heat and oxygen production method in the UniVessel® (5 L) based on the decomposition of H_2O_2.

Prior to all experiments, the concentration of the H_2O_2 stock solution was tested, to guarantee a constant quality and reproducible results. The stock solution was stored at 5 °C and warmed up to room temperature before it was used, to ensure a constant density and therefore, a constant flow.

4.6 Determination of UA in the UniVessel® (5 L)

For the measurement of UA the experiments were performed in the UniVessel® (5 L) and executed like described above (4.5). To overcome the dilution- and inactivation effect, which were discovered in later experiments (5.3), the following feeding strategy was used: In the beginning a MnO_2 concentration of 6 $\frac{g}{L}$ was introduced and after every hour, a feed of 3 $\frac{g}{L}$, suspended in 40 mL RO-water, was added. Temperature probes were installed at the in- and outlet of the cooling jacket and a mass flow measurement device was assembled in the cooling circulation (Figure 11).

For comparative studies, not only a heat supply by the degradation of hydrogen peroxide was studied, but also an electrically heat supply by calibration heaters was utilised (Figure 12). These calibration heaters had a maximum power input of 250 W and, respectively, 500 W and were set with a high performance alternating voltage regulator to the required set points.

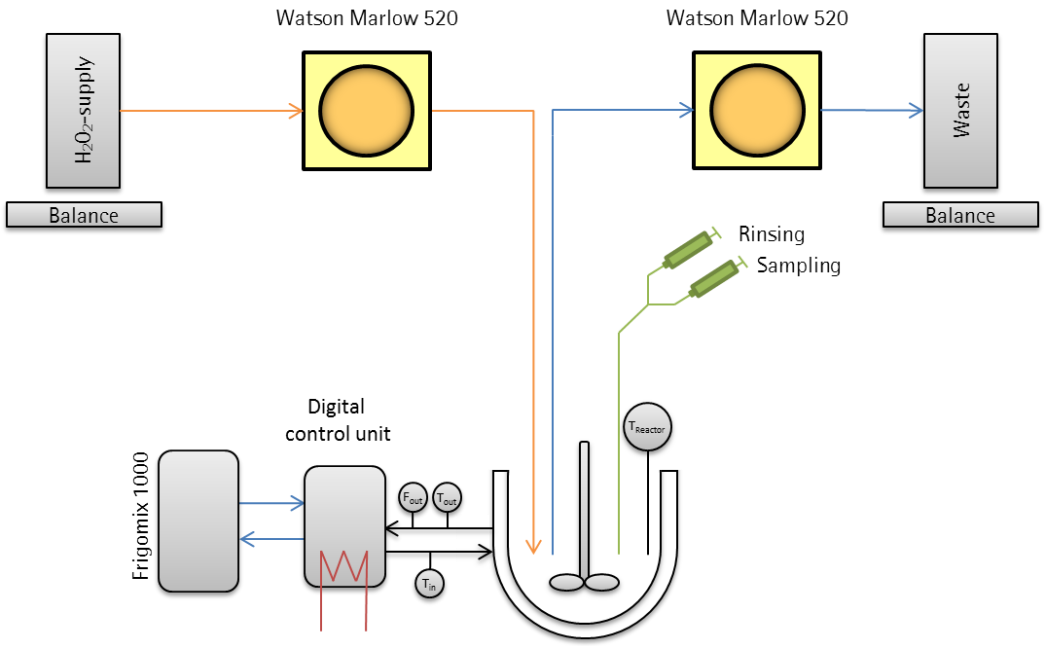

Figure 11: Experimental setup for the investigation of the heat transfer through the wall of the UniVessel® (5 L). Heat is supplied chemically by the decomposition of H_2O_2. Compared to Figure 10 the temperature probes at the in- and outlet of the double jacket and, furthermore, the mass flow meter is shown.

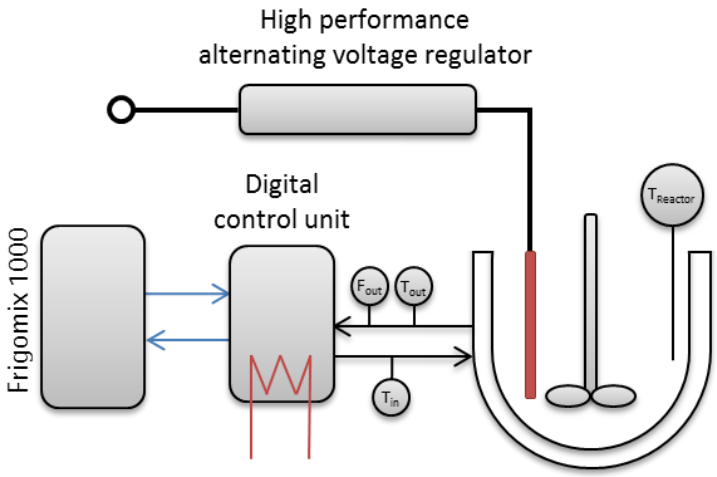

Figure 12: Experimental setup for the investigation of the heat transfer through the wall of the UniVessel® (5 L). Heat is supplied electrically by a calibration heater.

4.7 Determination of k_La in the UniVessel® (5 L)

The experimental setup for the measurement of the volumetric mass transfer coefficient (k_La) was similar to the heat transfer investigations (Figure 13). At first, the bioreactor was filled with 1x PBS-buffer (3.5 L), agitated (500 rpm), tempered (30 °C) and aerated with nitrogen ($1 \frac{L}{min}$). After the pO_2 and the temperature probe showed constant values, the pO_2 probe was recalibrated, if necessary. Subsequently, $6 \frac{g}{L}$ MnO_2 was added and the aeration was stopped. Then, 10 mL of H_2O_2 was added to check the pO_2 probe. Due to the O_2 production, the pO_2 rose above the measuring range of the probe. Next, the aeration was started again, so that the pO_2 adjusted quickly to 0 %. If necessary, the probe was recalibrated. Afterwards, H_2O_2 was pumped into the reactor. After a steady state of the temperature and the oxygen level was reached, the conditions were held for at least 15 minutes and a sample was taken to determine the current H_2O_2 concentration and therefore, the turnover (4.3). The sample was taken at the end of every steady state phase to prevent a falsification due to the air, which was pushed back to the sampling system for cleaning issues.

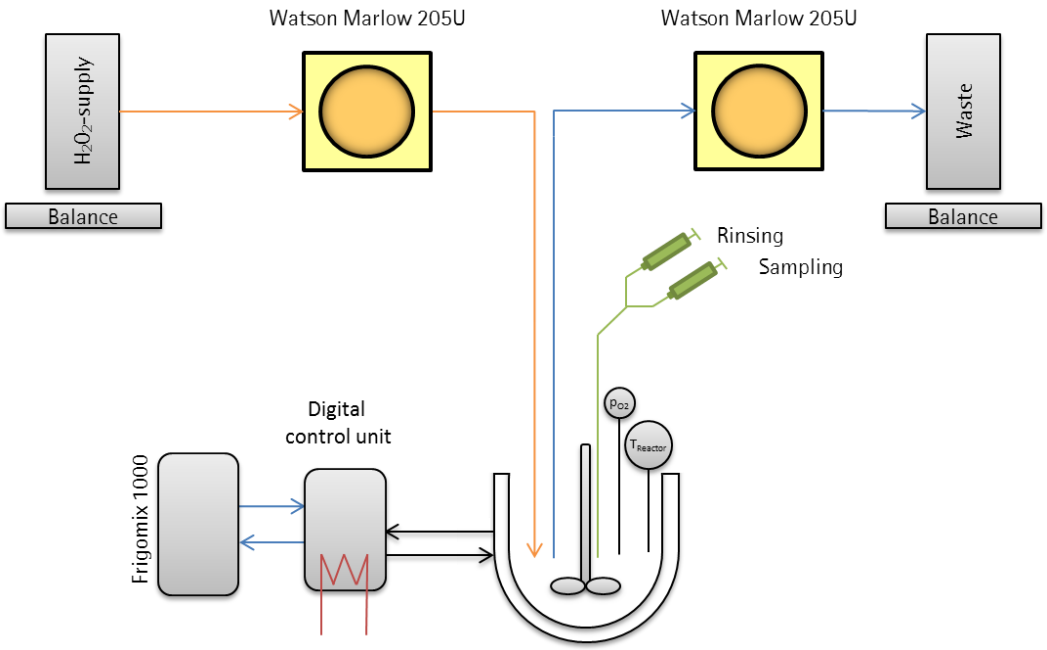

Figure 13: Experimental setup for the investigation of the mass transfer of oxygen supplied by the decomposition of H_2O_2 in the UniVessel® (5 L).

Then, the dilution rate was varied, to study the impact of different inflow rates on the dissolved oxygen concentration and their effect on the k_La. An example of the pO_2 profile is given in the appendix in Figure 57.

The k_La, calculated as an absolute value, due to the inverted oxygen transfer, is calculable by the following equation

$$|k_L a| = \left|\frac{OTR}{c_l^* - c_l}\right| \tag{49}$$

which can be substituted with the following equations (provided that an ideally mixed gas phase exists):

$$OTR = D \cdot c(H_2O_2)_i \cdot \frac{X}{100} \cdot \frac{1}{2} \tag{50}$$

$$c_l^* = c_{g,o} \cdot H^{cc} \tag{51}$$

$$c_{g,o} = \frac{c_{g,i} \cdot \dot{V}_{g,i} + OTR \cdot V}{\dot{V}_{g,o}} \tag{52}$$

$$\dot{V}_{g,o} = \dot{V}_{g,i} + OTR \cdot V \cdot \frac{R \cdot T}{p} \tag{53}$$

$$c_l = \frac{p_{O_2}}{100} \cdot c_s \tag{54}$$

Oxygen concentration in the gas phase at the reactor outlet	$c_{g,o}$	$\left[\frac{mole}{L}\right]$
Henry constant (dimensionless)	H^{cc}	$[-]$
Oxygen concentration in the gas phase at the reactor inlet	$c_{g,i}$	$\left[\frac{mole}{L}\right]$
Gas volume flow at the reactor inlet	$\dot{V}_{g,i}$	$\left[\frac{L}{s}\right]$

Gas volume flow at the reactor outlet	$\dot{V}_{g,o}$	$\left[\frac{L}{s}\right]$
Percentage dissolved oxygen saturation concentration in PBS medium	p_{O_2}	[%]
Oxygen saturation concentration in PBS medium	c_s	$\left[\frac{mole}{L}\right]$

An example calculation is given in the appendix (Table 15).

Finally, the k_La was determined by means of the gassing-out method (Meusel *et al.*, unpublished). At first, the dissolved oxygen was deaerated with nitrogen and subsequently aerated with air. Then, the k_La was calculable with the help of the differential algorithm (equation (29)).

4.8 Scanning electron microscope

For studies concerning the catalytic activity MnO_2 samples were analysed by a scanning electron microscope. The samples were sputtered with gold for 3 min (layer thickness 3-5 nm) and analysed with a scanning electron microscope (FEI Quanta 200F). The pictures were taken with an Everhart-Thornley-detector (secondary electron detector).

Chapter 5

Results and Discussion

5.1 Establishment of a H_2O_2 measuring method

The determination of the current hydrogen peroxide concentration is important for the calculation of the turnover in a continuous reactor. Therefore, an exact measurement of the consumption within the range of 0 to 99.5 % of the stock solution is needed, which corresponds to a concentration of 0.05 to 9.81 $\frac{mole}{L}$. The titrimetric approach, recommended in the literature (Vogel and Mendham, 2000; Dokuzovic, 2015), showed a very good correlation between the measured and the theoretical value. The highest average deviation from the expected concentration was -2.08 % at 2.45 $\frac{mole}{L}$. The standard deviation was never above 0.12 % and the coefficient of determination was 1.0 (Figure 14). Thus, these results show that the described method is valid for a quick and exact determination of the H_2O_2 concentration in the studied section.

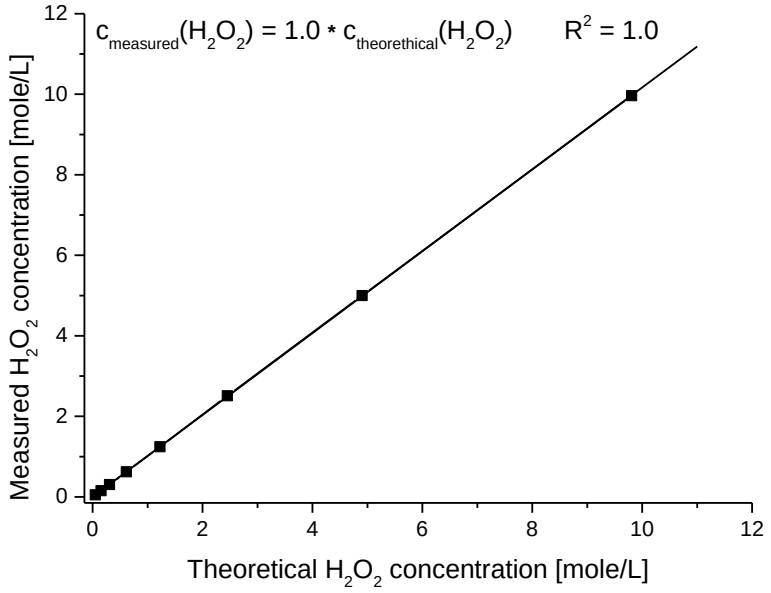

Figure 14: Illustration of the titrimetric measured H_2O_2 concentrations and their related theoretical values.

5.2 Establishment of an appropriate catalyst for the decomposition of H_2O_2

Since the degradation of H_2O_2 at standard conditions only takes place by the support of a catalyst, a suitable candidate had to be found. As already mentioned, the literature cites the enzyme catalase, the soluble iron nitrate ($Fe(NO_3)_3$) and the insoluble pyrolusite (MnO_2) as possible compounds (3.3.1). Research was carried out about their stability, their possible range of concentrations, safety issues and their reaction kinetics in a scale of 0.1 L. Knowledge about the latter is useful for the design of the procedure in a continuous mode. Since the literature declares the reaction as first-order (3.3.2), an accurate determination of the pseudo reaction rate k' is possible by batch experiments with different catalyst concentrations (equation (48)).

5.2.1 Catalase

The degradation of H_2O_2 by catalase (0.48 mg, >10,000 $\frac{units}{mg}$) followed as postulated a first order reaction kinetic (Reißmann, 2015) and led to a temperature increase of 13.8 K (Figure 15). However, the reduction from initially 1 $\frac{mole}{L}$ was not complete and stopped after 42 minutes at a turnover of 84 %. This might be explained by a decrease of

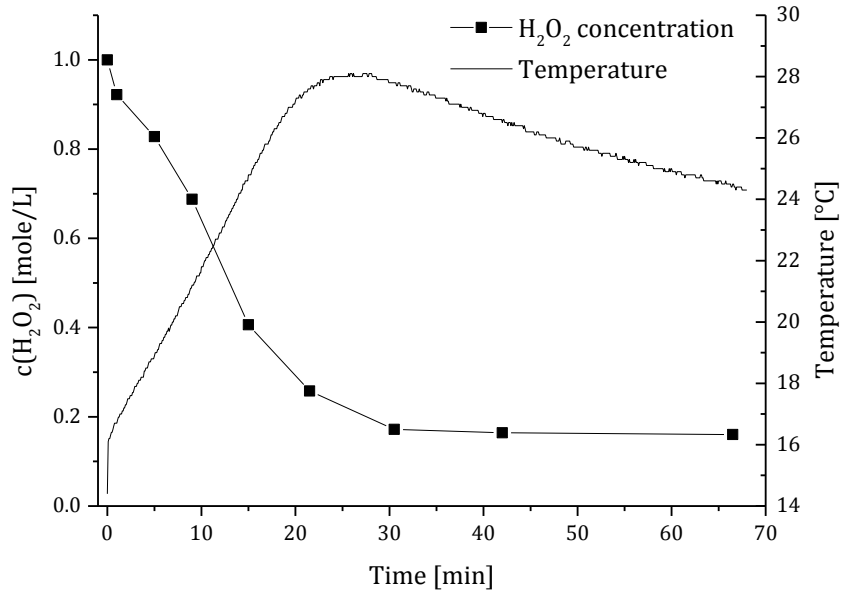

Figure 15: H_2O_2 concentration and temperature profile of the H_2O_2 decomposition by catalase (initial H_2O_2 concentration: 1 $\frac{mole}{L}$).

the enzymatic activity by a time- or turnover-dependent inactivation of the enzyme. For further investigations of this phenomenon, experiments with different initial H_2O_2 concentrations were executed. An increase of the concentration to 1.5 $\frac{mole}{L}$ engendered a consumption of 0.64 mole substrate in 50 minutes before the reaction stopped. After a feed of 0.48 mg fresh catalase (>10,000 $\frac{units}{mg}$) the degradation continued for 16.5 min and stopped again. During this interval 0.69 mole H_2O_2 was digested (Figure 16).

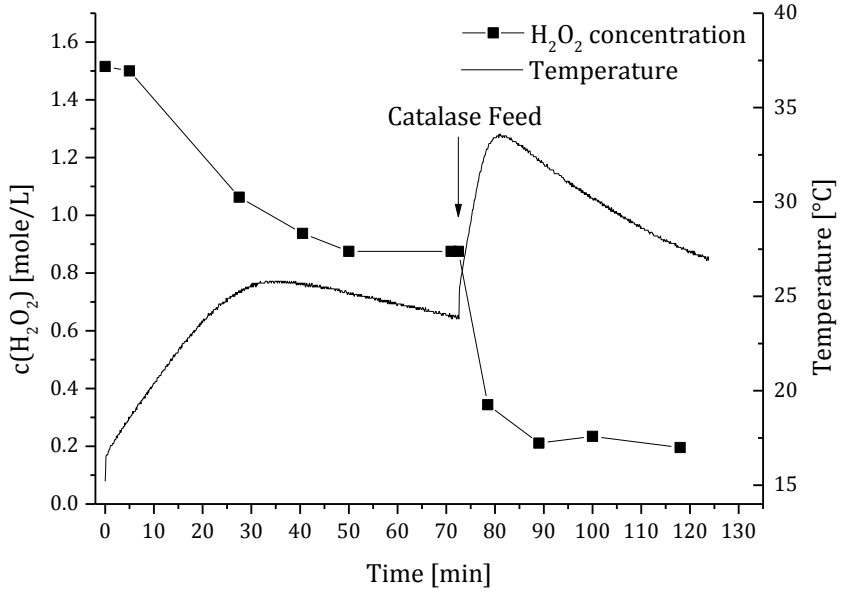

Figure 16: H_2O_2 concentration and temperature profile of the H_2O_2 decomposition by catalase (initial H_2O_2 concentration: 1.5 $\frac{mole}{L}$, Catalase Feed (4.8 $\frac{mg}{L}$) after 72 min).

The obtained temperature profile fit to the obtained hydrogen peroxide progression. During the first phase the temperature rose in 39 minutes by 11.1 K, while in the second phase an increase of 9.8 K in 8.5 minutes was observed. The timespan difference is explainable by the Arrhenius-equation:

$$k = B \cdot e^{\frac{-E_A}{R \cdot T}} \tag{55}$$

Pre-exponential factor	B	$\left[\frac{1}{h}\right]$
Activation energy	E_A	$\left[\frac{J}{mole}\right]$

Since the reaction rate constant depends on the temperature, it was much quicker after the catalase feed due to the increased temperature while the released heat stayed almost the same.

Furthermore, the effect of a decreased start concentration ($0.5\,\frac{mole}{L}$) was examined (Figure 17). After 9 minutes the entire initial hydrogen peroxide was dissipated and a feed of fresh H_2O_2 to $1.0\,\frac{mole}{L}$ led to a continuation of the reaction until it stopped again. 0.33 mole H_2O_2 was broken down. As before, the temperature curve showed a direct dependency to the turnover of the substrate.

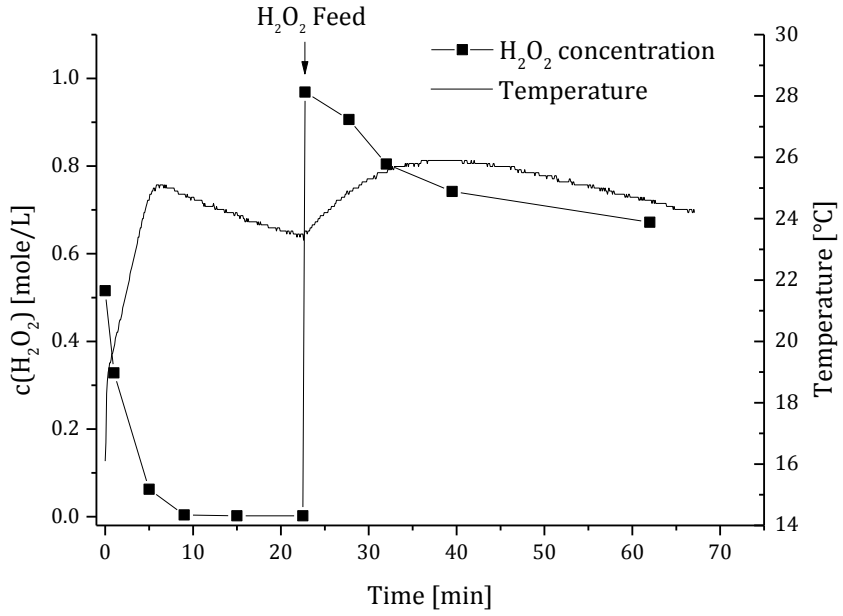

Figure 17: H_2O_2 concentration and temperature profile of the H_2O_2 decomposition by catalase (initial H_2O_2 concentration: $0.5\,\frac{mole}{L}$, H_2O_2 Feed ($1\,\frac{mole}{L}$) after 22.5 min).

The described results reinforced the assumption of dissipation and inactivation of catalase. In these batch experiments the enzyme transformed 0.17, 0.13, 0.14 or, respectively, 0.18 mole substrate per applied mg enzyme. Afterwards, it was unable to continue the degradation. A modelling of the time depended enzyme- and H_2O_2 diminution was performed for the experiment shown in Figure 15 with the following differential equation taken as a basis:

$$\frac{d\,c(H_2O_2)}{dt} = -k' \cdot c(Catalase_{active}) \cdot c(H_2O_2) \tag{56}$$

$$\frac{d\,(Catalase_{active})}{dt} = -k'' \cdot c(Catalase_{active}) \tag{57}$$

Concentration of active catalase	$c(Catalase_{active})$	$\left[\frac{mg}{L}\right]$
Inactivation rate	k''	$\left[\frac{1}{h}\right]$

Equation (56) represents the time dependent reduction of the H_2O_2 concentration, whereas equation (57) describes the inactivation of catalase. The Matlab (Mathworks) calculation (Figure 18) resulted in reaction rate velocities of $1.2\,\frac{L}{h \cdot mg}$ for k' and $3\,\frac{1}{h}$ for k'' (`ode45` solver, least square algorithm, source code in the appendix).[2]

Since 50 % of the incipiently catalase was inactivated after 15 minutes a high frequently feeding of fresh enzyme would be necessary. Furthermore, the exact inactivation kinetic was unknown. Therefore, this enzyme was not an appropriate catalyst for experiments in a continuous mode. Hence, other catalysts were tested on their potential.

[2] Since the catalase concentration is given in $\frac{mg}{L}$ the resulting pseudo reaction rate was given in $\frac{L}{h \cdot mg}$ instead of $\frac{L}{h \cdot mole}$.

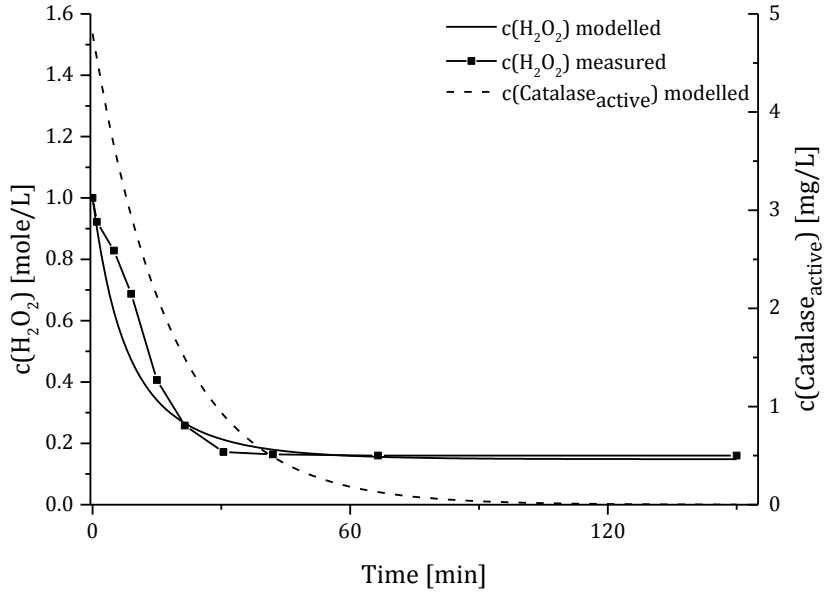

Figure 18: Illustration of the modelled H_2O_2 concentration and catalase profile of a batch experiment and comparison with the measured values.

5.2.2 Iron nitrate

5.2.2.1 Reaction kinetic

As described above, Fe^{3+} is another possible catalyst for the decomposition of H_2O_2 (3.3.1.2) and can be applied e.g. as $Fe(NO_3)_3$-salt. The catalysis can undergo a radical chain reaction or a three-step process, where the iron changes its oxidation number from +III to +IV and back (3.3.1.2). Independent from the mechanism, the iron (+III) forms in water a complex with six water molecules, which is, due to the high charge-size-ratio, able to emit a proton (Hancock, 2015). The resulting complex gives the solution an amber colour (Marzzacco, 2015):

$$\underset{\text{(colourless)}}{Fe(H_2O)_6{}^{3+}} \leftrightarrow \underset{\text{(amber)}}{Fe(H_2O)_5OH^{2+}} + H^+ \tag{58}$$

The literature is split over the need of acidification of the $Fe(NO_3)_3$ solution (Marzzacco, 2015; Brehm, 2015). Hence, the effect of 0.19 $\frac{\text{mole}}{\text{L}}$ HNO_3 on a 1.5 $\frac{g}{L}$ $Fe(NO_3)_3$ solution was

tested (Figure 19). These concentrations were recommended by Brehm. The curve progression showed a very slow decomposition for the acidified solution (0.4 % turnover after 14 min) while the pure $Fe(NO_3)_3$ solution depicted a 70-fold quicker reaction. The difference may be due to the chain breaking process by the interaction of two radicals, which is supported by protons and thus, at a low pH (Haber and Weiss, 1934). As described above, the pseudo reaction rate is exactly computable with equation (48) by batch experiments with different catalyst concentrations (5.2). Based on the obtained results, these studies were performed without HNO_3 (Figure 19).

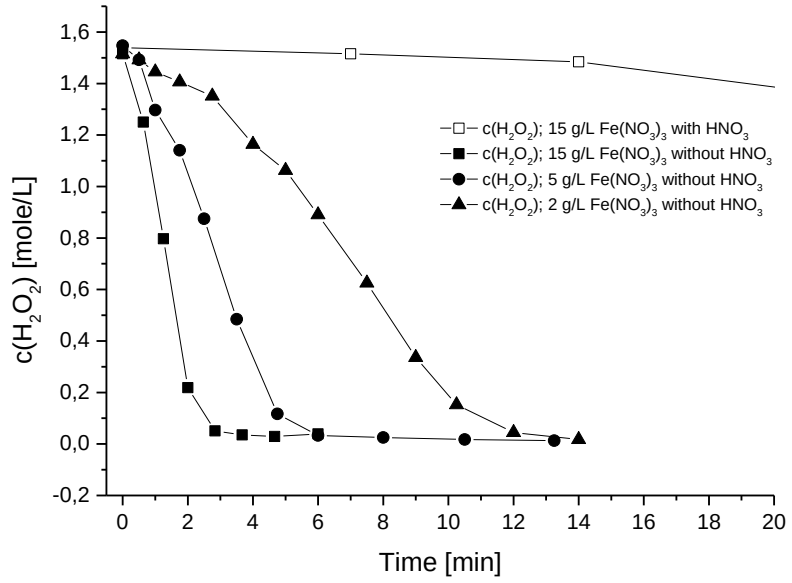

Figure 19: Profile of the H_2O_2 decomposition by $Fe(NO_3)_3$ with and without HNO_3.

5.2.2.2 Normalisation of the reaction rate

The reaction rate depends very strongly on the current temperature in the medium (equation (55)). Since the temperature rises during the experiment, the reaction rate changes as well. To approximately estimate the catalyst independent reaction rate k' for the design of the continuous procedure, the reaction rate velocities were standardized with a temperature correction.

For this standardisation, at first, the reaction rate k has to be defined.

$$k_{i,i+1} = ln\left(\frac{c(H_2O_2)_{i+1}}{c(H_2O_2)_i}\right) \cdot \frac{1}{t_{i+1} - t_i} \tag{59}$$

Average reaction rate for two adjacent measurement points	$k_{i,i+1}$	$\left[\frac{1}{h}\right]$
H_2O_2 concentration at the measurement point i+1	$c(H_2O_2)_{i+1}$	$\left[\frac{mole}{L}\right]$
H_2O_2 concentration at the measurement point i	$c(H_2O_2)_i$	$\left[\frac{mole}{L}\right]$
Time at the measurement point i + 1	t_{i+1}	$[h]$
Time at the measurement point i	t_i	$[h]$

The mean temperature is described by

$$\bar{T}_{i,i+1} = \frac{T_i + T_{i+1}}{2} \tag{60}$$

Average temperature for two adjacent measurement points	$\bar{T}_{i,i+1}$	$[K]$
Temperature at the measurement point i	T_i	$[K]$
Temperature at the measurement point i + 1	T_{i+1}	$[K]$

To obtain a comparable k-value all measured reaction rates have to be normed to 30 °C. This is possible, by calculating the increase of the reaction rate, which is only caused by the elevated temperature.

$$\frac{k(\bar{T}_{i,i+1})}{k(30\,°C)} = \frac{B \cdot e^{-\frac{E_A}{R \cdot \bar{T}_{i,i+1}}}}{B \cdot e^{-\frac{E_A}{R \cdot (30\,K + 273{,}15\,K)}}} = \bar{\kappa}_{i,i+1} \tag{61}$$

Standardisation factor	$\bar{\kappa}_{i,i+1}$	$[-]$
Reaction rate at 30 °C	$k(30\,°C)$	$\left[\frac{1}{h}\right]$
Reaction rate at the temperature $\overline{T}_{i,i+1}$	$k(\bar{T}_{i,i+1})$	$\left[\frac{1}{h}\right]$

Although the pre-exponential factor B is unknown, the equation is solvable, because it can be condensed to

$$\frac{k(\bar{T}_{i,i+1})}{k(30\,°C)} = \frac{e^{-\frac{E_A}{R \cdot \bar{T}_{i,i+1}}}}{e^{-\frac{E_A}{R \cdot (30\,K + 273{,}15\,K)}}} = \bar{\kappa}_{i,i+1} \tag{62}$$

Division of the measured reaction rate by the standardisation factor leads to the standardised reaction rate.

$$\frac{k(\bar{T}_{i,i+1})}{\bar{\kappa}_{1,i+1}} = k_{i,i+1}(30\,°C) \tag{63}$$

Standardised reaction rate	$k_{i,i+1}(30\,°C)$	$\left[\frac{1}{h}\right]$

Since, for each pair of measurement points a reaction rate was determined, every obtained and standardised reaction rate has to be rated time-dependently.

$$\frac{1}{t_0 - t_{end}} \cdot \sum_{i=1}^{n} (t_{i+1} - t_i) \cdot k_{i,i+1}(30\,°C) = k_{corrected} \tag{64}$$

Corrected reaction rate	$k_{corrected}$	$\left[\frac{1}{h}\right]$
Time at the end of the measurement	t_{end}	$[h]$
Time at the beginning of the measurement	t_0	$[h]$

An example calculation is given in the appendix in Table 12 and Table 13.

The standardised results were plotted against the corresponding catalyst concentration (Figure 20). Based on equation (48), the slope of the resulting linear equation ($5.1\,\frac{L}{h \cdot g}$) describes the pseudo reaction rate k'. A clear proof was given for the postulated kinetic (equation (37) and (38)). Therefore, a dimensioning of continuous modes was possible with $Fe(NO_3)_3$.

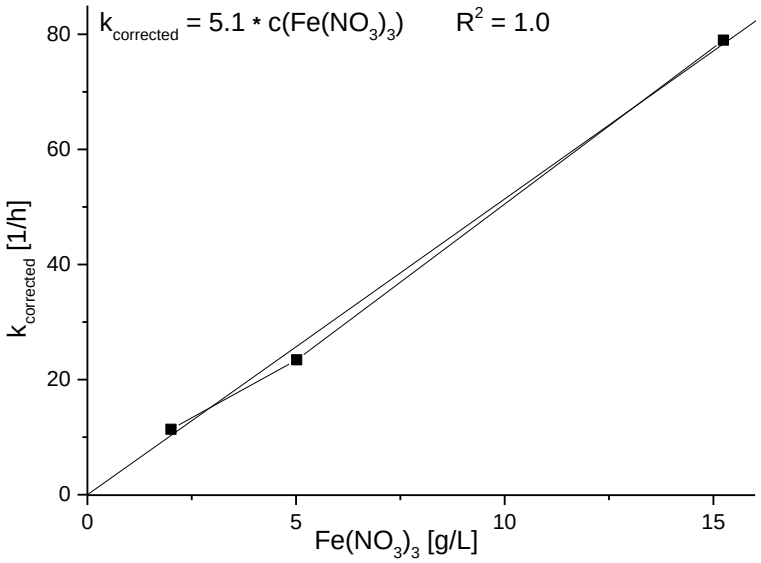

Figure 20: Determination of k' by comparison of several $Fe(NO_3)_3$ concentrations and their related reaction rates.

5.2.2.3 pH-dependency of iron nitrate

However, Fe^{3+} is very acidic, due to its large size, high charge and its electronegativity, which influence the acidity of a metal ion strongly (Table 3). A $Fe(NO_3)_3$ solution with a concentration of $5\ \frac{g}{L}$ has a pH of 2.3 without addition of HNO_3. Due to safety reasons and material issues this was not acceptable. Investigations were carried out, to shift the pH to the neutral section without reducing its catalytic activity.

An increase of the pH to 7 with NaOH was not possible because the iron (+III) reacted with the hydroxide ions to an insoluble compound (solubility product: $2.79 \cdot 10^{-39}\ \frac{mole^4}{L^4}$ (Lide, 1998) before the solution reached a pH of 3 (Figure 21) (Holleman *et al.*, 2007).

$$3\ NaOH\ (aq) + Fe(NO_3)_3\ (aq) \rightarrow\ 3\ NaNO_3(aq) + Fe(OH)_3\ (s) \downarrow$$

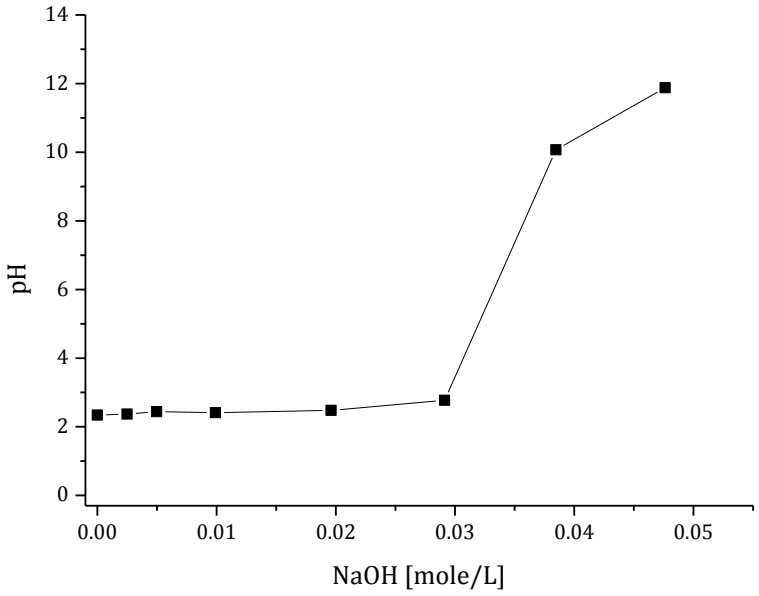

Figure 21: Influence of NaOH on the pH of a $Fe(NO_3)_3$ solution ($5\ \frac{g}{L}$).

Table 3: Dependency of the ionic radius and the charge of metal ions on their pK_a (Hancock, 2015).

	Be^{2+}	Mg^{2+}	Ca^{2+}	Sr^{2+}	Ba^{2+}
Ionic radius (Å)	0.27	0.74	1.00	1.18	1.36
pK_a	5.6	11.4	12.7	13.2	13.4

	Na^{+}	Ca^{2+}	La^{3+}	Th^{4+}
Ionic radius (Å)	1.02	1.00	1.03	0.94
pK_a	14.1	12.7	8.5	3.2

During the titration a colour change from a slight yellow to red-brown was visible (Figure 22). This shift is explainable by the change of the chemical formula due to the increased pH (Table 4).

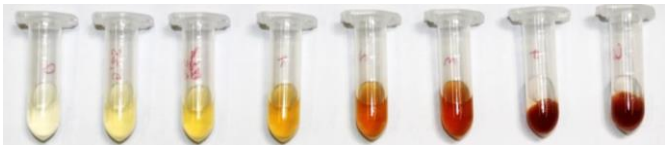

Figure 22: Photographic illustration of the influence of NaOH on the pH of a $Fe(NO_3)_3$ solution ($5\ \frac{g}{L}$). From left to right: 0, 2.5, 5.0, 9.9, 19.6, 29.1, 38.5, 47.6 $\frac{mmole}{L}$ NaOH.

Table 4: Influence of the pH on the chemical formula and other properties of Fe^{3+} (Holleman *et al.*, 2007; Hancock, 2015; Holdt, 2015)

pH	Chemical formula	Colour
<0	$[Fe(H_2O)_6)^{3+}]$	Colourless / pale lilac
0 – 2	$[Fe(OH)(H_2O)_5)^{2+}]$ and $[Fe(OH)_2(H_2O)_4)^{+}]$	Yellow-brown
2 - 3	$[(H_2O)_4Fe(\mu\text{-}OH)_2Fe(H_2O)_4]^{4+}$ and $[(H_2O)_5Fe\text{-}O\text{-}Fe(H_2O)_5]^{4+}$	Yellow-brown
3 - 5	Multiple-core Isopolyoxo-Cations	Yellow-brown
> 5	$FeOH_3$	Red-brown

To circumvent the formation of $Fe(OH)_3$ during the pH increases, the use of NH_3 instead of NaOH is not an option. Compared to Fe^{2+}, where $[Fe(NH_3)_6]^{2+}$ emerges, no $[Fe(NH_3)_6]^{3+}$ and only $Fe(OH)_3$ is formed. The reason for this is the low affinity of Fe^{3+} to

ammonia. However, EDTA (Ethylenediaminetetraacetic acid) is a potential chelating agent for Fe^{3+}. As a sixtoothed-ligand it is able to form $[Fe(EDTA)(H_2O)]^-$ (Ferric coordination number: 7 (similar to haemoglobin)) (Holleman *et al.*, 2007).

A titration of NaOH to an EDTA-$Fe(NO_3)_3$-solution ($5\,\frac{g}{L}$ $Fe(NO_3)_3$, $46\,\frac{g}{L}$ EDTA) showed the typical pH-progress of a multiple-protonic acid with several plateaus (probably due to the EDTA) (Figure 23). Compared to the $Fe(NO_3)_3$-solution without EDTA, only a slow pH increase was detected. Furthermore, precipitations were firstly perceived at a pH of 8.37 (Figure 24). Therefore, an adjustment of pH 7 was possible.

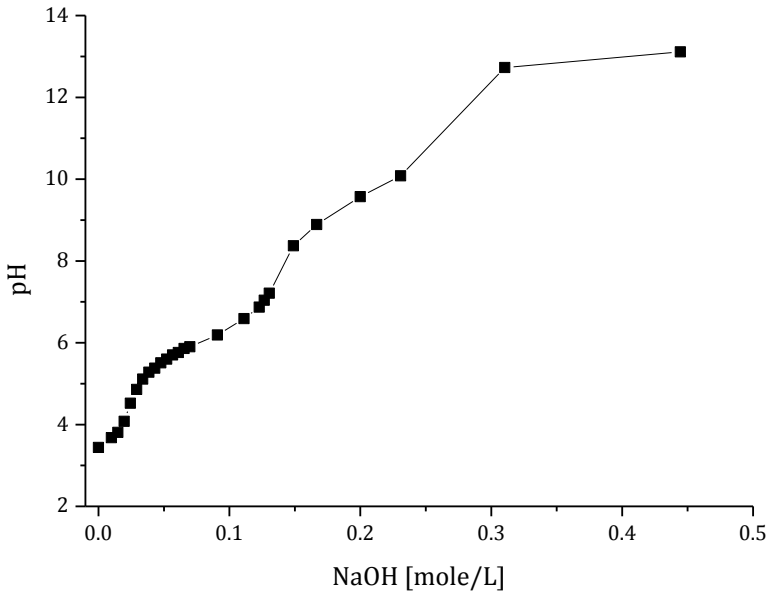

Figure 23: Influence of NaOH on the pH of an EDTA-$Fe(NO_3)_3$ solution.

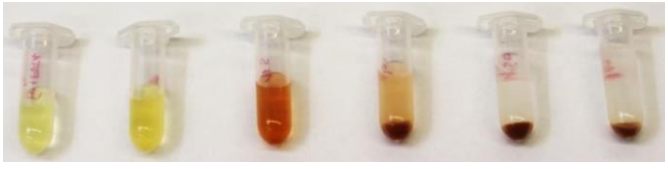

Figure 24: Photographic illustration of the influence of NaOH on the pH of an EDTA-$Fe(NO_3)_3$ solution. From left to right: 0, 65, 149, 231, 310 and 444 $\frac{mmole}{L}$ NaOH.

However, the concentration of EDTA might be too high and hence, influence the catalytic activity. Thus, experiments with a decreased amount of EDTA were performed (Figure 25). However, smaller concentrations of EDTA than the initially one ($46\,\frac{g}{L}$ EDTA) led to an increased pH and precipitations (Figure 26).

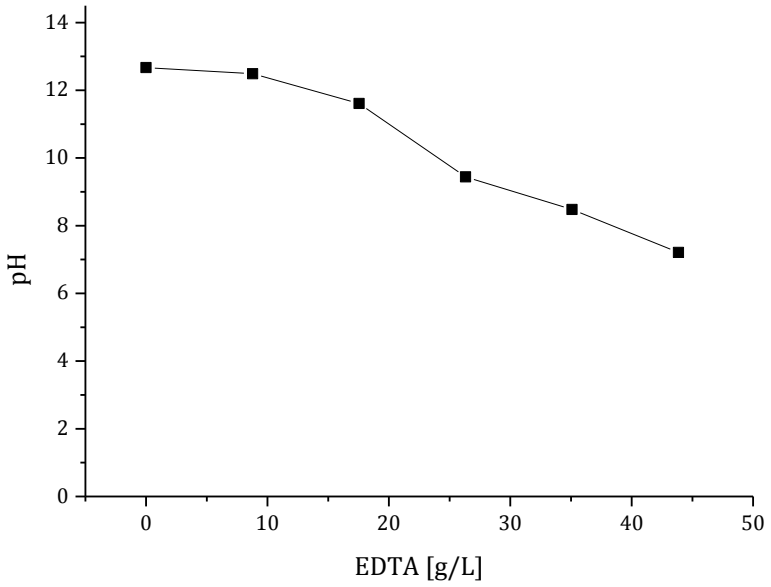

Figure 25: Illustration of the influence of EDTA on the pH of a $Fe(NO_3)_3$ solution ($5\,\frac{g}{L}$) with $123\,\frac{mmol}{L}$ NaOH.

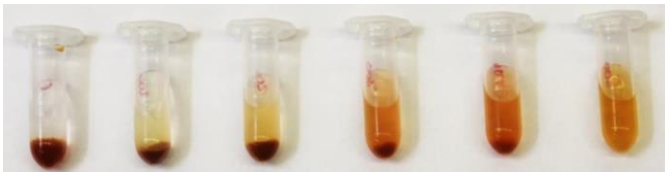

Figure 26: Photographical illustration of the influence of EDTA on the pH of a $Fe(NO_3)_3$ solution ($5\,\frac{g}{L}$). From left to right: 0, 8.8, 17.5, 26.3, 35.1 and $43.9\,\frac{g}{L}$ EDTA with $123\,\frac{mmol}{L}$ NaOH.

However, the incipiently problem of a too low pH was solved with an EDTA concentration of $46\,\frac{g}{L}$ for a $5\,\frac{g}{L}$ $Fe(NO_3)_3$ solution. Next, the decomposition activity of $[Fe(EDTA)(H_2O)]^-$ was investigated. A 0.1 L batch experiment resulted in a decrease of the initial H_2O_2 concentration (Figure 27). Therefore, $[Fe(EDTA)(H_2O)]^-$ was still able to

decompose hydrogen peroxide. The pH ranged from 7.2 in the beginning to 7.6 in the end and was thus, in the required scope. However, the reaction was slower (compared to the obtained results with $5\,\frac{g}{L}$ $Fe(NO_3)_3$ and without EDTA) and the catalyst seemed to be inactivated by time, because the temperature profile showed no further heat production and according to this, no further decomposition. Merely $0.72\,\frac{mole}{L}$ was converted to H_2O and O_2 after 80 minutes, which comply with 48 % of the initial value. In addition to that, the exact reaction kinetic for these settings was still unclear.

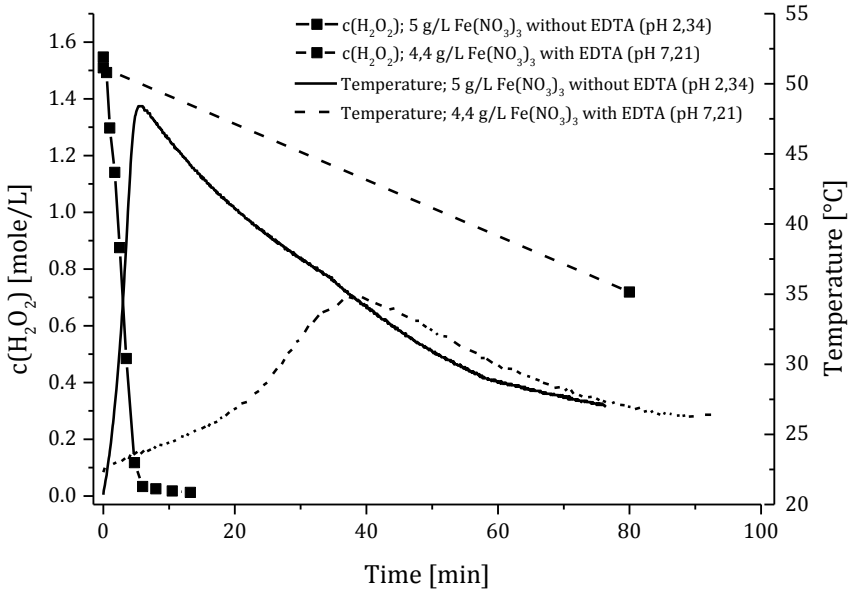

Figure 27: Comparison of the temperature profile and the H_2O_2 concentration of a $Fe(NO_3)_3$-solution with and without EDTA in a scale of 0.1 L processed in batch mode.

5.2.3 Manganese-(IV)-oxide

5.2.3.1 Reaction kinetic

Due to the quick inactivation of catalase and the safety issues of $Fe(NO_3)_3$ manganese dioxide was studied for its potential concerning a steady and safe decomposition of H_2O_2. Just as the other catalysts, the breakdown by MnO_2 depicted a first order kinetic (Figure 28), which is also referred in the literature (Akhtar *et al.*, 2012). As distinguished from catalase, the reaction led to a complete decline of H_2O_2 and thus, showed no time depended inhibition or inactivation in the range of 5.4 $\frac{g\ MnO_2}{mole\ H_2O_2}$ (Figure 29) to 0.1 $\frac{g\ MnO_2}{mole\ H_2O_2}$ (Figure 30). The latter did not display an entire turnover during a measuring time of 20.6 hours due to the smaller amount of MnO_2, but followed as well a first order kinetic. The low reaction rate is explainable as well by the temperature profile of the liquid. It only depicted an increase of 2.7 K. During the night, the solution cooled down (3.8 K under the initial temperature), which further decreased the reaction rate.

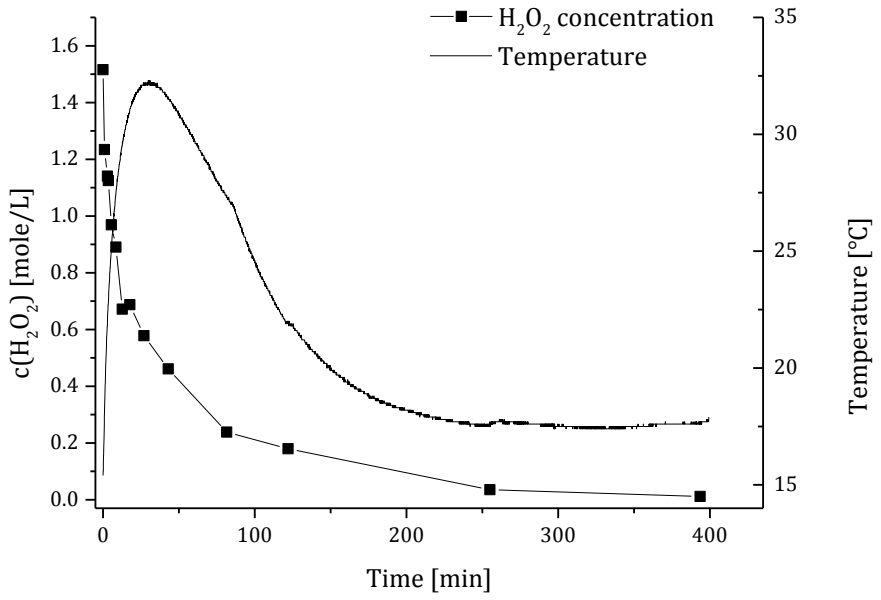

Figure 28: H_2O_2 concentration and temperature profile of the H_2O_2 decomposition by MnO_2 (0.86 $\frac{g\ MnO_2}{L}$, 0.6 $\frac{g\ MnO_2}{mole\ H_2O_2}$).

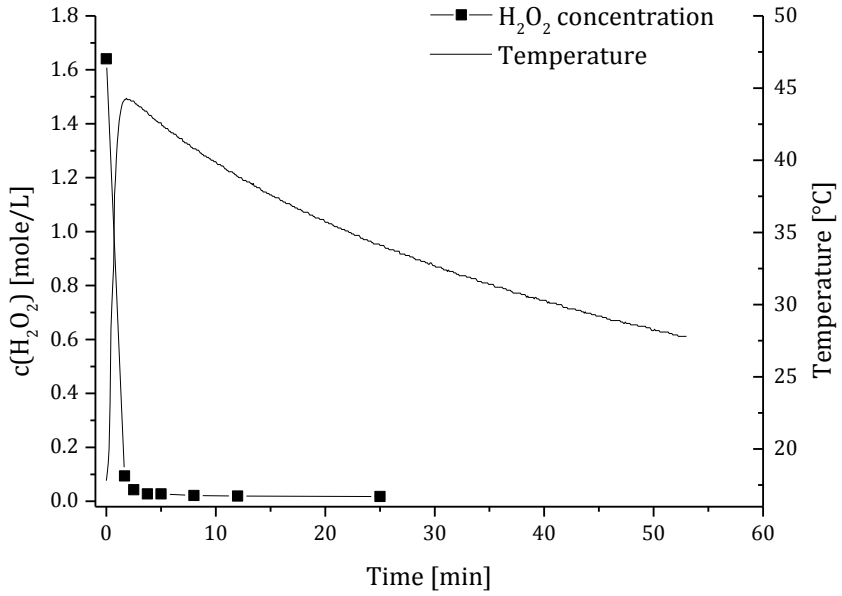

Figure 29: H_2O_2 concentration and temperature profile of the H_2O_2 decomposition by MnO_2 (8.08 $\frac{g\ MnO_2}{L}$, 5.4 $\frac{g\ MnO_2}{mole\ H_2O_2}$).

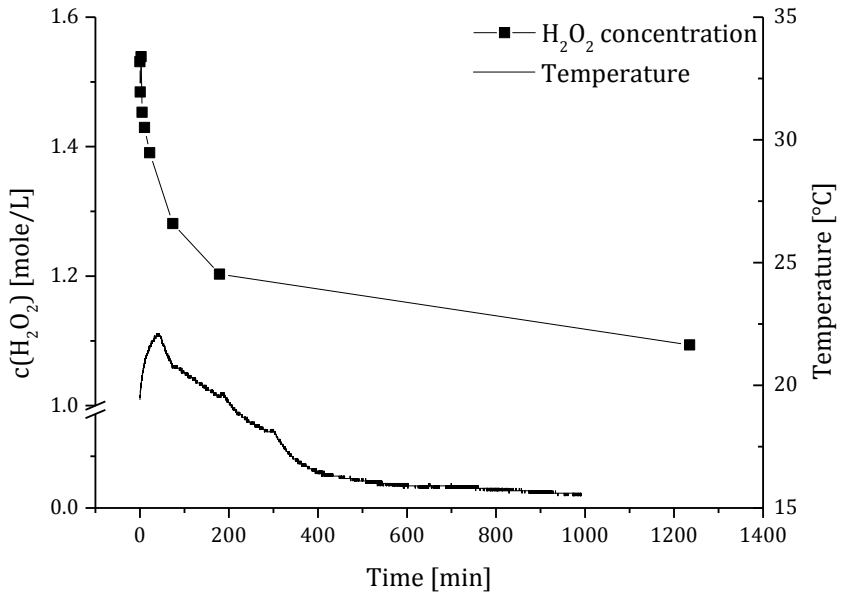

Figure 30: H_2O_2 concentration and temperature profile of the H_2O_2 decomposition by MnO_2 (0.10 $\frac{g\ MnO_2}{L}$, 0.1 $\frac{g\ MnO_2}{mole\ H_2O_2}$).

Nevertheless, an inactivation, similar (but slower) to the one observed with catalase, should be kept in mind. Martin mentioned a deactivation but did not describe this further (Martin, 1996). In this case, it was difficult to give evidence for that, due to the temperature curve and the related changing reaction rate.

Similar to $Fe(NO_3)_3$, the resulted decomposition profiles were normalised. However, this standardisation gives only a rough estimation, because the activation energy (E_A) is needed. The literature is unclear about E_A for the MnO_2 catalysed reaction and states two different values (58 and 82 $\frac{kJ}{mole}$). Hence, an average activation energy of 70 $\frac{kJ}{mole}$ was assumed. Nevertheless, this should refine the measured results and be sufficient for a first dimensioning.

The corrected reaction rates were plotted against their corresponding catalyst concentration and a linear regression was made (Figure 31). The slope of the straight line represents the pseudo reaction rate k'. In this case it was 1.4 $\frac{L}{h \cdot g}$.

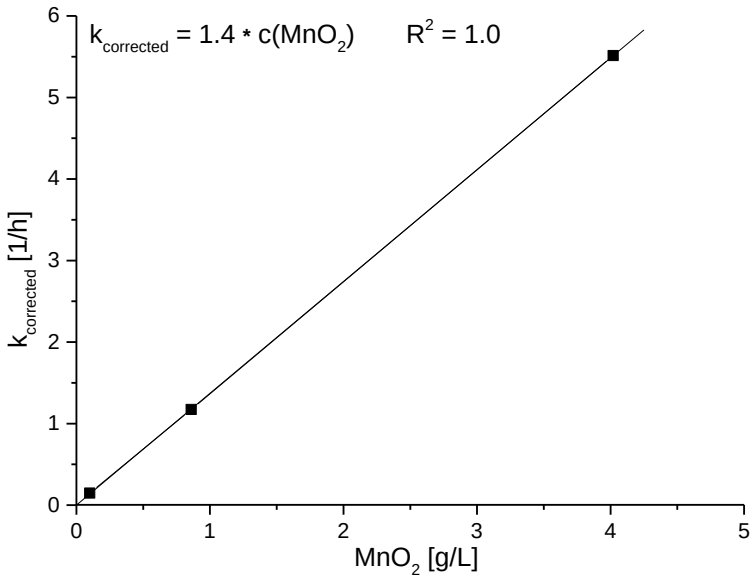

Figure 31: Determination of k' by comparison of several MnO_2 concentrations and their related reaction rates.

However, the data from 8.08 $\frac{g}{L}$ MnO_2 showed a high deviation compared to the other measurements (k' = 5.9 $\frac{L}{h \cdot g}$). A possible explanation for this phenomenon is the very short time of the reaction (the substrate was decomposed in less than 1.7 min). Therefore, less measuring points were possible during this time span. Furthermore, the sampling was difficult due to strong foam formation, not only in the beaker but also in the pipette tip. According to that, precise pipetting was not possible. However, the results of the other measurements showed a strong linear relationship, which allowed a first assessment of a continuous reactor, by which a constant heat production is possible.

5.2.3.2 Disposal strategy

Since MnO_2 cannot be just disposed to the sewage due to environmental regulations, a strategy of waste management was established. Reducing the amount of waste is possible by filtration of the insoluble solid material. The choice of the utilised membrane depends on the size of the MnO_2 particles. Therefore, a light microscopically investigation was executed. It revealed that the majority of the particles were bigger than 30 µm (Figure 32), wherefore a membrane with a pore wideness of 0.2 µm is capable to hold them back.

With a single-use Büchner funnel (180C6, 0.22 µm PES membrane, Sartorius) plugged to a vacuum pump, a complete separation of the MnO_2 was possible (Figure 53, appendix). Furthermore, a multi-use Büchner funnel with a Microsart polyethersulfone-(PESU)-membrane (0.2 µm) was checked for its potential (Figure 54, appendix). Exactly like the single-use solution, the manganese oxide was separated completely. The results of a scanning electron microscopically analysis supported the assumption, that the pore wideness of the PESU-membrane was narrow enough, to hold the MnO_2 particles back (Figure 33).

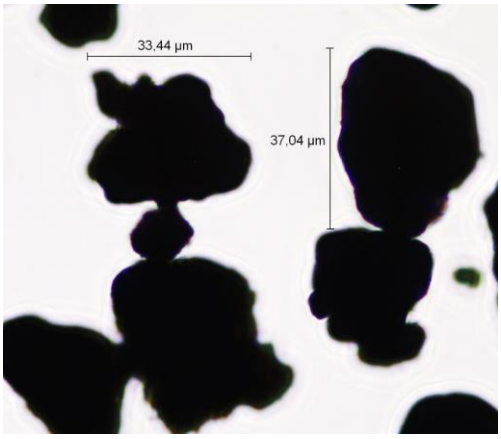

Figure 32: Light microscope picture of MnO_2 (400-fold-optical enlargement).

Since the filter area of the multi-use device was smaller compared to the single-use one, the possible amount of separated MnO_2 was less. On the other side, the costs of the membrane for the multi-use Büchner funnel were estimated as much lower than the costs for the single-use device.

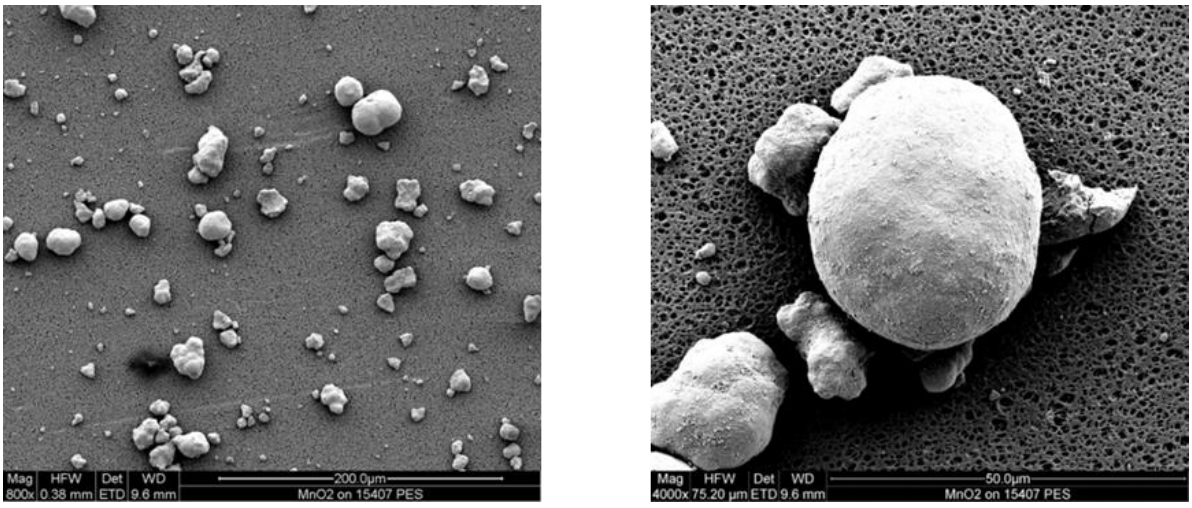

Figure 33: Electron-scan microscope picture of MnO_2 on a Microsart PESU-membrane (0.2 µm).

However, both disposal strategies are only suitable for relatively small volumes and volume flows of the MnO_2 suspension and a constant refilling of the Büchner funnel is necessary. In addition, it is not possible to prevent fine dust formation from the dried filter cake. Hence, another solution had to be found to realise higher flows with easier handling and without safety issues. On this account, a filtration capsule (Sartopore 2

(0.45 + 0.2 µm), PESU-membrane) in combination with a pump (Watson Marlow 520) was tested and found to be appropriate (Figure 55, appendix). No residues were found in the filtrate just like in the experiments made before. Additionally, in contrast to them, a sealing of the tubes before and after the filtration capsule (e.g. with the BioSealer (Sartorius)) was possible, which implies a safe locking from the ambient air. As mentioned before, this is important, because a whirl up should be prevented due to fine dust formation and would not be possible for the filter in the Büchner funnel. For the sealing, a special tubing material was added (C-flex), which is not pumpable.

5.2.4 Conclusion

Three different catalysts were studied for their potential of decomposing H_2O_2 in a continuous reactor. Catalase, an enzyme found e.g. in the liver, was excluded, due to its quick inactivation. In contrast to that, $Fe(NO_3)_3$ showed no change in the reaction rate. However, it was found as inappropriate, due to its low pH. A complexation with EDTA and a subsequent increase of the pH by NaOH led to a strong decrease of the reaction rate.

The third studied catalyst was MnO_2. Similar to iron nitrate the reaction rate did not decrease over time in the batch experiments. Since it was investigated in PBS-buffer, the pH was in a neutral range. A possible problem can be the washing out effect of the catalyst in a continuous reactor. A permanent addition of MnO_2 is not practicable, since it is not dissolved and quickly sediments. In Table 5 the pros and cons of the studied catalysts are summarized. On these grounds the continuous experiments were performed with MnO_2.

Table 5: Advantages and disadvantages of possible catalysts for the digestion of H_2O_2.

Catalyst	pH	Kinetic	Inactivation detected in batch mode	Type of catalysis	Miscellaneous
Catalase	7	Unknown	Yes	Biological	Expensive
$Fe(NO_3)_3$	~ 2	Known	No	Homogenous	/
EDTA-$Fe(NO_3)_3$	~ 7	Unknown	No	Homogenous	Very slow reaction
MnO_2	7.4	Known	No	Heterogeneous	Fine dust formation

5.3 Establishment of a continuous heat and oxygen production method

5.3.1 Studies concerning the steady state regarding temperature and quantity of substance

One of the major advantages of a continuous procedure is the simplified calculation of the specific heat transfer coefficient (UA), the volumetric mass transfer coefficient (k_La) and different kinetic parameters like the reaction rate during the stationary phase. This phase is defined by no time-depended change, neither of the temperature, nor the concentration. In case of a varying volume (e.g. due to vaporizing or a decreased outflow out of the system caused by sucking of bubbles formed in the medium) instead of the concentration, the amount of substance has to be taken into account and will not vary.

During the steady state, a stable turnover lower than 100 percent is needed, because the calculation of kinetic parameters like the activation energy (E_A), the pre-exponential factor (B) and the catalyst-independent pseudo reaction rate (k') are based on experiments with various turnovers. If the difference between them is too small, big mistakes will occur and the results would be inaccurate.

Since MnO_2 was shown to be an appropriate catalyst due to stability and disposal, a continuous process was established with this compound, to enable a constant heat and oxygen release for the determination of UA and k_La. Since only two relatively different references for E_A were found in the literature (5.2.3), the already calculated reaction rate (k') should be verified, because an inaccuracy might falsify k' relatively strong (equation (55)).

The first experiment in a scale of 0.1 L depicted an initial slope of H_2O_2, which seemed to tend towards the steady state concentration. However, after 80 minutes the slope of H_2O_2 reached its minimum and the amount of hydrogen peroxide ran through (Figure 34), whereas the temperature reached a maximum of 32.1 °C. Therefore, the stationary phase was not achieved. The observed behaviour might be explained by the long span, which increased more and more the washing out effect of the catalyst. In reference to the theoretically calculated and illustrated MnO_2 concentration, it became apparent, that the catalyst concentration already reduced from 0.50 $\frac{g}{L}$ to 0.42 $\frac{g}{L}$. Probably due to the time-depended increase of this effect or a possible inactivation, it was not possible, to reach a stationary phase.

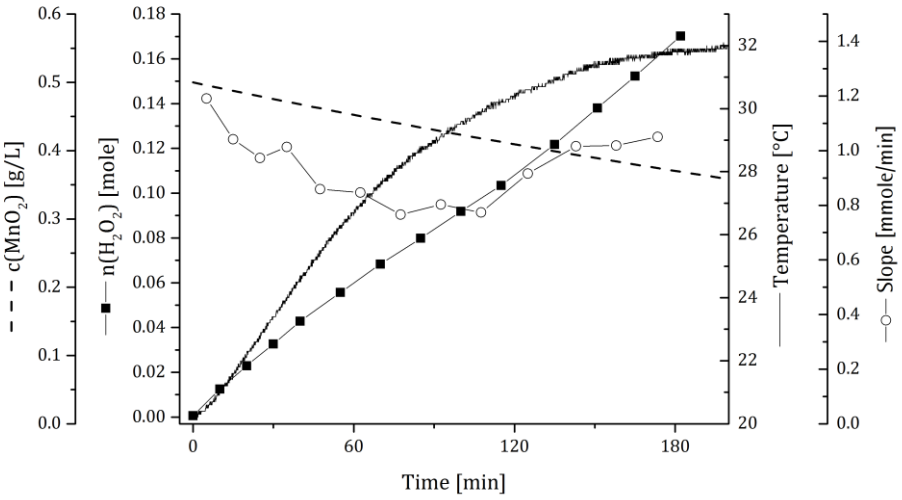

Figure 34: Temporal course of the temperature and the amount of substance of H_2O_2 in a scale of 0.1 L processed in continuous mode (MnO_2 start concentration: 0.50 $\frac{g}{L}$, dilution rate: 0.1 $\frac{1}{h}$).

To shorten the long transient oscillation, the initial amount of H_2O_2 was increased to reach the saturation condition quicker (Figure 35). However, the great amount of

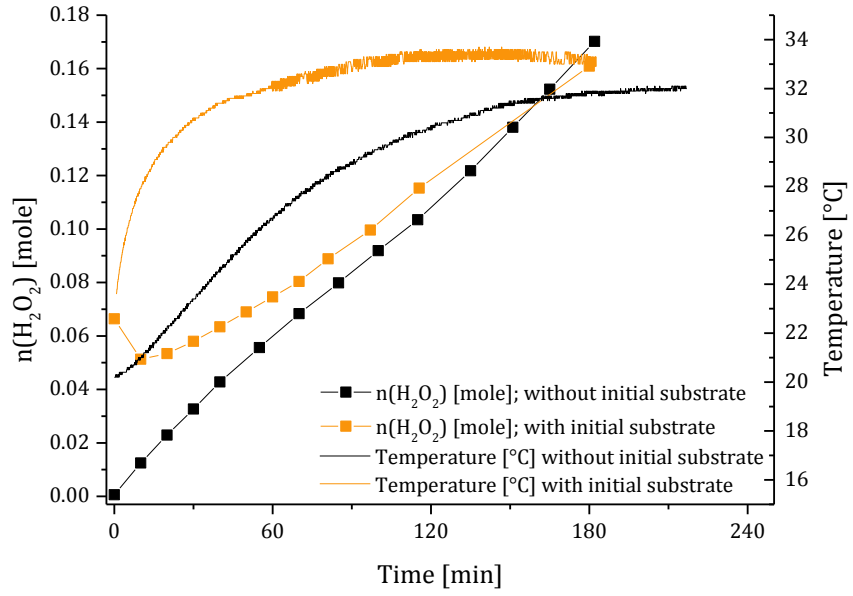

Figure 35: Illustration of the influence of an initial H_2O_2 concentration on the temporal course of the temperature and the amount of substance of H_2O_2 in a scale of 0.1 L processed in continuous mode (MnO_2 start concentration: 0.50 $\frac{g}{L}$, dilution rate: 0.1 $\frac{1}{h}$).

hydrogen peroxide led to a higher reaction velocity and, as a consequent to a higher heat release, which in turn supported the combustion. The progression converged with the results sighted before.

Due to the fact, that increased dilution rates led to a quicker increase of the amount of substance (Figure 36), a process cascade with a higher initial dilution rate ($0.8\,\frac{1}{h}$ (0 - 12.5 min) and $0.1\,\frac{1}{h}$ (12.5 - 182 min)) was performed (Figure 37). The desired quantity of substance was achieved in the beginning by this method; however, the catalyst was probably washed out in the same way. Therefore, the process was shortened but the stationary phase was not reached again.

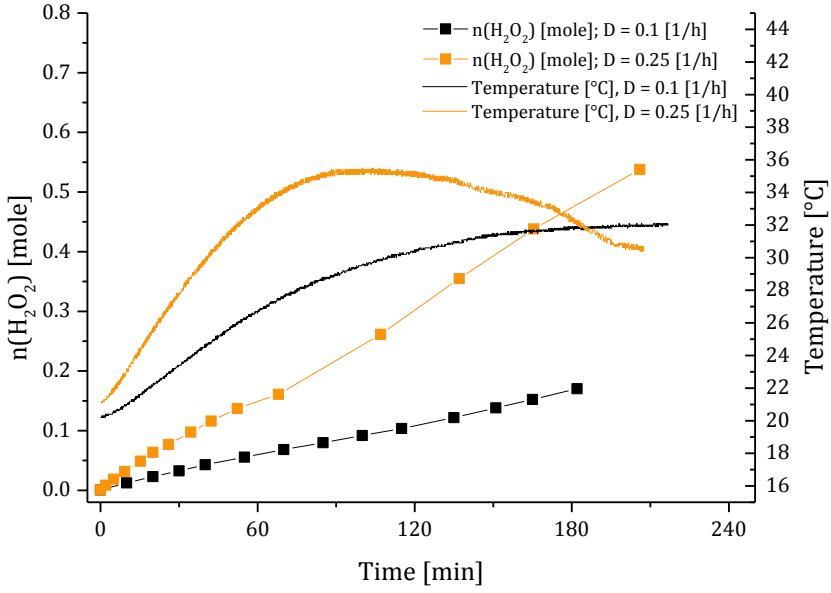

Figure 36: Illustration of the influence of different dilution rates ($0.1\,\frac{1}{h}$ and $0.25\,\frac{1}{h}$) on the temporal course of the temperature and the amount of substance of H_2O_2 in a scale of 0.1 L processed in continuous mode (MnO_2 start concentration: $0.50\,\frac{g}{L}$).

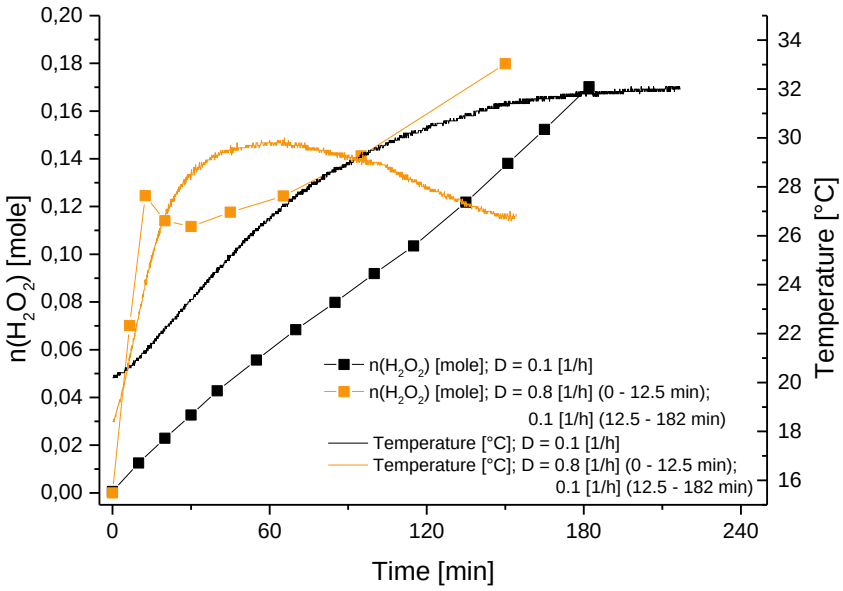

Figure 37: Illustration of the influence of a dilution rate profile on the temporal course of the temperature and the amount of substance of H_2O_2 in a scale of 0.1 L processed in continuous mode.

The theoretical coherence of the catalyst concentration and the turnover was plotted in Figure 38 according to equation (43). This correlation made clear, that over a wide range (> $1\,\frac{g}{L}$) a decrease of the concentration has no impact and thus, the washing out should not affect the turnover and the amount of substance in the stationary stage. Below this threshold of $1\,\frac{g}{L}$, a slight decrease leads to a large decline. Nevertheless, it would not be reasonable to use too high amounts of MnO_2, due to the effort for the disposal. Furthermore, larger quantities of H_2O_2 would be associated for a high, but not complete turnover. This would demand high dilution rates and beside that, it would increase the washing out effect again.

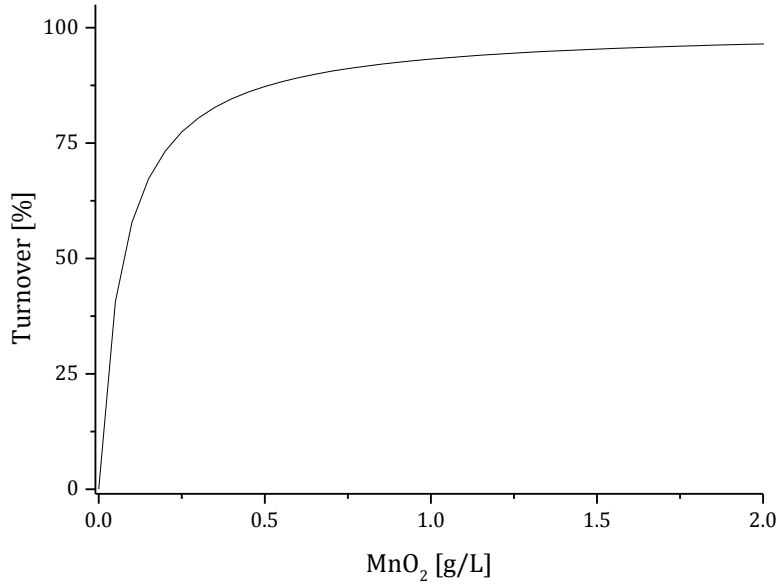

Figure 38: Theoretical coherence of the MnO_2 concentration and the linked turnover (D = 0.1 $\frac{1}{h}$, k' = 1.4 $\frac{L}{h \cdot g}$).

Based on this, higher catalyst concentrations (0.86, 1.50 and 4.00 $\frac{g}{L}$) were examined to study this relationship (Figure 39). With these settings, a stationary phase was

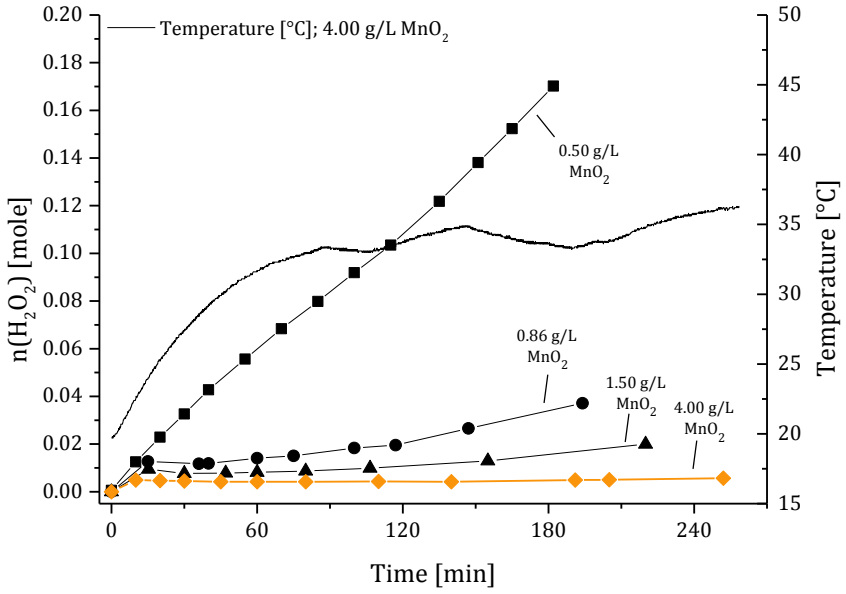

Figure 39: Illustration of the influence of different MnO_2 concentrations on the temporal course of the temperature and the amount of substance of H_2O_2 in a scale of 0.1 L processed in continuous mode (D = 0.1 $\frac{1}{h}$).

observed for 4.00 $\frac{g}{L}$ MnO_2 (labelled orange). Merely the temperature profile showed its maximum shifted (after 250 min) and besides oscillated. The reason for this shifting was the required time for the medium to heat up, and can be solved by a temperature regulation. Since this was not possible in the utilised 250 mL beaker, a process transfer to the UniVessel® (2 L) with a heating jacket was performed.

Furthermore the MnO_2 rinsing needs to be prevented, because the decreasing of the catalyst concentration over time results in a constantly changing steady state concentration. Wirges solved the problem with a continuous addition of the catalyst (Wirges, 1977). Since he used the soluble $Fe(NO_3)_3$, instead of the insoluble MnO_2, he balanced this rinsing effect. For a MnO_2 suspension this runs into difficulties, because the particles sediment quickly. Therefore, an evenly feeding is not possible. A feasible solution is a filtration probe at the medium outlet instead of a common tube. As mentioned before (5.2.3.2) a 0.2 µm membrane withheld the MnO_2 particles reliably.

5.3.2 Prevention of the washing-out effect

To stop the steady rinsing of MnO_2 from the reactor, a filtration probe was manufactured out of a Microsart PESU-Membrane (0.2 µm), a seal ring and a plastic case (Figure 40). The probe was plugged to the outlet tubing, fixed at the sleeve of the temperature probe and directed towards the stirrer to prevent the forming of a filter cake and therefore, the clogging of the filter.

Figure 40: Filtration probe with a Microsart PESU-membrane

To test the device for its potential a MnO_2 suspension ($4.00\,\frac{g}{L}$) was filled into the 2 litre vessel. The reactor was operated like before in the continuous experiments, merely no H_2O_2 was added and the dilution rate was set to $0.3\,\frac{1}{h}$ to make sure that no blocking of the filter occurs for higher mass flows. Since the filtrate was clear, the test showed that no MnO_2 passed the membrane. On top of this, the flow rate only deviated about 1 % during more than 2.5 hours of examination and did not decrease over time (Figure 41). Therefore, the suction was not significantly influenced by the attached filtration probe.

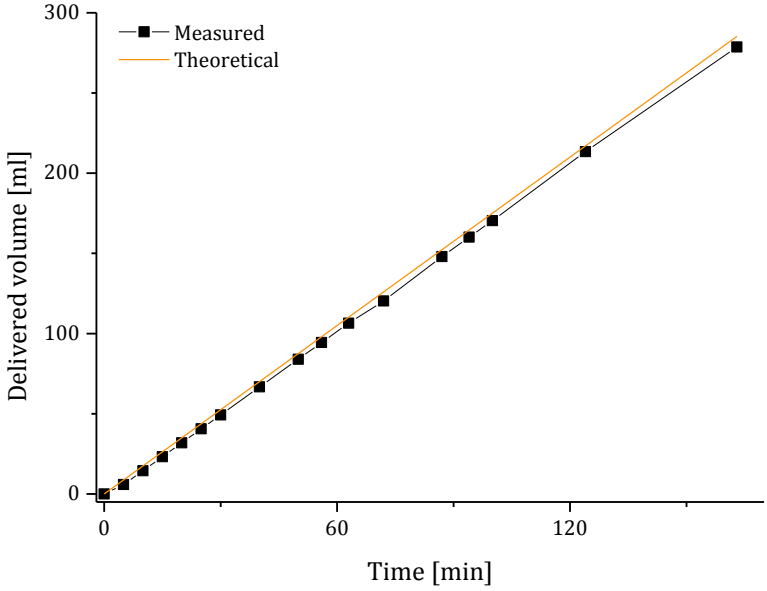

Figure 41: Temporal course of the delivered volume with the filtration probe for the validation of the unresisted pump capacity (D = $0.3\,\frac{1}{h}$).

After the experiment, a slight filter cake was found on the membrane. However, it can be removed mainly by rinsing with RO-water (Figure 42). Subsequently, the filter was reusable and applicable.

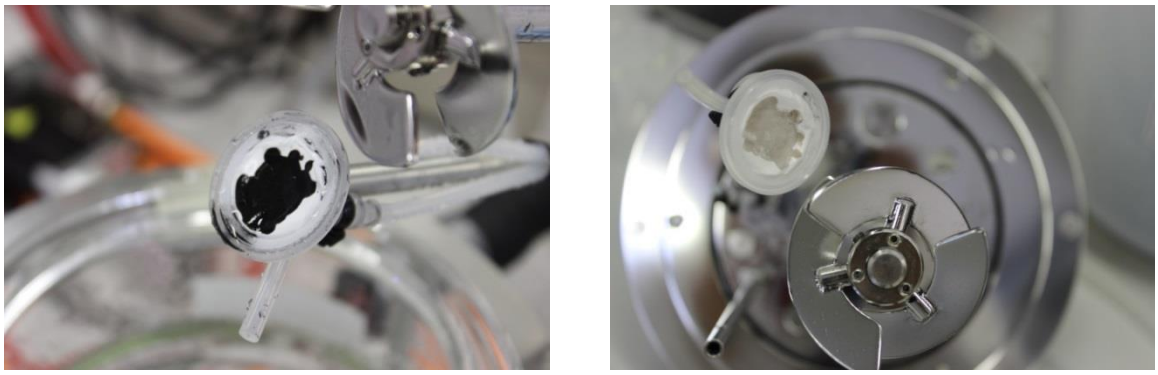

Figure 42: Filtration probe before (left) and after rinsing (right).

By the use of the filtration probe, lower catalyst concentrations are possible and therefore, a turnover less than 100 percent without the threat of unstable hydrogen peroxide concentrations caused by the dilution of the catalyst. As described above (5.3.1) these states are needed, because the calculation of many kinetic parameters are based on experiments with different balance conditions. Sufficient accuracy is only given for significant differences between them. The following experiments with the filtration probe (and 0.1 or, respectively, $0.5\,\frac{g}{L}\,MnO_2$) were carried out with 0.35 L in the UniVessel® (2 L). This small scale was chosen, to minimise the H_2O_2 consumption and MnO_2 waste production in this early phase of development. The agitation was set to 500 rpm, because higher speeds led to stronger squirting at this small amount of medium. The temperature was set to 30 °C instead of the common used temperature for fermentations (37 °C) to shorten the initial heating up time span. For comparisons with results from fermentations, subsequent measurements at 37 °C and 1500 rpm are recommended.

Despite of the filtered sampling and the additional temperature regulation, no steady state was achieved. After approximately 80 minutes a buckling was observed and a linear increasing of the amount of H_2O_2 occurred (Figure 43). The stopping of the continuous inflow of the hydrogen peroxide and the outflow of the medium after 260 minutes, (thus, switching in batch mode) resulted for the suspension with $0.5\,\frac{g}{L}\,MnO_2$ in a slight decomposition of H_2O_2. Compared to previous studies, the reaction velocity was

strongly decreased. Only 0.18 mole H_2O_2 were decomposed in 13 minutes (initial concentration 2.0 $\frac{mole}{L}$) with 0.5 $\frac{g}{L}$ MnO_2, whereas 0.84 mole H_2O_2 were decomposed in 12.8 minutes (initial concentration 1.5 $\frac{mole}{L}$) with 0.86 $\frac{g}{L}$ MnO_2 in earlier experiments. As already mentioned, an inactivation of MnO_2 for long-term experiments was brought up in the literature (Martin, 1996). However, no further investigation has been made and no more data has been published. That was why studies concerning the catalytic activity of MnO_2 were executed.

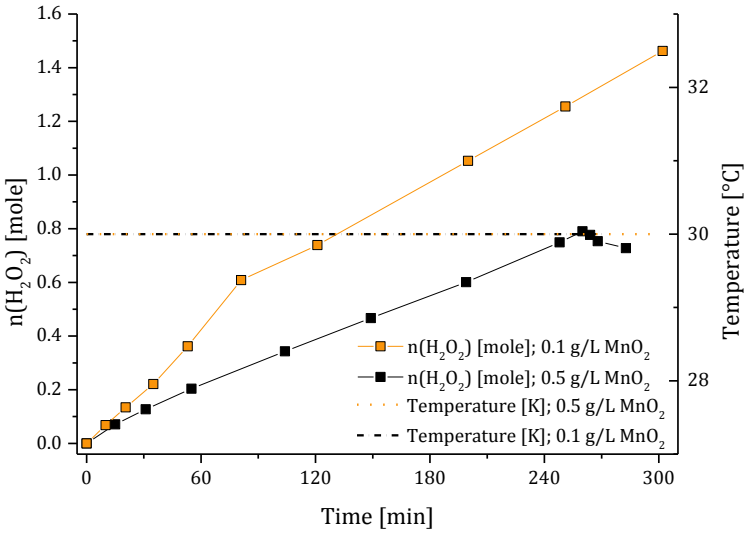

Figure 43: Temporal course of the temperature and the amount of substance of H_2O_2 in a scale of 0.35 L (UniVessel® 2L) processed in continuous, temperature regulated mode (30 °C) with a filtration probe and different MnO_2 concentrations.

5.3.3 Investigations concerning the catalytic activity of MnO_2

In preliminary experiments with low amounts of substrate no inactivation or decrease of the MnO_2 catalytic activity were observed (5.2.3.1). However, the H_2O_2 concentration did not stop to increase in continuous mode. Since the prevention of the rinsing effect did not solve this problem, an inactivation of the catalyst may be present. To understand this phenomenon a repeated fed-batch was performed. 0.5 $\frac{g}{L}$ MnO_2 was added to 350 mL of a 0.88 $\frac{mole}{L}$ H_2O_2 solution and the decreasing concentration of hydrogen peroxide was measured. Every 90 minutes fresh H_2O_2 was supplied so that the initial concentration was reached again. During the whole process, the temperature was regulated and set to

30 °C (Figure 44). The experimental conditions (500 rpm, 30 °C and 350 mL) were chosen due to the reasons already mentioned in chapter 5.3.2.

The behaviour of the hydrogen peroxide concentration revealed an ongoing retardation of the reaction velocity (Figure 45). During the first and the second feed, the MnO_2 decomposed only 65 % and, respectively, 47 % of the amount degraded in the initial batch. Beyond that, the swings of the temperature profiles got narrower after each feed, which leads to the assumption, that less heat was produced and hence, the reaction did not take place in the same strength like before. Compared to the experiments made before in the 0.1 L scale, this time the temperature was kept constant and had therefore no influence on the reaction (except the first minutes after the feeds where the temperature had to settle again). Since Martin wrote that salts do not affect the activity of MnO_2, the inactivation has to depend on time or on the decomposed amount of substance (Martin, 1996). Scanning electron microscopically analysis showed no difference in the surface structure of fresh and inactivated MnO_2 (Figure 56, appendix).

The obtained inactivation effect reveals the reason for the unachievable steady-state conditions both in small scale (0.1 L, unregulated temperature) and in bigger scale (0.35 L, regulated temperature). The inactivation effect seems to be much stronger than the rinsing effect because, independent of the utilisation of the filtration probe, the same decrease of the reaction rate occurred again.

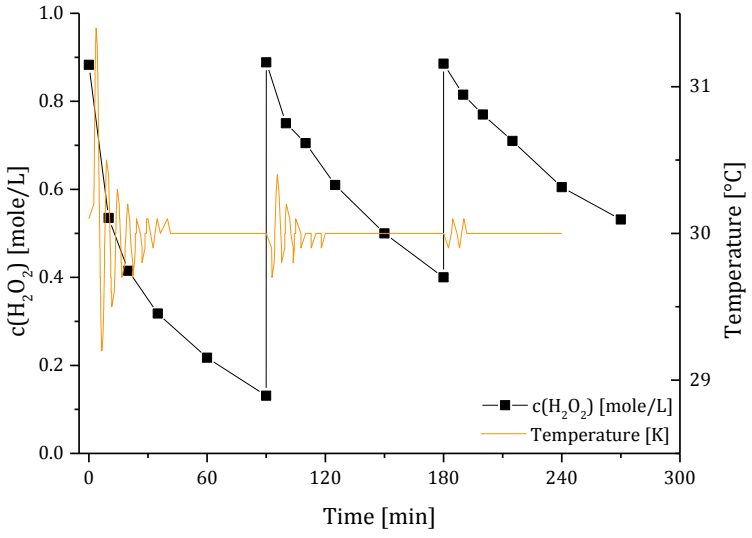

Figure 44: Temporal course of the temperature and the H_2O_2 concentration of a repeated fed-batch in a scale of 0.35 L.

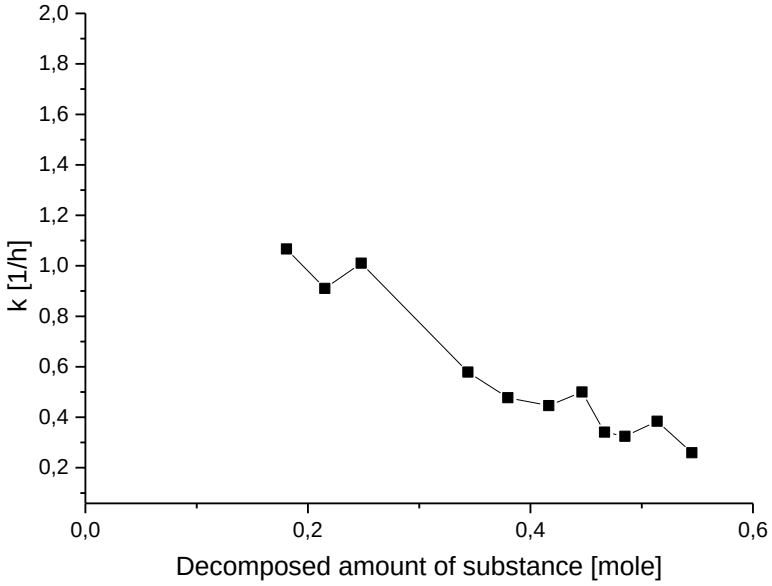

Figure 45: Illustration of the reaction rate in connection with the decomposed amount of substance.

5.3.4 Development of a feeding strategy to overcome MnO_2 inactivation

Generally, kinetic parameters like the activation energy (E_A), the pre-exponential factor and the pseudo reaction rate (k') are determinable by several experiments with various turnovers (caused by varied dilution rates) or, respectively, diverse temperatures in the stationary phase. Then the calculation can be made by equation (65), (66) and (67) (derived by equation (43)).

$$E_A = R \cdot \ln(2) \cdot \frac{T_1 \cdot T_2}{T_1 - T_2} \tag{65}$$

Temperature in experiment number 1	T_1	$[K]$
Temperature in experiment number 2	T_2	K

$$B = \frac{k' \cdot c(CAT)}{e^{\frac{E_A}{R \cdot T}}} \tag{66}$$

$$k' = \frac{X \cdot D}{c(CAT) \cdot (1 - X)} \tag{67}$$

However, up to this point no steady state was achieved. The unknown inactivation kinetic of MnO_2 made it difficult to feed the exact needed amount during a process to hold not only a specific concentration but as well a certain catalytic activity and consequently, a certain turnover. On that score it had to be resigned to identify the exact kinetic parameters of the process. However, investigations regarding the heat and mass transfer can be still performed. At very high catalyst concentrations the dilution and inactivation effects are no issue (Figure 38). To overcome a possible drop of the turnover, periodical catalyst feeds are recommendable, which consider both mentioned effects. According to this, a turnover of almost 100 % during the whole process is expected and the delivered amount of heat is rigorously calculable.

In a scale of 0.35 L these assumptions were tested. Because preliminary experiments showed a steady state for $4\,\frac{g}{L}$ MnO_2 and a dilution rate of $0.1\,\frac{1}{h}$ (Figure 39), the trial was executed with higher MnO_2 concentration ($6\,\frac{g}{L}$) in the beginning to enable analyses with higher dilution rates. To prevent a decrease of the turnover during the measurement by inactivation and rinsing, $3\,\frac{g}{L}$ MnO_2 were fed every 60 minutes. During the entire procedure the estimated progression was detected in the presumed way. The turnover only fluctuated between 99.2 and 99.4 %. The same experimental setting in a bigger scale (1 L medium in the UniVessel® (2 L) and 3.5 L medium in the UniVessel® (5 L)) resulted in very similar measurements. The turnover was always between 99.0 and 99.4 % and the scale-up was therefore successful. Since two feeds are applied, three measurements of the H_2O_2 turnover and the temperature of the cooling water are possible in the steady states after 0, 60 and 120 minutes.

5.3.5 Cost calculation

The higher recommended amount of MnO_2 leads to higher costs of the whole process. Since a standard method should be cheap, a cost calculation for the catalyst and H_2O_2 was made (Table 6 - Table 8). The favoured feeding strategy of MnO_2 resulted in costs up

to 23.52 € per execution in a 10 L bioreactor. In addition, the costs for the PBS-Buffer should be kept in mind.

Table 6: Cost calculation of MnO_2 with a total usage of 12 $\frac{g}{L}$[3].

Volume of the bioreactor [L]	Needed amount of MnO_2 for 10 executions [kg]	Recommended MnO_2 container [kg]	Average costs per execution
1	0.12	0.25	2.99 €
2	0.24	0.25	2.99 €
5	0.6	1	4.99 €
10	1.2	2.5	10.90 €

Table 7: Cost calculation of H_2O_2 with a total usage of 0.3 $\frac{L\ H_2O_2}{L\ Medium}$ (D = 0.1 $\frac{1}{h}$, time span: 3 h)[4].

Volume of the bioreactor [L]	Needed amount of H_2O_2 for 10 executions [L]	Recommended H_2O_2 container [L]	Average costs per execution
1	3	10	4.15 €
2	6	10	4.15 €
5	15	2 x 10	8.30 €
10	30	1 x 10 + 1 x 25	12.62 €

Table 8: Overall cost calculation of H_2O_2 and MnO_2[5].

Volume of the bioreactor [L]	Average MnO_2 costs per execution	Average H_2O_2 costs per execution	Total costs per execution
1	2.99 €	4.15 €	7.14 €
2	2.99 €	4.15 €	7.14 €
5	4.99 €	8.30 €	13.20 €
10	10.90 €	12.62 €	23.52 €

[3] Data obtained on the 10.09.2015 at www.carlroth.com
[4] Data obtained on the 10.09.2015 at www.carlroth.com
[5] Data obtained on the 10.09.2015 at www.carlroth.com

5.4 Determination of procedurally parameters in the UniVessel® (5 L)

The newly developed technique for the determination of the heat and mass transfer showed a constant heat and oxygen production in preliminary experiments (5.3.4). To prove its reliability, it was compared with conventional approaches. In case of the heat transfer, a stationary power input by an electrical calibration heater was applied. Furthermore, the oxygen transfer was studied in addition to the H_2O_2 technique with the dynamic gassing-out method.

5.4.1 Determination of UA

There are various sources and sinks of heat flows in a bioreactor (Figure 46) (Storhas, 1994; Regestein, 2012). The system can be described by two balancing spaces, which are related with each other by the heat flow $\dot{Q}_{Jacket}$ (highlighted in orange).

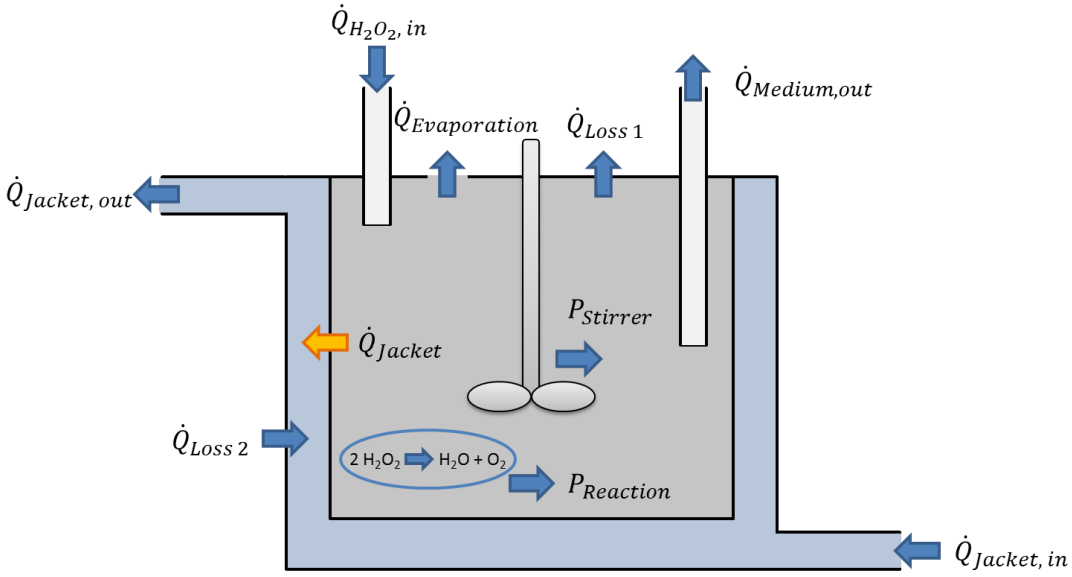

Figure 46: Schematic representation of possible heat flows in a bioreactor. In particular, the decomposition of H_2O_2 is stated as a model reaction for the heat production by a chemical or microbial reaction. The system is divided in two sections (balancing space 1: the reactor (grey), balancing space 2: the double jacket (blue)).

The first balancing space (the inner part of the reactor) can be described with the following balances:

$$P_{Reaction} + P_{Stirrer} + \dot{Q}_{H_2O_2,in} = \dot{Q}_{Jacket} + \dot{Q}_{Evaporation} + \dot{Q}_{loss\,1} + \dot{Q}_{Medium,out} \quad (68)$$

Power input by the reaction to the reactor	$P_{Reaction}$	$[W]$
Power input by the stirrer to the reactor	$P_{Stirrer}$	$[W]$
Heat flow by the inflowing H_2O_2	$\dot{Q}_{H_2O_2,in}$	$[W]$
Heat flow from the reactor to the jacket	$\dot{Q}_{Jacket}$	$[W]$
Heat flow by the evaporating oxygen	$\dot{Q}_{Evaporation}$	$[W]$
Heat flow from the reactor through the lid to the environment	$\dot{Q}_{loss\,1}$	$[W]$
Heat flow by the outflowing medium	$\dot{Q}_{Medium,out}$	$[W]$

The listed heat flows are given by:

$$P_{Reaction} = (-\Delta H_R) \cdot \dot{V}_E \cdot c(H_2O_2)_i \cdot X \quad (69)$$

$$P_{Stirrer} = 2 \cdot \pi \cdot N \cdot M_t = Ne \cdot \rho \cdot N^3 \cdot d^5 \quad (70)$$

$$\dot{Q}_{H_2O_2,in} = \dot{m}_{H_2O_2} \cdot c_{p,H_2O_2} \cdot T_{Environment} \quad (71)$$

$$\dot{Q}_{Jacket} = UA \cdot (T_{Reactor} - T_{Jacket,out}) \quad (72)$$

$$\dot{Q}_{Evaporation} = \dot{m}_{O_2} \cdot c_{p,O_2} \cdot T_{Reactor} \quad (73)$$

$$\dot{Q}_{loss\,1} = UA_2 \cdot (T_{Reactor} - T_{Environment}) \quad (74)$$

$$\dot{Q}_{Medium,out} = \dot{m}_{Medium} \cdot c_{p,Medium} \cdot T_{Reactor} \quad (75)$$

Reaction enthalpy	ΔH_R	$\left[\frac{J}{mole}\right]$
Inflowing volume flow rate	$\dot{V}_E$	$\left[\frac{L}{s}\right]$
Amount of rotations of the stirrer per time	N	$\left[\frac{1}{s}\right]$
Torque	M_t	$[N \cdot m]$
Newton number	Ne	$[-]$
Density	ρ	$\left[\frac{kg}{L}\right]$
Diameter of the stirrer	d	$[m]$
Mass flow of the inflowing H_2O_2	$\dot{m}_{H_2O_2}$	$\left[\frac{kg}{s}\right]$
Specific heat capacity of H_2O_2	c_{p,H_2O_2}	$\left[\frac{J}{K \cdot kg}\right]$
Temperature of the environment	$T_{Environment}$	$[K]$
Temperature of the reactor	$T_{Reactor}$	$[K]$
Temperature of the outflowing cooling water	$T_{Jacket,out}$	$[K]$
Mass flow of the evaporating O_2	$\dot{m}_{O_2}$	$\left[\frac{kg}{s}\right]$
Specific heat transfer coefficient for the reactor lid	UA_2	$\left[\frac{W}{K}\right]$
Mass flow of the outflowing medium	$\dot{m}_{Medium}$	$\left[\frac{kg}{s}\right]$
Specific heat capacity of the medium	$c_{p,Medium}$	$\left[\frac{J}{K \cdot kg}\right]$

In addition to that, the heat balance equation in the jacket (balancing space 2) comprises by:

$$\dot{Q}_{Jacket,in} + \dot{Q}_{Jacket} = \dot{Q}_{loss\,2} + \dot{Q}_{Jacket,out} \tag{76}$$

Heat flow by the inflowing cooling water	$\dot{Q}_{Jacket,in}$	$[W]$
Heat flow from the jacket chamber to the environment	$\dot{Q}_{loss\,2}$	$[W]$
Heat flow by the outflowing cooling water	$\dot{Q}_{Jacket,out}$	$[W]$

The enumerated heat flows can be specified by:

$$\dot{Q}_{Jacket,in} = \dot{m}_{H_2O} \cdot c_{p,H_2O} \cdot T_{Jacket,in} \tag{77}$$

$$\dot{Q}_{loss\ 2} = UA_3 \cdot (T_{Jacket,out} - T_{Environment}) \tag{78}$$

$$\dot{Q}_{Jacket,out} = \dot{m}_{H_2O} \cdot c_{p,H_2O} \cdot T_{Jacket,out} \tag{79}$$

Mass flow of the cooling water	$\dot{m}_{H_2O}$	$\left[\frac{kg}{s}\right]$
Specific heat capacity of water	c_{p,H_2O}	$\left[\frac{J}{K \cdot kg}\right]$
Temperature of the inflowing cooling water	$T_{Jacket,in}$	$[K]$
Specific heat transfer coefficient for the outer wall of the jacket chamber	UA_3	$\left[\frac{W}{K}\right]$

Since the power input by the stirrer is unclear, the heat sources in the reactor cannot be calculated completely. However, comparative measurements can be carried out, if the stirrer speed is the same in both experiments. Similar to the impact of the stirrer, it is not necessary to bear the heat loss to the surrounding environment ($\dot{Q}_{Loss\,1}$ and $\dot{Q}_{Loss\,2}$) for the comparison in mind, since it occurs during the chemical and the electrical heat release in the same way. However, for studies about the absolute value of UA, this has to be regarded.

Furthermore, the inflow of H_2O_2 and outflow of medium, respectively, is only given in the continuous mode. Therefore, these influences have to be included. Their combined heat flow is described by

$$\dot{Q}_{in-and\ outflow} = \dot{m}_{H_2O_2} \cdot c_{p,H_2O_2} \cdot T_{Environment} - \dot{m}_{Medium} \cdot c_{p,Medium} \cdot T_{Reactor} \quad (80)$$

Overall heat flow from the H_2O_2 inflow and the medium outflow	$\dot{Q}_{in-and\ outflow}$	$[W]$
Volume flow rate of the H_2O_2 inflow and the medium outflow	$\dot{V}_{i,o}$	$\left[\frac{L}{s}\right]$

and

$$\dot{Q}_{in-and\ outflow} = \dot{V}_{i,o} \cdot \left(\rho_{H_2O_2} \cdot c_{p,H_2O_2} \cdot T_{Environment} - \rho_{Medium} \cdot c_{p,Medium} \cdot T_{Reactor}\right) \quad (81)$$

Density of H_2O_2	$\rho_{H_2O_2}$	$\left[\frac{kg}{L}\right]$

respectively.

In addition, the heat sink by the evaporated oxygen has to be taken into account. For its calculation the mass flow of oxygen is needed, which is given by

$$\dot{m}_{O_2} = \dot{V}_i \cdot c(H_2O_2)_i \cdot M_{O_2} \cdot \frac{1}{2} \cdot X \quad (82)$$

Volume flow rate of the H_2O_2 inflow	$\dot{V}_i$	$\left[\frac{L}{s}\right]$
Molarity of O_2	M_{O_2}	$\left[\frac{g}{mole}\right]$

As a result of this, it is possible to measure different heat flows from the reactor to the jacket for various power inputs. Since $\dot{Q}_{loss,2}$ is insignificant as explained before, the balance equation for the jacket is given by

$$\dot{m}_{H_2O} \cdot c_{p,H_2O} \cdot T_{Jacket,out} = UA \cdot \left(T_R - T_{Jacket,out}\right) + \dot{m}_{H_2O} \cdot c_{p,H_2O} \cdot T_{Jacket,in} \quad (83)$$

and can be transformed to

$$\dot{m}_{H_2O} \cdot c_{p,H_2O} \cdot \left(T_{Jacket,out} - T_{Jacket,in}\right) = UA \cdot \left(T_R - T_{Jacket,out}\right) \quad (84)$$

and furthermore, to

$$\frac{\dot{m}_{H_2O} \cdot c_{p,H_2O} \cdot \left(T_{Jacket,out} - T_{Jacket,in}\right)}{\left(T_R - T_{Jacket,out}\right)} = UA \quad (85)$$

The experimental data showed for higher specific power inputs a decrease of the in- and outlet temperature and, furthermore, an increase of their difference (Figure 47 and Figure 48). This trend was the same for the chemical and the electrical approach.

For the later, two different calibration heaters were studied (250 W and 500 W) for precision reasons. With a high performance alternating voltage regulator the power input was set to the required set points.

Based on this data, UA was calculated for both methods at different specific power inputs. The profile showed a constant UA in the range of 18.2 – 24.2 $\frac{W}{K}$ (250 W calibration heater) and 19.5 – 23.0 $\frac{W}{K}$ (500 W calibration heater). The results, obtained with the chemical approach, fitted very well to the electrical ones. Despite of the measurement point at 32.4 $\frac{W}{L}$, a specific heat transfer coefficient between 19.1 – 24.2 $\frac{W}{K}$ was determined. These fluctuations of all measurements and especially of the outlier from the mean value might be explainable by the influence of the environmental temperature. Since no insulation was used, a cooling effect (in case of outlet temperatures above the environmental temperature (Figure 47) and, respectively, a heating effect (during experiments with very low cooling water temperatures (Figure 48) occurred. In addition, the changing room temperature might have a further impact.

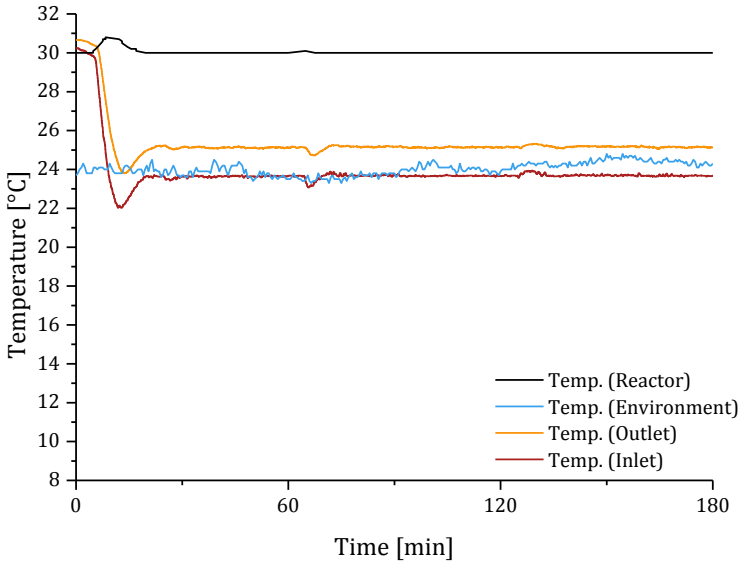

Figure 47: Temperature profile due to chemical heat production ($P_{spec.}$ = 32.4 $\frac{W}{L}$).

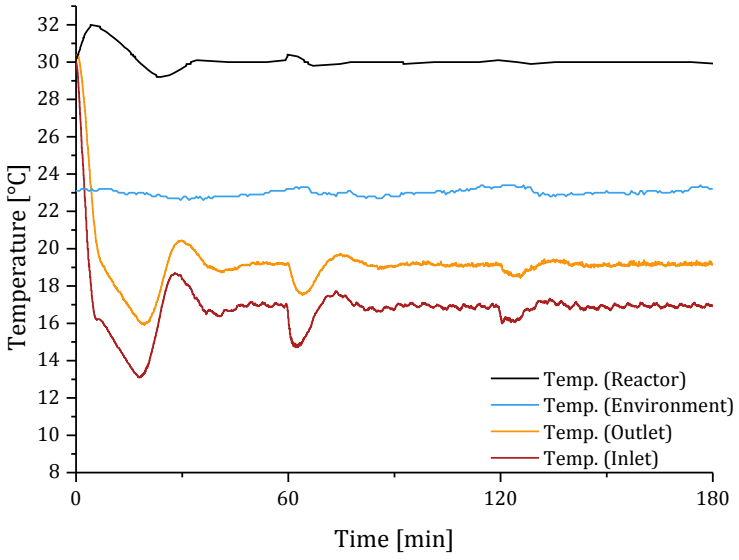

Figure 48: Temperature profile due to chemical heat production ($P_{spec.}$ = 67.9 $\frac{W}{L}$).

By a nonlinear least square minimisation the influence of the environment was analysed and $\dot{Q}_{loss\ 2}$ was taken into account. Then, the differential equation concerning the heat flows for steady state conditions are given by:

$$\dot{m}_{H_2O} \cdot c_{p,H_2O} \cdot (T_{Jacket,out} - T_{Jacket,in}) - UA \cdot (T_R - T_{Jacket,out}) + UA_{loss\ 2} \cdot (T_{Environment} - T_{Jacket,out}) = 0 \quad (86)$$

The calculated results are presented in Figure 49. $UA_{loss\ 2}$ was quite constant in a range of 1.98 – 2.04 $\frac{W}{K}$ for all measurements, independent of the used heat source. Besides, the specific heat transfer coefficient from the reactor and the double jacket to the environment accounted only 8 % of UA. Considering of $UA_{loss\ 2}$ changed the profile of UA and the outlier at 32.4 $\frac{W}{L}$ only slightly. Apart from this deviation of 34.6 $\frac{W}{K}$, UA was still in the range of 17.1 – 24.8 $\frac{W}{K}$ for both methods.

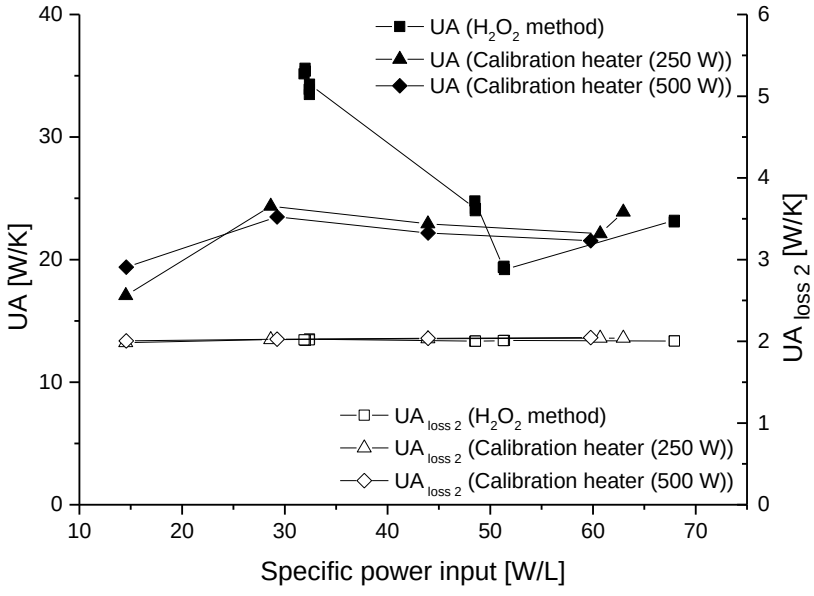

Figure 49: Illustration of UA and UA_{loss} for different specific power inputs.

The main expected diverging factor on the findings is the feeding velocity. Lower feeding rates led to a more unsteady flow. In addition, the feeding tube was set above the surface

of the medium. Hence, a very thin tube, which is placed in a zone of high mixing, is suggested for upcoming experiments to enable a steadier flow and ideal mixing. Since the Watson Marlow 205U pump offers, compared to the Watson Marlow 520 pump, a more regular flow, due to the higher amount of pressure rollers, the utilisation of the first might be favourable.

All in all, additional examinations have to be made to find out the causing influence for the described deviation. Measurements should be made as well with specific power inputs less than $32\,\frac{W}{L}$ to screen the UA profile for possible further high specific heat transfer coefficients, due to the described above coherence.

However, the newly developed method is suitable for the determination of UA in the range of about $50 - 70\,\frac{W}{L}$ and lead to comparative results like the outcomes of the electrical approach by calibration heaters.

5.4.2 Determination of k_La

The presented new method was not only tested for its potential regarding the determination of the heat transfer but as well for its feasibility concerning studies on the mass transfer. At first the coalescence behaviour of the utilised medium was analysed. Dissolved compounds (especially salts) have a strong impact on the formed gas bubbles in aerated liquids. With increasing amounts of salts, a coalescence inhibition is observable (Marrucci and Nicodemo, 1967). Hence, media, which are applied for biological processes, can be assumed as non-coalescent due to their containing nutrients and salts. Liepe et al. mentioned, that a medium with an ion strength <0.1 $\frac{g}{mole}$ has to be expected as coalescent, whereas a liquid with an ion strength >0.3 $\frac{g}{mole}$ can be assumed as coalescence-inhibited (Liepe *et al.*, 1998). For the newly developed H_2O_2 method 1x PBS-buffer was chosen, due to the recommendation of the literature (Meusel *et al*., unpublished). The utilised buffer has an ion strength of 0.2 $\frac{g}{mole}$ and is therefore in the transitional range. To proof non-coalescent conditions and therefore, similar circumstances compared with biological media, different concentrations were tested on their k_La by means of the gassing-out method (Figure 50) (Meusel *et al*., unpublished). The outcomes showed an average k_La of 287 $\frac{1}{h}$ in the range of the 0.8 – 3.8-fold of the

normal PBS-buffer-concentration. Higher dilutions led (after a transient zone) to a decreased k_La of about 133 $\frac{1}{h}$.

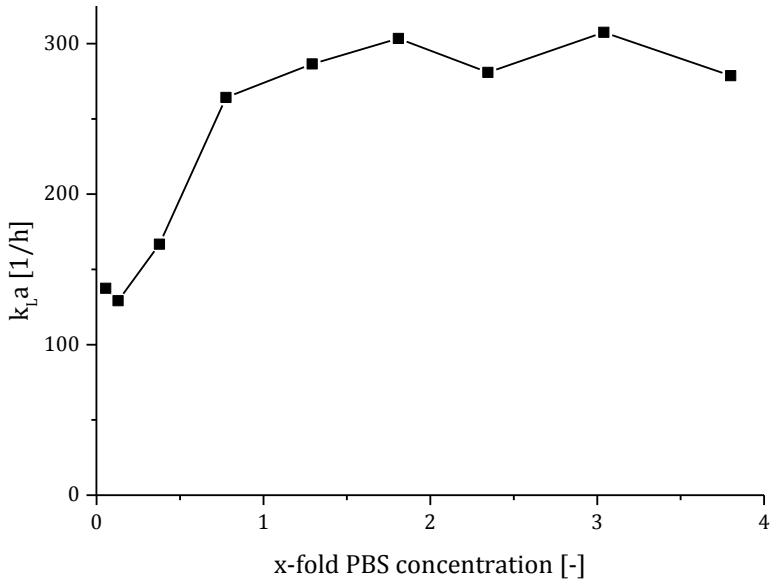

Figure 50: Dependency of the k_La on the PBS-buffer concentration. Experimental setting: 500 rpm, 1 vvm air, 30 °C, 6-blade disk-impeller (diameter of 75 mm), baffles, 3.5 L medium.

This phenomenon is explicable by the occurring coalescence in more diluted solutions, which involves bigger gas bubbles, a smaller total bubble surface and hence a decreased k_La. In contrast to that, for a 1x PBS-buffer a coalescence-inhibited medium is present, which results in smaller air bubbles with a bigger overall surface and a higher k_La.
In the sector of non-coalescent the specific boundary layer surface is independent from the exact salt concentration (Marrucci and Nicodemo, 1967). Hence, the slightly occurring dilution by the addition of the H_2O_2-solution and the formation of water by the reaction does not change the k_La.
The experimental settings were based on Hickmans k_La determination (Hickman, 1988). Because a flooding of the stirrer is possible at these configurations, a lower gassing rate was adjusted for the k_La determination with the hydrogen peroxide method at different dilution rates (Figure 51). Furthermore, nitrogen instead of air was utilised to decrease the stationary dissolved oxygen concentration and hence, increase the measurable range.

With increasing flow rates, the obtained k_La got higher until it almost reached a constant value of 431 h^{-1}. The obtained behaviour might be, similar to the inaccurate UA determination at low dilution rates (5.4.1), caused by an irregular flow. Further studies to investigate its stability with a higher mass flow were not possible. Due to the limitations of the digital control unit (DCU), the computer was not able to deal with higher currents than about 170 nA. A possible solution of this problem could be a current divider, to diminish the registered current.

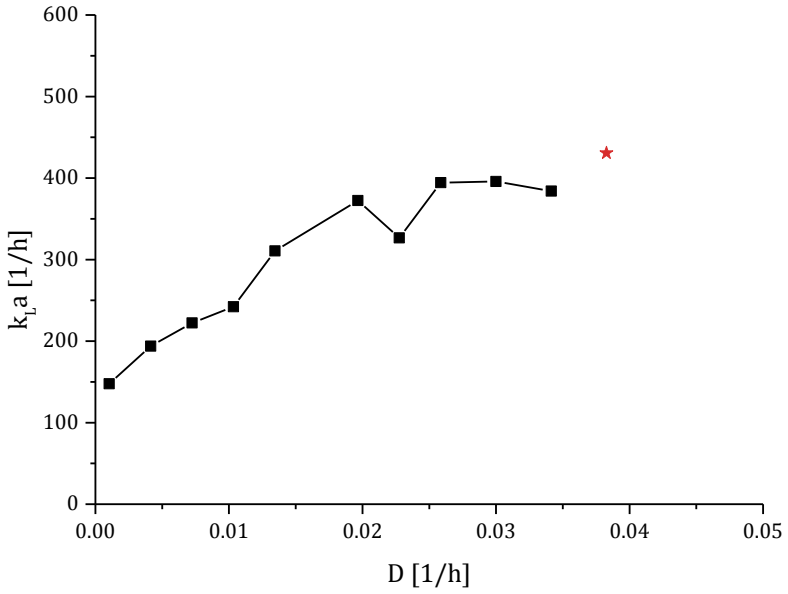

Figure 51: Measured k_La for different dilution rates. The measurement point at 0.04 h^{-1} (red) might be incorrect, due to the measurement limitations of the DCU. Experimental setting: 500 rpm, 0.3 vvm nitrogen, 30 °C, 6-blade disk-impeller (diameter of 75 mm), baffles, 3.5 L medium.

Due to this limitation, the measurement point with the highest dilution rate ($38 \cdot 10^{-3}$ h^{-1}) has already to been seen as critically and too high, because the recorded value was in a zone directly next to the registration border. It has to be taken into account, that the current varied in this area about 20 nA from the mean measurement, wherefore a distance of minimum 30 nA is needed for a distinct result (Figure 52).

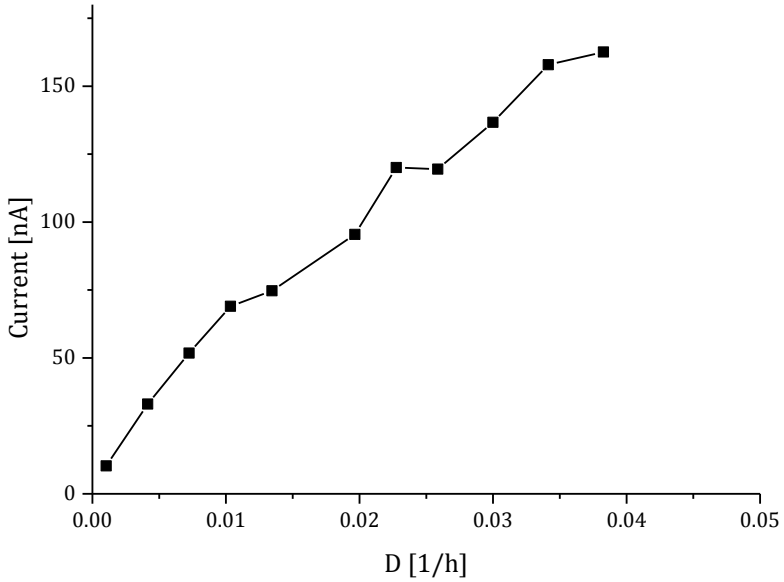

Figure 52: Illustration of the current for different dilution rates.

The obtained results showed a higher k_La compared with the outcomes made before with the gassing-out method (264 - 287 h^{-1}). Since this technique is a dynamic determination, a lower mass transfer is expected, due to the response time of the dissolved oxygen probe. Additionally, the driving force decreases over time, which influences the measurement as well (Garcia-Ochoa and Gomez, 2009). However, the lower gassing rate in the H_2O_2 experiments has to be considered (Table 9).

Hickmann found a constant k_La of 162 – 173 h^{-1} in his experiments (Hickman, 1988). He investigated the dilution rate range of $1.2 \cdot 10^{-3} - 9.4 \cdot 10^{-3}\ h^{-1}$, where the measured k_La in this thesis was 194 – 242 h^{-1}. His experimental setting was very similar to the installation presented in this work. However, he used water instead of a salt solution like PBS. Hence, he worked in a coalescent medium, which leads to a decreased mass transfer. A contrary effect was introduced by a higher adjusted gas flow rate. Finally, other process affecting parameters, like the medium temperature, were not mentioned. These reasons explain his lower k_La.

The formation of oxygen takes place in the medium, wherefrom it diffuses to gas bubbles. Therefore, unlike the sodium thiosulfate method (3.2.3), where the oxygen is already consumed in the boundary layer (which increases the k_La), the Hatta number has not to

be considered for this approach. The Hatta number describes the ratio of the reaction rate to the mass transfer (equation (86)) (Hertwig and Martens, 2011; Liepe *et al.*, 1998).

$$Ha = \frac{\sqrt{k \cdot D_c}}{k_L} \quad \text{(for first order reactions)} \tag{87}$$

Hatta number	Ha	$[-]$
Diffusion coefficient	D_c	$\left[\frac{m^2}{s}\right]$

However, the causes for the unstable k_La are still unclear, especially because Hickman reported a steady k_La in the studied dilution rate range. Therefore, the H_2O_2 method is still in the development phase and not ready to apply. Subsequent experiments are recommended in view of these obscurities. Furthermore, to enhance the comparability of this method with more results from the literature, it would be helpful to adjust the process conditions to settings occurring in fermentations (37 °C, 1500 rpm, 4.5 L, 1.1 vvm , Air)

Table 9: Comparison of the experimental settings and the obtained k_La with different methods.

	H_2O_2-method (own results)	H_2O_2-method (Hickman, 1988)	Gassing-out method (own results)
Temperature	30 °C	Not mentioned	30 °C
Gassing rate	0.3 vvm	1.1 vvm	1 vvm
Gas	N_2	Air	Air
Volume	3.5 L	5 L	3.5 L
Medium	PBS-buffer	Water	PBS-buffer
Agitation	500 rpm	500 rpm	500 rpm
k_La	$431\ \frac{1}{h}$	$162 - 173\ \frac{1}{h}$	$264 - 287\ \frac{1}{h}$

The exact Henry constant has a strong impact on the calculated k_La and depends on various parameters (e.g. the salinity, the temperature and the pressure). Thus, it should be determined preliminary to further experiments. Since it is known for pure water, an easy procedure would be to calculate ${H_{PBS,MnO_2}}^{cc}$ by comparative measurements with a Clark electrode for pure water and PBS medium with MnO_2. Subsequently, the Henry constant is calculable by

$$ {H_{PBS,MnO_2}}^{cc} = \frac{{c_{l,\ PBS,MnO_2}}^{*} \cdot {H_{Water}}^{cc}}{{c_{l,\ Water}}^{*}} \tag{88} $$

Henry constant for PBS/MnO_2 medium (dimensionless)	${H_{PBS,MnO_2}}^{cc}$	$[-]$
Oxygen saturation concentration of PBS/MnO_2 medium	${c_{l,\ PBS,MnO_2}}^{*}$	$\left[\frac{mole}{L}\right]$
Henry constant for pure water (dimensionless)	${H_{Water}}^{cc}$	$[-]$
Oxygen saturation concentration of pure water	${c_{l,\ Water}}^{*}$	$\left[\frac{mole}{L}\right]$

Chapter 6

Conclusion and Outlook

Knowledge about the heat and mass transfer in bioreactors is fundamental for a sufficient process regulation in both, microbial fermentation and cell culture cultivation. Present attempts are limited due to their dynamic measurement principle. Furthermore, in case of the heat transfer, they are restricted towards larger scales and uncommon geometries such as various single-use bioreactors. In this thesis, a new method is developed, which overcomes this limitations. This approach is based on the degradation of hydrogen peroxide, which is on the one hand a possible source of heat by its reaction enthalpy of -98.2 $\frac{kJ}{mole}$ and offers on the other hand the formation of oxygen. In a continuous process the stationary heat and oxygen production makes the measurement of the specific heat transfer coefficient and volumetric mass transfer coefficient comparatively more accurate than in dynamic attempts. In contrast to an electrical power input, this chemical heat production approach is independent of the design and scale of the bioreactor.

In order to develop such a continuous process, three different catalysts (catalase, $Fe(NO_3)_3$ and MnO_2) were studied concerning their kinetic, possible inactivation and safety issues. Based on these results, manganese oxide was chosen to be the most suitable candidate.

Subsequently, experiments in continuous mode were executed, but at first no steady state was achieved. It was shown, that this was due to the long term washing out effect and an inactivation. Therefore, a feeding strategy with an excess of MnO_2 and, related to that, with a constant turnover of almost 100 % was developed (6 $\frac{g}{L}$ initially + 3 $\frac{g}{L}$ every 60 minutes). The process was successfully scaled-up from 100 mL to the UniVessel® (5 L). In this scale, the newly established chemical method was compared with another one, based on an electrical power input by two calibration heaters to show its usability. The results showed the comparability of both methods, due to similar UA determinations in the range of 17.1 – 24.8 $\frac{W}{K}$ at power inputs of about 50 – 70 $\frac{W}{L}$.

However, at a specific power input of 32.4 $\frac{W}{L}$ the chemical method obtained a higher UA of 34.6 $\frac{W}{K}$. To investigate this specific section, more measurement points in this span should be analysed. Further research will deal with the determination of UA by this

chemical approach in single-use-bioreactors, especially in the wave-mixed BIOSTAT® RM due to its uncommon geometry. In addition, it seems to be promising to process a further scale-up to volumes of 50 L in a stirred bioreactor to proof its capability for larger scales.

The investigations regarding the volumetric mass transfer coefficient showed that the determination of k_La is not feasible yet. Stable results could not be measured. However, steady results are expected with dilution rates higher than 0.04 h^{-1}. Hence, further studies are necessary to overcome these problems. Subsequent experiments with settings similar to fermentation conditions (regarding agitation, gassing rate, etc.) are advisable for better comparability to other approaches like the exhaust gas analysis. Finally, an exact determination of the Henry constant in the studied medium was suggested and described to overcome an imprecise calculation of the k_La.

Chapter 7

References

Akhtar, K., Khalid, N. and Ali, M. (2012), "Effect of pH and temperature on the catalytic properties of manganese dioxide", *Journal of The Chemical Society of Pakistan*, Vol. 34 No. 2.

Baehr, H.D. and Stephan, K. (2013), Wärme- und Stoffübertragung, *SpringerLink Bücher,* 8., aktual. Aufl. 2013, Imprint: Springer Vieweg, Berlin, Heidelberg.

Biener, R., Steinkämper, A. and Hofmann, J. (2010), "Calorimetric control for high cell density cultivation of a recombinant Escherichia coli strain", *Journal of biotechnology*, Vol. 146 No. 1-2, pp. 45–53.

Brehm, A. (2015), "Thermisches Verhalten von Reaktoren", available at: http://www.gmehling.chemie.uni-oldenburg.de/download/ThermVerhalten.pdf (accessed 29 September 2015).

Broughton, D.B. and Wentworth, R.L. (1947), "Mechanism of Decomposition of Hydrogen Peroxide Solutions with Manganese Dioxide. I", *Journal of the american chemical society*, Vol. 69 No. 4, pp. 741–744.

Chmiel, H. (2011), Bioprozesstechnik, 3., neu bearb. Aufl, Spektrum Akad. Verl., Heidelberg.

Do, S.-H., Batchelor, B., Lee, H.-K. and Kong, S.-H. (2009), "Hydrogen peroxide decomposition on manganese oxide (pyrolusite): kinetics, intermediates, and mechanism", *Chemosphere*, Vol. 75 No. 1, pp. 8–12.

Dokuzovic, L. (2015), "Iodometrie", available at: http://www.lickl.net/doku/iodometrie.pdf (accessed 15 June 2015).

Dolhun, J. (2015), "Chemical Transformation I, Decomposition of H_2O_2 with MnO_2", available at: http://ocw.mit.edu/high-school/chemistry/demonstrations/videos/the-steaming-gun/steaming_gun.pdf (accessed 9 July 2015).

Eduard-Job-Stiftung für Thermo- und Stoffdynamik (2015), "H_2O_2-Zersetzung durch verschiedene Katalysatoren", available at: http://www.job-stiftung.de/pdf/versuche/H_2O_2_Zersetzung.pdf (accessed 1 June 2015).

Elprince, A.M. and Mohamed, W.H. (1992), "Catalytic decomposition kinetics of aqueous hydrogen peroxide and solid magnesium peroxide by birnessite", *Soil Science Society of America Journal*, Vol. 56 No. 6, pp. 1784–1788.

Elprince, A.M., Mohamed, W.H. and El-Wakil, E.M. (2008), "Kinetics of nonenzymatic decomposition of hydrogen peroxide by torrifluvents", *Soil Science Society of America Journal*, Vol. 72 No. 1, pp. 83–89.

Garcia-Ochoa, F. and Gomez, E. (2009), "Bioreactor scale-up and oxygen transfer rate in microbial processes: an overview", *Biotechnology advances*, Vol. 27 No. 2, pp. 153–176.

Haber, F. and Weiss, J. (1934), "The Catalytic Decomposition of Hydrogen Peroxide by Iron Salts", *Proceedings of the Royal Society A: Mathematical, Physical and Engineering Sciences*, Vol. 147 No. 861, pp. 332–351.

Hancock, R. (2015), "Stability of complexes of metal ions in aqueous solution", Vorlesungsskript, University of North Carolina Wilmington, available at: http://www.uncw.edu/chem/documents/acidityofmetalionsinaqueoussolution.doc (accessed 2 July 2015).

Hertwig, K. and Martens, L. (2011), Chemische Verfahrenstechnik, 2., überarbeitete Aufl, Oldenbourg, R, [S.l.].

Hickman, A.D. (1988), "Gas-liquid oxygen transfer and scale-up. A novel experimental technique with results for mass transfer in aerated agitated vessels", *6th European Conference on Mixing, Pavia, Italy*.

Holdt, H.-J. (2015), "Experimentalvorlesung zur Allgemeinen und Anorganischen Chemie", available at: http://www.chem.uni-potsdam.de/groups/anorganik/Kapitel31.pdf (accessed 3 July 2015).

Holleman, A.F., Wiberg, E. and Wiberg, N. (2007), Lehrbuch der anorganischen Chemie, 102., stark umgearbeitete und verb. Aufl, de Gruyter, Berlin, New York.

Kanungo, S.B., Parida, K. and Sant, B.R. (1981), "Studies on MnO_2—III. The kinetics and the mechanism for the catalytic decomposition of H_2O_2 over different crystalline modifications of MnO_2", *Electrochimica Acta*, Vol. 26 No. 8, pp. 1157–1167.

Knoll, A., Maier, B., Tscherrig, H. and Büchs, J. (2005), "The Oxygen Mass Transfer, Carbon Dioxide Inhibition, Heat Removal, and the Energy and Cost Efficiencies of High Pressure Fermentation", *Adv Biochem Eng Biotechnol.*, Vol. 92, pp. 77–99.

Koepp-Bank, H.-J. (2012), "Bioverfahrenstechnik", Vorlesungsskript, Hochschule Darmstadt.

Lide, D.R. (1998), CRC handbook of chemistry and physics: A ready-reference book of chemical and physical data, 79th ed, CRC, Boca Raton, Fla., London.

Liepe, F., Sperling, R. and Jembere, S. (1998), Rührwerke: Theoretische Grundlagen, Auslegung und Bewertung, 1. Aufl, Fachhochsch., Köthen.

Linek, V., Havelka, P. and Sinkule, J. (1996), "Supersaturation effect in steady-state and dynamic methods for measuring kLa in gas-liquid dispersions", *Chemical Engineering Science*, Vol. 51 No. 23, pp. 5223–5226.

Marrucci, G. and Nicodemo, L. (1967), "Coalescence of gas bubbles in aqueous solutions of inorganic electrolytes", *Chemical Engineering Science*, Vol. 22 No. 9, pp. 1257–1265.

Martin, T. (Ed.) (1996), Gas dispersion with radial and hydrofoil impellers in fluids with different coalescence characteristics*, Verfahrenstechnik*, H. Utz, München.

Marzzacco, C. (2015), "The effect of a change in the catalyst on the enthalpy of decomposition of hydrogen peroxide", available at: https://uwaterloo.ca/chem13news/sites/ca.chem13news/files/uploads/files/catalyst-enthalpy-hydrogen-peroxide.pdf (accessed 17 June 2015).

Meusel, W., Löffelholz, C., Husemann, U., Dreher, T., Greller, G., Kauling, J., Eibl, D., Kleebank, S., Bauer, I., Glöckler, R., Huber, P., Kuhlmann, W., John, G. T., Pörtner, R. and Kraume, M. (unpublished), "Recommendations for process engineering characterization of single-use bioreactors and mixing systems by using experimental methods", DECHEMA Working group, Upstream processing.

Müller, M. (2015), "Wärmetechnische Charakterisierung von Bioreaktoren mittels einer chemischen Wärmequelle", Sartorius Stedim Biotech - internal Document.

Nagraik, T. (2015), "Establishing and characterizing of an Escherichia coli model process", Masterthesis, Sartorius Stedim Biotech / Technische Universität Harburg-Hamburg.

Omar, K.A. (2014), “Catalytical decomposition of hydrogen peroxide on manganese dioxide nanoparticles at different pH values”, *IMPACT: International Journal of Research in Engineering & Technology*, No. 5, pp. 241–248.

Regestein, L. (2012), “Design and Application of Calorimeters for Monitoring Biological Processes in Stirred Tank Bioreactors”, Dissertation, Rheinisch-Westfälischen Technischen Hochschule Aachen.

Reiss, M. (2015), “Einführung in die Bioreaktortechnik II: Sauerstoff-Transfer und Leistungseintrag”, available at: http://www.biotec.rwth-aachen.de/uploads/V2%20Skript%20Sauerstofftransfer_Leistungseintrag_WS2011.pdf (accessed 1 June 2015).

Reißmann, S. (2015), “Bestimmung der Katalaseaktivität und der Aktivierungsenergie der durch die Katalase katalysierten Reaktion”, available at: http://www2.uni-jena.de/biologie/biochemphys/biochem/Lehre/versuch_1.pdf (accessed 1 June 2015).

Stanbury, P.F., Whitaker, A. and Hall, S.J. (1995), Principles of fermentation technology, 2nd ed, Pergamon, Oxford, U.K., Tarrytown, N.Y., U.S.A.

Stephan, P. (2013), “Wärme und verschiedene Arten der Wärmeübertragung”, in VDI-Gesellschaft Verfahrenstechnik und Chemieingenieurwesen (GVC) (Ed.), *VDI-Wärmeatlas*, Springer Berlin Heidelberg, Berlin, Heidelberg, pp. 19–22.

Storhas, W. (1994), Bioreaktoren und periphere Einrichtungen, Friedr. Vieweg & Sohn Verlagsgesellschaft mbH, Braunschweig / Wiesbaden.

Türker, M. (2004), “Development of biocalorimetry as a technique for process monitoring and control in technical scale fermentations”, *Thermochimica Acta*, Vol. 419 No. 1-2, pp. 73–81.

Van't Riet, K. (1979), “Review of Measuring Methods and Results in Nonviscous Gas-Liquid Mass Transfer in Stirred Vessels”, *Industrial & Engineering Chemistry Process Design and Development*, Vol. 18 No. 3, pp. 357–364.

VDI-Gesellschaft Verfahrenstechnik und Chemieingenieurwesen (GVC) (Ed.) (2013), *VDI-Wärmeatlas*, Springer Berlin Heidelberg, Berlin, Heidelberg.

Vogel, A.I. and Mendham, J. (2000), Vogel's textbook of quantitative chemical analysis, 6th ed., Prentice Hall, Harlow.

Wirges, H.-P. (1977), “Oszillationen von Temperatur und Umsatz im gekühlten Durchflußrührkessel”, *Dissertation,* Technische Universität Berlin.

Zlokarnik, M. (1999), Rührtechnik: Theorie und Praxis, *Chemische Technik/Verfahrenstechnik*, Springer Berlin Heidelberg, Berlin, Heidelberg.

Zühlke, J. (2015), “Evaluation of the heat transfer for a small scale glass bioreactor”, Masterthesis, Sartorius Stedim Biotech/ Hamburg University of applied sciences.

Chapter 8

Appendix

Table 10: Chemicals and enzymes

Chemicals	Manufacturer
Starch	Roth, Art. nr.: 9441.1
$Na_2S_2O_3$	Roth, Art. nr.: HN 25.4
KI	Roth, Art. nr.: 8491.2
H_2O_2 (30%)	Roth, Art. nr.: CP26.1
HCl (32 %)	Roth, Art. nr.: P074.1
MnO_2	Roth, Art. nr.: 7751.1
HNO_3	Roth, Art. nr.: 4989.3
$Fe(NO_3)_3$	Roth, Art. nr.: CN84.1
NaOH	Roth, Art. nr.: K021.1
NaCl	Roth, Art. nr.: 3957.2
KCl	Roth, Art. nr.: 6781.1
Na_2HPO_4	Roth, Art. nr.: P030.3
KH_2PO_4	Roth, Art. nr.: 3904.3
EDTA-$Na_2 \cdot 2\ H_2O$	Sigma-Aldrich, Art. nr.: 03685
Catalase	Sigma-Aldrich, Art. nr.: C40

Table 11: Devices

Devices	Article number, Manufacturer
Graduated burette (25 mL)	Hirschmann
Graduated flasks (0.5, 1 and 2 L)	Isolab Germany
Balances	CPA 10001, Sartorius LA6 20S, Sartorius GENIUS ME215S, Sartorius
Magnetic stirrer	IKA, RCT basic
Beaker (250 mL)	Schott Duran
Escape	Bense Laborbau
Camera	Canon EOS 600D
Camera lens	Canon EF-S 18-55mm f/3.5-5.6 IS II
Temperature measurement device	Testo 435-2
Pumps	205 U, Watson Marlow 520, Watson Marlow
Bioreactors	UniVessel® (2 L) (multi-use), Sartorius UniVessel® (5 L) (multi-use), Sartorius
Cooling unit	Frigomix 1000, Sartorius
Digital control unit	Biostat B plus, Sartorius
Vacuum pump	16692, Sartorius
Single-use Büchner funnel	Sartolab 180C6 (0.22 µm PES), Sartorius
Multi-use Büchner funnel	Not labelled, Sartorius
Scanning electron microscopically	FEI Quanta 200F
Sputter coater	Emitech K550
Mass flow meter	10 DX 3312 A, Fischer Porter
Filtration capsule	Sartopore 2 (0.45 + 0.2 µm), Sartorius
Tube sealer	BioSealer, Sartorius
Tubes (50 mL)	Sarstedt
Insulation	Armaflex, Armacell
pO2-probe	OxyFerm FDA 225, Hamilton
Exhaust-gas-analyser	Biopat Xgas, Sartorius

Table 12: Calculation and normalisation of the reaction rate (part 1). Results obtained with 0.86 $\frac{g}{L}$ MnO_2 and 1.5 $\frac{mole}{L}$ H_2O_2 in a batch experiment (Figure 28). Constants: E_A = 70,000 $\frac{J}{mole}$, $e^{\frac{E_A}{R\cdot(30+273,15)}} = 8.6722E\text{-}13$.

Time $[h]$	$c(H_2O_2)$ $\left[\frac{mole}{L}\right]$	$k_{i,i+1}$ $\left[\frac{1}{min}\right]$	Average temperature $[K]$	$e^{\frac{E_A}{R\cdot T_{i,i+1}}}$ $[-]$
0.00	1.52			
0.02	1.23	12.32	289.9	2.43688E-13
0.05	1.14	2.37	293.3	3.39565E-13
0.06	1.13	1.66	295.6	4.2663E-13
0.09	0.97	4.49	297.1	4.92612E-13
0.14	0.89	1.68	299.5	6.15305E-13
0.21	0.67	3.98	302.5	8.13224E-13
0.30	0.69	-0.28	304.8	1.00335E-12
0.45	0.58	1.12	305.0	1.0217E-12
0.72	0.46	0.85	302.6	8.24524E-13
1.36	0.24	1.03	297.8	5.26544E-13
2.03	0.18	0.42	292.9	3.28113E-13
4.25	0.04	0.74	290.9	2.69273E-13

Table 13: Calculation and normalisation of the reaction rate (part 2). Results obtained with 0.86 $\frac{g}{L}$ MnO_2 and 1.5 $\frac{mole}{L}$ H_2O_2 in a batch experiment (Figure 28). Constants: E_A = 70,000 $\frac{J}{mole}$, $e^{\frac{E_A}{R\cdot(30+273,15)}} = 8.6722E\text{-}13$.

$\kappa_{i,i+1}$ [−]	$k_{i,i+1}(30\,°C)$ $\left[\frac{1}{h}\right]$	$\frac{t_{i+1}-t_i}{t_0-t_{end}}\cdot k_{i,i+1}(30\,°C)$ $\left[\frac{1}{h}\right]$	$k_{corrected}$ $\left[\frac{1}{h}\right]$
			1.76
0.28	43.83		
0.39	6.05	0.15	
0.49	3.36	0.02	
0.57	7.90	0.20	
0.71	2.37	0.09	
0.94	4.24	0.22	
1.16	-0.24	-0.01	
1.18	0.95	0.11	
0.95	0.89	0.18	
0.61	1.69	0.81	
0.38	1.11		
0.31	2.37		

Figure 53: Single-use büchner funnel (180C6, 0.22 µm PES), plugged to a vaccum pump for the separation of MnO_2.

Figure 54: Multi-use büchner funnel with a polyethersulfone-(PESU)-membrane (0.2 µm), plugged to a vaccum pump for the separation of MnO_2.

Figure 55: Filtration capsule (Sartopore 2 (0.45 µm + 0.2 µm)), plugged to a peristaltic pump for the separation of MnO_2.

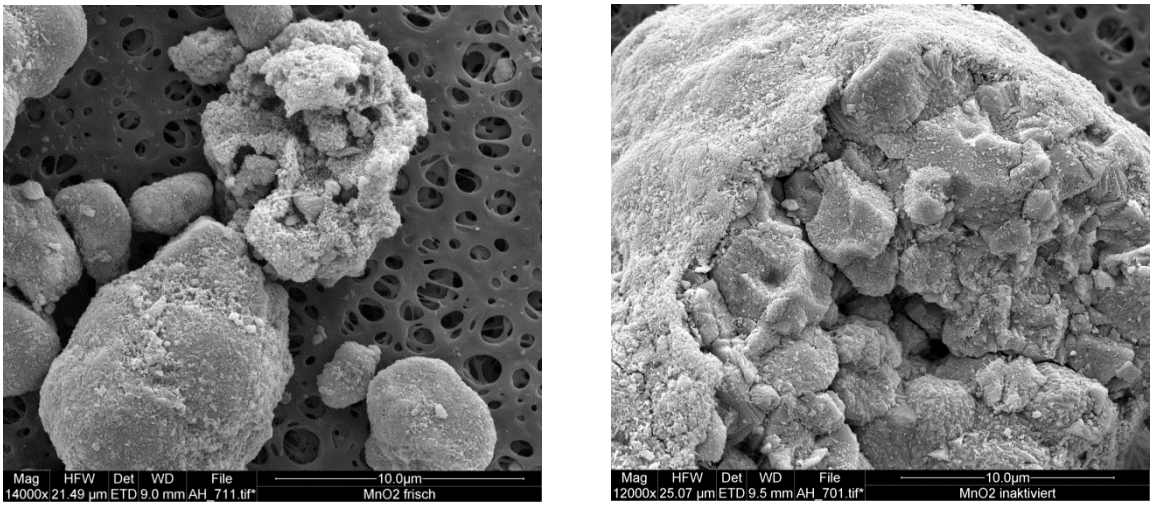

Figure 56: Scanning electron microscopically analysis of fresh (left) and inactivated MnO_2 (right).

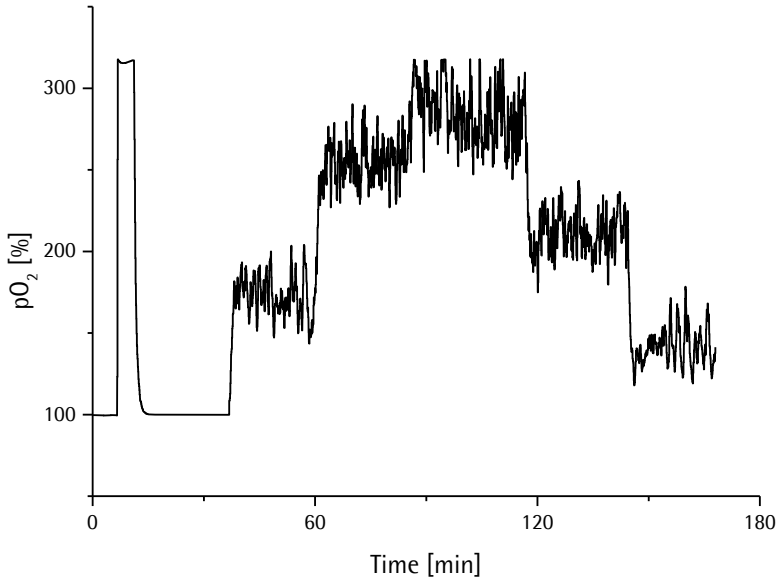

Figure 57: Supersaturation of dissolved oxygen due to the steady digestion of H_2O_2. 7 min – 15 min: 10 ml of H_2O_2 (test of the pO_2-probe). Dilution rates according to Table 14. $\dot{V}_{gas}$ = 1 $\frac{L}{min}$ (air), 500 rpm.

Table 14: Dilution rate profile.

Time [min]	D $\left[\frac{1}{h}\right]$
40 – 60	$11 \cdot 10^{-3}$
60 – 85	$28 \cdot 10^{-3}$
85 – 115	$45 \cdot 10^{-3}$
115 – 145	$19 \cdot 10^{-3}$
145 – 165	$4 \cdot 10^{-3}$

Example for the calculation of k_La

Table 15: List of process parameters for the determination of k_La.

Process parameters	Values
V	$3.5\ L$
T	$303.15\ K$
p	$10^5\ Pa$
$c(H_2O_2)_i$	$9.8\frac{mole}{L}$
c_s	$223 \cdot 10^{-6}\frac{mole}{L}$
D	$38.28 \cdot 10^{-3}\frac{1}{h} = 10.6 \cdot 10^{-6}\frac{1}{s}$
Gas	$Nitrogen$
$\dot{V}_{g,i}$	$1\frac{L}{min} = 16.7 \cdot\ 10^{-3}\frac{L}{s}$
$c_{g,i}$	$0\frac{mole}{L}$
H^{cc}	$27.2\ \cdot 10^{-3}(salt\ solution, 10\ \%\ salinity)$
X	99.4 %
p_{O_2}	298.3 %

$$|k_La| = \left|\frac{OTR}{c_l^* - c_l}\right| \tag{89}$$

$$OTR = D \cdot c(H_2O_2)_i \cdot \frac{X}{100} \cdot \frac{1}{2} \tag{90}$$

$$OTR = 10.6 \cdot 10^{-6}\frac{1}{s}\ \cdot 9.8\frac{mole}{L} \cdot \frac{99.4\ \%}{100} \cdot \frac{1}{2} \tag{91}$$

$$OTR = 51.8 \cdot 10^{-6}\frac{mole}{L \cdot s} \tag{92}$$

$$c_l^* = c_{g,o} \cdot H^{cc} \tag{93}$$

$$c_{g,o} = \frac{c_{g,i} \cdot \dot{V}_{g,i} + OTR \cdot V}{\dot{V}_{g,o}} \tag{94}$$

$$\dot{V}_{g,o} = \dot{V}_{g,i} + OTR \cdot V \cdot \frac{R \cdot T}{p} \tag{95}$$

$$\dot{V}_{g,o} = 16.7 \cdot 10^{-3} \frac{L}{s} + 51.8 \cdot 10^{-6} \frac{mole}{L \cdot s} \cdot 3.5\ L \cdot \frac{8.3\ \frac{J}{mole \cdot K} \cdot 303.15\ K \cdot 1000}{10^5 Pa} \tag{96}$$

$$\dot{V}_{g,o} = 21.2 \cdot 10^{-3} \frac{L}{s} \tag{97}$$

$$c_{g,o} = \frac{0.21 \cdot \left(\frac{8.3\ \frac{J}{mole \cdot K} \cdot 303.15\ K \cdot 1000}{10^5 Pa} \right) \cdot 0\ \frac{L}{s} + 51.8 \cdot 10^{-6} \frac{mole}{L \cdot s} \cdot 3.5\ L}{21.2 \cdot 10^{-3} \frac{L}{s}} \tag{98}$$

$$c_{g,o} = 8.5 \cdot 10^{-3} \frac{mole}{L} \tag{99}$$

$$c_l{}^* = 8.5 \cdot 10^{-3} \frac{mole}{L} \cdot 27.2 \cdot 10^{-3} \tag{100}$$

$$c_l{}^* = 0.2 \cdot 10^{-3} \frac{mole}{L} \tag{101}$$

$$c_l = \frac{p_{O_2}}{100} \cdot c_s \tag{102}$$

$$c_l = \frac{298.3\ \%}{100} \cdot 223 \cdot 10^{-6} \frac{mole}{L} \tag{103}$$

$$c_l = 0.6 \cdot 10^{-3} \frac{mole}{L} \tag{104}$$

$$c_l{}^* - c_l = 0.2 \cdot 10^{-3}\ \frac{mole}{L} - 0.6 \cdot 10^{-3}\,\frac{mole}{L} \tag{105}$$

$$c_l{}^* - c_l = -0.4 \cdot 10^{-3}\,\frac{mole}{L} \tag{106}$$

$$|k_L a| = \left|\frac{51.8 \cdot 10^{-6}\,\frac{mole}{L \cdot s}}{-0.4 \cdot 10^{-3}\,\frac{mole}{L}}\right| \tag{107}$$

$$|k_L a| = 112 \cdot 10^{-3}\ s^{-1} = \ 431\ h^{-1} \tag{108}$$

Modelling of the H_2O_2 decomposition and Catalase inactivation

Matlab source code

```
function Catalase_Modellierung ()

clear all
close all
clc

% Prozessmodell Peroxid-Zerfall und Catalase Inaktivierung (Batch)
% 21.05.2015
% Ulf Dehio, Matthias Müller

% Experimentelle Daten
time = [0 1 5 9 15 21.5 30.5 42 66.5 130]';
H2O2 = [1.00858 0.92978 0.83523 0.69340 0.40974 0.26002 0.17335 0.16547 0.16153
0.16153]';

% Equidistante Interpolation mit definierter Stepanzahl
numStep = 100;
expTimeInterp = (linspace(time(1),time(end),numStep));
expDataInterp = interp1(time,H2O2,expTimeInterp);
expTimeInterp = (linspace(time(1),time(end),numStep)).*60;

k1 = 2.2622e-002;
k2 = 4.3342e-002;
parameter0=[k1 k2];


options = optimset('Display','off','TolX',1e-007);
[parameter] = fminsearch(@optimizeParameter, parameter0, options);
Y
disp(['k1, beträgt: ',num2str(parameter(1)) char(10) 'k2, beträgt:
',num2str(parameter(2))]);

    function [RMSE] = optimizeParameter (parameter)


    % Aufsetzen des ODE-Sovers
    tspan = expTimeInterp;
    yzero = [1.00858; 0.96*0.5/0.1];

    options = odeset('NonNegative',2);
    [t,Y] = ode45(@(t,Y)ODE1(t,Y,parameter),tspan,yzero);

        if parameter(1) < 0 || parameter(2) < 0;
            RMSE = 1e06;
        else
            RMSE = sum(sqrt((Y(:,1)-expDataInterp').^2));
        end
```

```
        % Nested function %
        %  Prozessmodell  %
        function dYdt = ODE1(t,Y,parameter)

        dYdt=zeros(2,1);

        % Y(1) entspricht dem H2O2-Verlauf, Stoffbilanz
        dYdt(1) = -parameter(1)*Y(2)*Y(1);

        % Y(2) entspricht der Änderung der Enzymmenge, Verdünnungseffekt
        dYdt(2) = -parameter(2)*Y(2);

        end


    end
    subplot(1,2,1);plot(expTimeInterp./60,Y(:,1));hold on;scatter(time,H2O2);
    subplot(1,2,2);plot(expTimeInterp./60,Y(:,2));
end
```

Chapter 9

Eidesstattliche Erklärung

Ich versichere hiermit, dass ich die vorliegende Arbeit selbstständig verfasst und keine anderen als die angegebenen Quellen und Hilfsmittel benutzt habe. Das bearbeitete Thema wurde nicht schon früher im Rahmen einer anderen Arbeit behandelt und/oder anderweitig als Prüfungsarbeit eingereicht.

Göttingen, den Unterschrift des Verfassers